HYBRID SCANNING ELECTROCHEMICAL TECHNIQUES: METHODS AND APPLICATIONS

Christine Kranz, Christophe Demaille

HYBRID SCANNING ELECTROCHEMICAL TECHNIQUES: METHODS AND APPLICATIONS

Christine Kranz[a] and Christophe Demaille[b]

[a] Institute of Analytical and Bioanalytical Chemistry, Ulm University, Ulm, Germany

[b] Université de Paris, UMR CNRS 7591, Paris, France.

Since the 2nd Edition of the book, significant progress has been made in all aspects of hybrid scanning electrochemical probe microscopy (SEPM) combining SECM with techniques such as AFM, STM, shear force and SICM. Given the ease of nanopipette fabrication, nanopipette-based hybrid SPM techniques have gained significant attention such that they will now be covered in a separate chapter (**[Editor please insert Chapter no.]**). One of the driving forces behind the hybrid SECM techniques is the precise knowledge of the tip-substrate separation, which is essential to extract quantitative information on surface processes. This is particularly a critical aspect if improved spatial resolution down to the nanometer regime is targeted, which requires nano-sized electrodes positioned with several electrode radii precision at the sample surface. To perform imaging experiments with nano-sized electrodes, distance-controlled positioning of the SECM tip using an electric feedback loop is highly recommended. For example, for real-world samples with surface morphology on the order of the radii of the electroactive area at SECM tips, fixed height imaging invariably may result in erroneous data or tip crash. However, the developments are also driven by addressing more complex problems which requires that several sample-characteristic parameters (e.g., like nanomechanical properties, spectroscopic and optical properties) are recorded simultaneously without the need of sequential mapping. With the update of this chapter, the combination of SECM with techniques such as AFM, STM, shear force but also complementary techniques including fluorescence, confocal laser scanning microscopy, surface plasmon resonance and attenuated total reflection (ATR) IR measurements will be covered, providing selected highlighted applications of these hybrid methods.

Index:

1. COMBINED SCANNING ELECTROCHEMICAL MICROSCOPY – ATOMIC FORCE MICROSCOPY (SECM-AFM)

1.1 Introduction

After shear force mode SECM (**section 3.1**), the combination of SECM with atomic force microscopy (AFM) is one of the most well-known and well-documented hybrid SECM technologies as it adds advantages to both SPM methods. In contrast to the first editions of the book, the abbreviation **AFM-SECM** will now be used throughout this chapter, as has evolved into a commonly used expression in the literature. AFM is frequently termed as "chemically blind"; hence adding information on (electro)chemical surface process during mapping of the sample surface allows the correlation of e.g., morphological changes with local reactivity. SECM requires reliable distance control if SECM tips with sub-micrometer dimensions are used for imaging. Traditionally, in amperometric SECM measurements the current that flows at the tip, when the tip is placed close to a surface, is due to the diffusional flux of a specific electroactive moiety to the electrode, which is dependent on both surface reactivity and tip-substrate separation, *d*. If *d* is not known accurately then the (electro)chemical process under investigation cannot be correctly interpreted. More than twenty years ago, the first approaches to combine AFM and SECM were demonstrated by Macpherson and Unwin [1] and Kranz et al. [2] by fabricating sub-micro- and nano-sized electrodes that can be used as cantilevers in AFM [3] or by integrating an electrode into a commercial AFM probe [2]. Since these seminal contributions, significance developments in hybrid AFM-SECM have been made. Various aspects have been discussed in recent reviews featuring SEPM with focus on AFM-SECM methodology and applications [4–9].

Atomic force microscopy (AFM), introduced by Binnig, Quate and Gerber in 1986 [10] is to date probably the most commonly used scanning probe microscopy technique, as high-resolution information of sample surfaces independent of their physical and chemical nature

can be obtained. Attractive and/or repulsive forces acting between an ultra-sharp tip at the end of a cantilever and the sample surface lead to a displacement of the cantilever following Hooke's law in contact mode AFM, or to changes in amplitude (i.e., amplitude-modulated AFM, AM-AFM), or in frequency (i.e., frequency-modulated AFM, FM-AFM) in dynamic mode AFM. For AFM imaging, the AFM probe scans across the sample surface, and a physical property of the cantilever varies in response to force interactions between the tip and substrate. Using an electronic feedback loop, the AFM tip-sample separation is kept constant and accurately maintained (constant force mode) providing high resolution 3D information with resolutions *z* resolutions of sub-Å and *x,y* resolutions in the nanometer range. The latter is controlled primarily by the radius of curvature of the sharp tip and the experimental conditions. However, the AFM is considered as 'chemically blind', if the AFM tip, which is usually made from silicon or silicon nitride, is not specifically modified [8]. In respect to SECM, the need to improve the lateral resolution using electrodes with radii in the nanometer range, requires that the distance between the sample and the SECM tip can be maintained accurately. By integration of an electrode into the AFM probe, the advanced positioning of the AFM tip can be simultaneously exploited for the tip-integrated electrode, thereby allowing precise control of the implemented electrode-sample distance. Thus, the inherent correlation of structural information with (electro)chemical surface activity is facilitated. The current response of the electrode, which can be located at various positions at the AFM tip, serves as a quantitative measure of the (electro)chemical properties of the interface, akin to SECM. The effect of local changes in solution composition, initiated electrochemically can be interrogated structurally.

1.2 Probe fabrication

For a long time, a limiting factor compared to other hybrid SECM methods was the lack of suitable AFM-SECM probes. Hence, it is evident that a significant body of AFM-SECM literature is focused on combined/integrated probe fabrication, which will be discussed in the following, including commercially available AFM-SECM probes, which appeared on the

market within the last decade. Predominantly, AFM-SECM probes have been reported with an electrode either at the apex of the AFM tip (i.e., mostly conical electrodes) or an electrode located below the non-conductive AFM tip (i.e., termed as “recessed from the tip”). Evidently, the co-location of electrode and AFM tip apex is more established, as the fabrication of such probes - either hand-fabricated or via well-established microfabrication – is less complex. Almost all fabricated AFM-SECM probes discussed in the following section were characterized via electron microscopy (i.e., shape and size) and cyclic voltammetry in terms of electrode size and quality of insulation quality.

1.2.1. Hand-fabricated AFM-SECM Probes

Hand-fabricated probes can be obtained without specialized equipment or the need of a cleanroom facility, as initially shown by Macpherson, Unwin and co-workers [3]. Nanoscopic electrode fabrication [11] and the fabrication of probes for electrochemical STM [12] are well-established procedures of electrochemical etching and insulation of microwires, leading to sharpened and insulated sub-micro- and nanoelectrodes, except at the very apex of the tip. For the fabrication of AFM-SECM probes, the wire is etched and then bent and flattened to form the force-sensing cantilever. Subsequently, the bent wire is insulated with an electrochemically induced deposition process of i.e., electrophoretic paint, which retracts from the apex during curing, so that only the very end of the tip is exposed, leaving a sub-micron, “cone-shaped” electrode at the tip apex. Due to the low resonant frequencies of these hand-fabricated AFM-SECM probes, topographical imaging is typically carried out in contact mode. As, electrochemical imaging is typically carried out with the tip maintained at a 'constant distance' from the substrate of interest, the AFM-SECM probe scans each line twice. In the first pass, sample topography is recorded whilst, in the second pass this information is used to hold the tip at a constant, defined distance from the surface while electrochemical data is acquired [13]. This methodology is also used for magnetic- and electrostatic-AFM imaging and is usually

termed as “lift mode”. In this way the tip-substrate separation is always known, which is not possible with conventional SECM imaging.

This seminal approach was adapted and modified e.g., to fabricate sub-micrometer-sized gold AFM-SECM electrodes of well-defined conical or spherical geometry [14,15]. The apex of the etched gold microwire is molded into a defined spherical or conical structure by local melting using a controlled arc discharge. The whole structure is then coated with an electrodeposited insulating paint and the very end of the tip exposed by applying a high voltage pulse to the gold wire. These probes can then be further labeled with redox-active groups as introduced by Demaille and co-workers [16] by tethering redox molecules such as ferrocene moieties via flexible PEG cross-linkers to the gold tip. A crucial requirement of all AFM-SECM probe developments is that the only exposed metallic area on the probe is that of the electrode itself, thus it is essential that no pinholes are present in the insulating coating, which is quite challenging, when experiments are carried out in organic electrolyte solution or at harsh conditions such as strong acidic or basic pH values. Glass is mostly used for conventional micro-sized SECM tips, and is among the best methods to seal micro-wires. Glass-insulated AFM-SECM probes with nanometer-sized Pt electrodes or protruding conical Pt electrodes, which are fabricated via laser pipette pulling are commercially available e.g., from Nanonics Imaging Ltd. [17]. An overview of hand-fabricated AFM-SECM probes is shown in **Figure 1**.

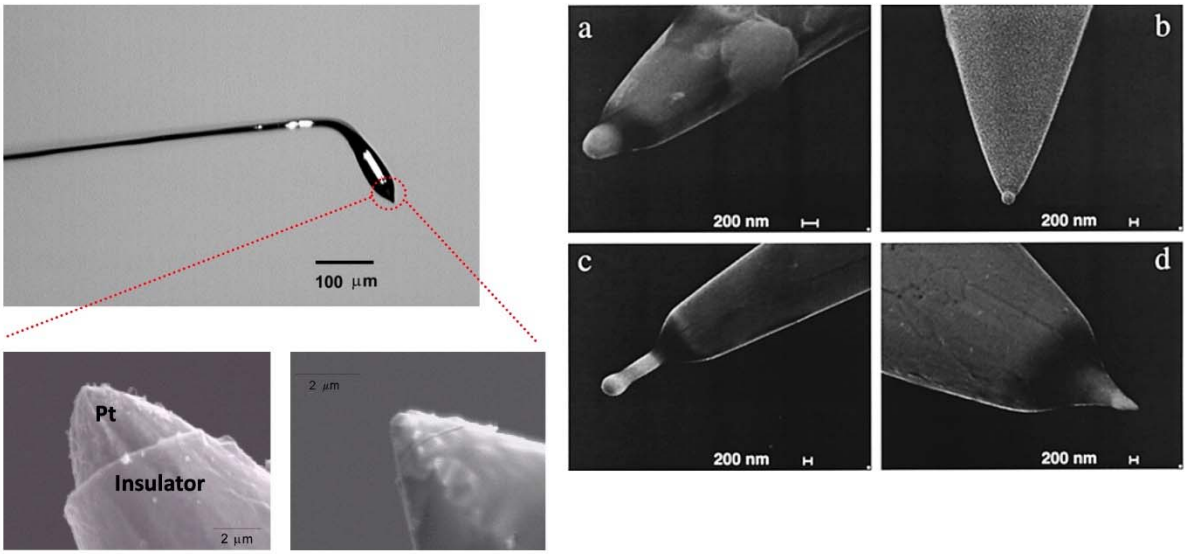

Figure 1. Left) Micrograph of a coated SECM-AFM probe. scanning electron micrographs of the end micrometer- and sub-micrometer-sized SECM-AFM tips. Adapted with permission from J.V. Macpherson et al., *Anal. Chem.* 72, 276-285 (2000). Copyright 2000 American Chemical Society. Right: SEM micrographs of gold sub-microelectrodes. The electrodes are made from gold wires bearing sub-micrometer-sized structures formed as a result of the controlled arc discharge technique. The body of the wire is insulated by a layer of electrophoretic paint; only the preformed tip end is bare gold. (a) – (d) represent the different structures formed by varying the settings of the spark generator.; Reproduced with permission from J. Abbou et al., *Anal. Chem.* 74, 6355-6363 (2002). Copyright 2002 American Chemical Society.

Spherical AFM-SECM probes with radii ranging from 150 to 550 nm were initially reported by Abbou et al. [14] and later reduced radii of 20–100 nm have been reported [15]. Conical AFM-SECM probes with effective tip radii ranging from 50 nm to 2.5 µm were reported within a batch of 50 fabricated tips [1]. For hand-fabricated AFM-SECM probes, the electrode is also at the same location as the apex of the imaging AFM tip.

L-shaped AFM-SECM probes ("iProbe"), developed by a former AFM distributor (Windsor Scientific Ltd) with microscopic electrodes were employed for corrosion studies by Davoodi and colleagues [18–23]. The fabrication steps of these AFM-SECM probes included embedding of a Pt microwire in an insulating epoxy, to produce an insulated ultramicroelectrode (UME) of 1-5 µm in diameter followed by a flattening and bending step adapted from the approach by Macpherson and Unwin [1]. Thereby, the probe can be used as cantilever, for sufficient laser deflection the bent part was coated with gold. The insulated end was cut with FIB to reveal a small tip next to the Pt disc electrode [21]. Alternatively, the probes

were fabricated by pulling and embedding the Pt in quartz glass, again flattened and bent, and then polished at an angle of 15-25° [18]. For both designs, the bent part for AFM laser deflection was not immersed in the electrolyte solution. These probes were used for investigating structure-activity problems related to corrosion as discussed in **section 1.5.2**. Velmurugan et al. [24] fabricated glass-insulated nanoelectrodes by laser-pulling, which were then attached to a quartz tuning fork. Although, the nanoelectrode is produced by benchtop methods, a series of milling steps and ion beam-induced deposition (IBID) steps for attachment of the probe to the quartz tuning fork were employed, which appears quite laborious, time and cost consuming.

1.2.2. Micro-fabricated AFM-SECM Probes

For more widespread application of AFM-SECM, probes with reproducible and defined characteristics such as tunable force constants, reproducible tip curvature radii, and robust insulation are required. In 1999, DeRooij and co-workers already presented a microfabrication process for NSOM probes and AFM probes with conical microelectrodes [25]. Currently, two microfabrication approaches for AFM-SECM probes, where the electrode is also at the same location as the apex of the imaging tip currently are reported: (1) modification of commercially available AFM probe to integrate electrochemical functionality [2,26,35–40,27–34] and (2) bottom-up fabrication, where the probe structure is built from first principles [**41–51**]. The latter can be divided again in two approaches: batch process using standard lithographic methods applicable to produce probes at the wafer-level and microfabrication steps with an additional serial step during fabrication or at the end of the fabrication process to expose the electroactive area, predominantly by focused ion beam (FIB) structuring. Owing to its precision, FIB milling evolved into a quite popular AFM-SECM probe fabrication step despite the requirement of serial processing. The bottom-up fabrication process, which applies standard lithographic processes used in AFM probe fabrication for rectangular cantilevers, has been reported by e.g., Staufer, Frederix, Engel and co-workers. [41,52,53] Frederix et al. presented an approach, where pyramidal etch pits in Si(100) were opened by etching and then coated with a film of

silicon nitride. These were used as the template for electrode and tip formation. The electrode (tip) was formed by depositing a film of polycrystalline silicon, restructured by ion etching, followed by a layer of platinum. Finally, a layer of silicon nitride was deposited to encapsulate the metal, and the surface was subject to etching to reveal the cantilever shape, resulting in a cantilever and tip totally insulated, except for the Pt_xSi_y apex. Although the probes are formed in a batch process, variation was found in the electrode base radii, between 40 – 400 nm, and ratio of electrode height to base radii from 2- 2.5. Despite these large variations, tip curvature radii as small as 10 nm were obtained.

Prinz and Fasching fabricated sharpened high aspect ratio silicon (HARS) AFM-SECM probes with base diameters as small as 600 nm and tip radii smaller than 50 nm, using isotropic and anisotropic deep-reactive etch processes including a serial FIB milling step [43]. Deposition of silicon nitride followed by a back etch step enabled the silicon tips to protrude through the silicon nitride layer. Layers of platinum, followed by silicon nitride were then deposited on the tips. Finally, using a mask in combination with FIB, the underlying metallic layer was exposed to reveal the Pt electrode sitting atop the HARS tip. The fabrication steps can also be used to fabricate linear probe arrays and two-dimensional probe arrays. Only electrochemical characterization using cyclic voltammetry, but no AFM-SECM measurements were reported. The same group reported the fabrication of planar and needle shaped probes with a dual electrode system (see **Figure 2**) for analyzing living cells [54]. In brief, the processes comprise two fabrication steps: (1) microfabrication of cantilevers and metal deposition and (2) serial FIB milling steps to precisely define the shape of the tip, resulting in radii as small as 50 nm and to remove the insulator in the vicinity of the apex and to define the electrode geometry. For dual probes fabrication, one needle was coated with Pt whereas the other one was modified with Ag to form the reference electrode. The probes were found to have an average electrode area of 0.1 μm^2 and both Pt and Ag/AgCl (formed by chloridizing Ag) sub-micrometer electrodes were formed on the AFM tips. The functionality of the probes for imaging was only

demonstrated for mapping the topography of a SiO_2 grating with step heights of 100 nm. The capability to use the microfabricated probe for live cells studies was demonstrated via a first proof-of-principle measurement, penetrating a rat fibroblast cell with a single Ag/AgCl AFM probe recording the cell membrane potential during penetrating the cell.

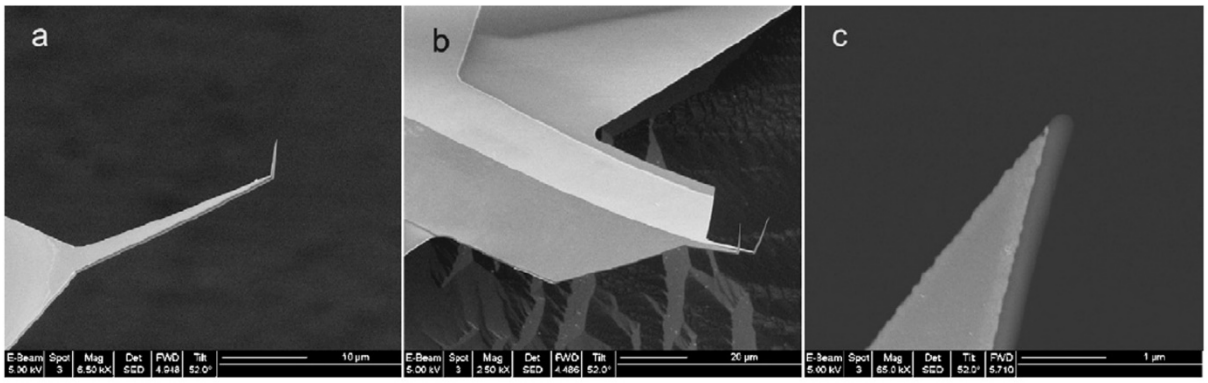

Figure 2. (a) Single and (b) dual probes with bent nano-probes for combined electrochemical and AFM analyses. (c) Tip of the single probe. Reproduced with permission from Bai, et al., *Sensors Actuators B Chem.* 130, 249–257 (2008). Copyright 2008 Elsevier B.V.

A similar fabrication process had been adopted earlier in 2005 by Macpherson and Weaver [45,46], except that in this study electron beam lithography was used to expose the defined electrode area as opposed to FIB. **Figure 3** shows a typical image of the final AFM-SECM probe with triangular shaped gold electrode with a base width of approx. 1 μm, defined at the apex of the tip. High yields of ~ 80 % were reported.

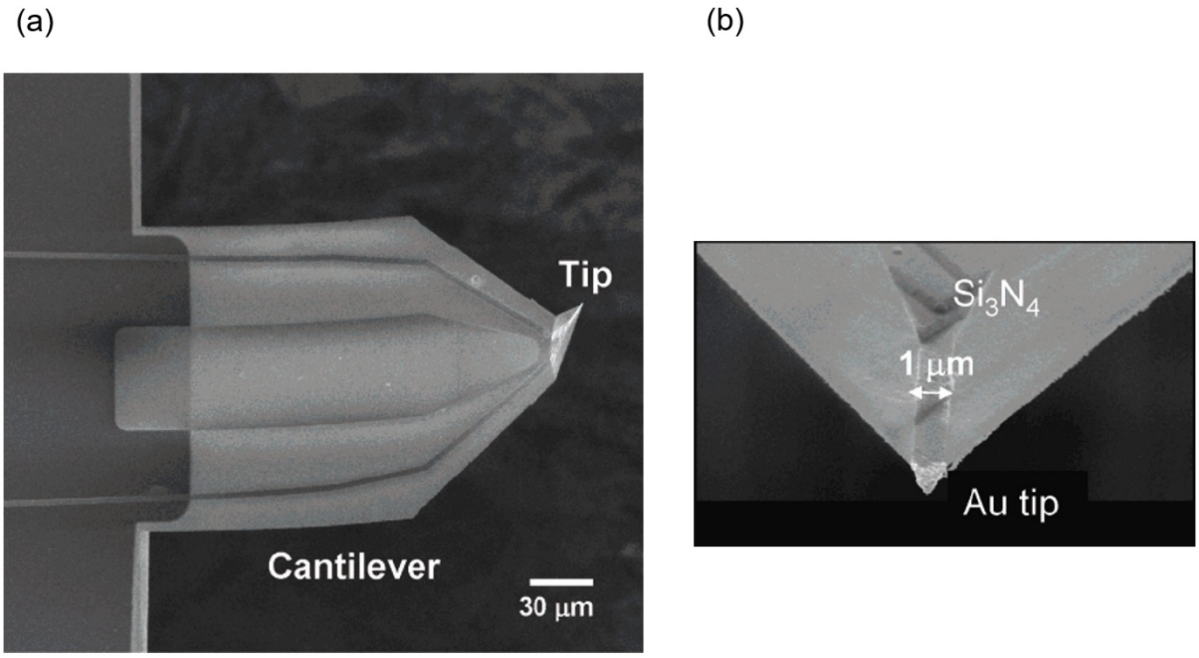

Figure 3: (a) Low- and (b) high-resolution FE-SEM images of the tip and cantilever geometry of a typical AFM-SECM probe fabricated using microfabrication and electron beam lithography. Adapted with permission from P. S. Dobson et al., *Anal. Chem.* 77, 424–434 (2005). Copyright 2005 American Chemical Society.

DeRooij and colleagues presented a bottom-up process using photolithography to fabricate AFM-probes with a gold apex, suitable for AFM-SECM, and single molecule force spectroscopy as the golf apex can be easily modified with specific molecules through thiol chemistry [55]. This FIB-less microfabrication process, which is based on photolithography and Si etching steps from the top surface of a SOI wafer allows processing of cantilevers with different length and the thicknesses resulting in force constants from 0.05 N/m to 13.67 N/m from the same wafer. The integrated electrode was defined by an electron beam lithographic step resulting after processing in a gold nanowire with a tip radius of approx.. 20 nm which is protruding from the side of the cantilever as visible in **Figure 4**. Although only the fabrication process was presented in this contribution, such batch bottom-up fabrication with tunable properties of the conductive probes is quite interesting.

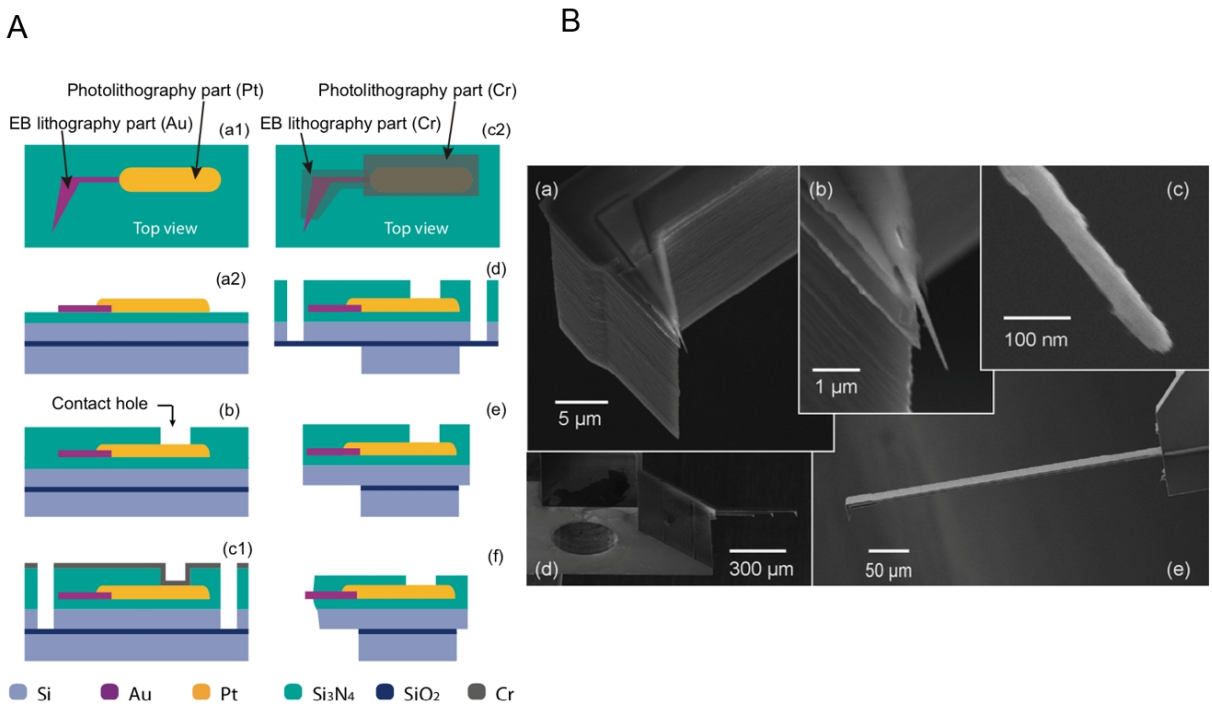

Figure 4. Left: Schematic view of the fabrication process. Top view (a1) and side view (a2) of the tip and interconnections after the lift-off process. (b) BHF etching to open the contact holes. (c1) DRIE etching through the device layer with the Cr mask which defines the chip shape. (c2) Top view of the Cr mask in step c1. (d) Backside patterned by DRIE. (e) BHF etching releases the chip. (f) KOH etching and BHF etching open the conducting tip apex. Right: SEM pictures of the fabricated probe: (a) Conductive probe. (b) Closer view of the passivation and gold tip. (c) Tip apex. (d) A bird's eye view of the chip from the handling layer. (e) 400 µm × 20 µm × 2 µm cantilever with a gold conductive tip. Reproduced with permission from Y. Wu et al., *Sensors Actuators A Phys*. 215, 184–188 (2014). Copyright 2014 Elsevier B.V.

Wain et al. fabricated AFM-SECM probes also using a bottom-up approach with a serial FIB modification step [51]. After defining the dimension and shape of the cantilever and forming an insulating SiO_2 layer by thermal oxidation, the tip side was coated with a Pt layer and a silicon nitride layer. As already previously applied in AFM-SECM probe microfabrication [30], a sacrificial Cr layer is deposited and selectively removed by FIB milling. Subsequent wet etching steps to remove the previously exposed silicon nitride, the remaining sacrificial Cr layer, resulted in AFM-SECM probes with an approximated base radius of 150 nm. Although the tip radius and tip height were not further specified, a tip radius of approx. 80-90 nm can be estimated from the SEM image shown in **Figure 5**. A yield of 80% of functional AFM-SECM probes was reported. Imaging of a gold patterned silicon oxide substrate was carried out in lift

mode recording first the topography followed by "lifting" the probe by 100 nm before recording the electrochemical image.

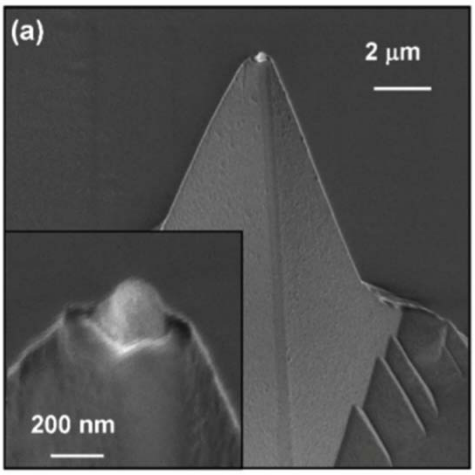

Figure 5. (a) SEM image of a batch-fabricated AFM-SECM tip with conical electrode apex. Reproduced with permission from A. J. Wain et al., *Anal. Chem.* 86, 5143−5149 (2014). Copyright 2014 American Chemical Society.

Wittstock and co-workers and Oesterschulze and co-workers microfabricated AFM-SECM probes with nanoscopic electrodes by back filling and coating a microfabricated aperture within a silicon dioxide pyramid [56] with an Au layer [47,48]. For handling, the processed cantilever structures were mounted to a rigid chip processed at a second wafer. To make electrical contact, a pyramidal feedthrough was etched into the holder chip to contact the Au layer on the cantilever. Initially, for insulation of the AFM-SECM probe, a 1 μm thin layer of Parylene C layer was used which was replaced later by silicon nitride. The electrode was exposed by slicing off the apex of the silicon dioxide tip using FIB under a certain angle, as shown in **Figure 6**.

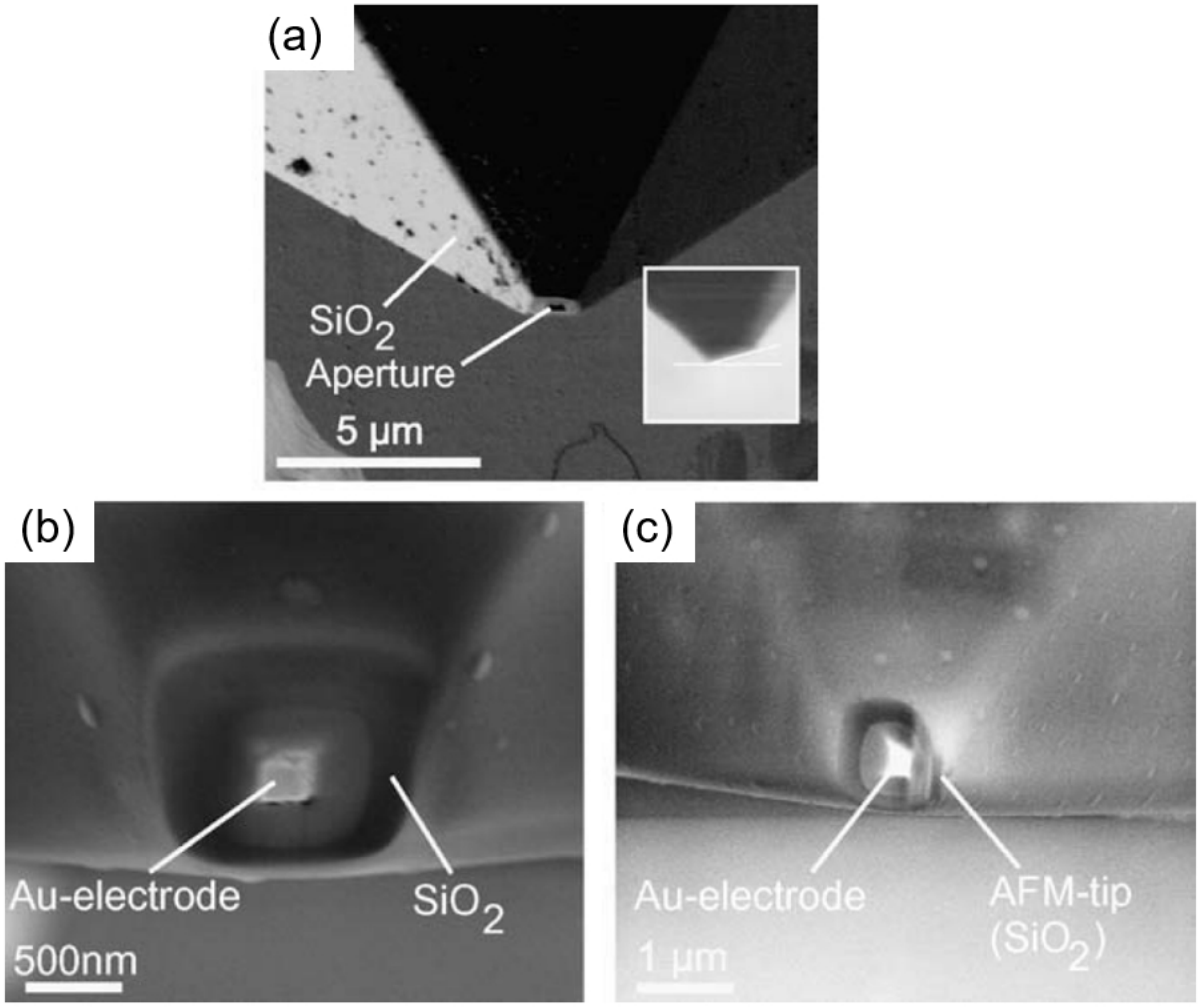

Figure 6: (a) Slice of the pyramidal tip yielding a small square electrode (inset shows the same tip at the same magnification but at a different angle in order to visualize the sloped cut of ~ 15°). (b) Electrode at the apex of the pyramid achieved by removing SiO_2 at the very tip. (c) Ion beam milling was performed so that one half of the top SiO_2 layer was left as distance holder in SECM and as AFM-tip. Reproduced with permission from M. Salomo et al., *Microelectron. Eng.* 87, 1537–1539 87 (2010). Copyright 2010 Elsevier B.V.

As can be seen the electrode is slightly offset from the imaging tip, which must be accounted for when interpreting the electrochemical images. AFM-SECM probes with electrodes as small as ~ 10 nm radius were fabricated using this approach [48]. It was noted that with this type of SECM-AFM design topographical features on the surface of a certain size (dependent on probe-electrode geometry) led to artifacts in the SECM current image [48].

Batch-fabrication process at the wafer-scale level for recessed electrodes using standard lithography techniques without any serial modification steps such as FIB milling at the

expensive of the achievable size of the electrode have been introduced by Shin et al., however, at the expense of the achievable electrode size [49,50]. Silicon AFM-SECM probes with micro-sized Pt ring-electrodes were fabricated by coating microfabricated silicon pillars on cantilever structures with Pt, followed by silicon carbide deposition. Preferentially, etching of the surface left a silicon carbide tip on the top of the pillar, surrounded by a ring of Pt, at the base of the tip. Typical yields were quoted at 60% [50]. Due to the standard lithographic process, the diameter of the ring electrode is in the range of 4-6 μm, thus limiting the achievable resolution in the current images. A batch fabrication for AFM probes with a conductive and an insulation layer except the contact pad and the tip has been presented by Birhane et al. [57] showing reduced capacitive coupling with the sample. The fabrication process is based on standard lithographic processes. Although the probes were designed for conductive AFM (contact mode) and electrostatic force microscopy (dynamic) mode, these probes may be also suitable for AFM-SECM measurements. Commercially available AFM-SECM probes with conical electrodes from Bruker are also fabricated via standard MEMS processes and will be discussed in **section 1.3**

1.2.3. Modification of commercially available AFM probes.

A quite popular approach for fabricating AFM-SECM probes is the modification of commercially available silicon and silicon nitride AFM cantilevers. Initially this approach was introduced by Kranz et al. [2] by coating silicon nitride AFM probes with a 100 - 300 nm thick layer of Au, followed by ~ 800 nm thick layer of silicon nitride. Alternatively, mixed silicon oxide/silicon nitride layers [58], Parylene C [59] or plasma-deposited fluorocarbon films [29] have been used for insulation. Via several FIB milling steps, a gold square-shaped electrode (given the pyramidal shape of the AFM tip) is exposed around the base of the non-conductive AFM tip. As the AFM tip is reshaped, the AFM-SECM probes have tip curvature radii comparable to commercial silicon nitride AFM probes. Alternatively, boron-doped diamond

(BDD) having an enhanced potential window and exhibiting chemical and physical inertness has also been implemented as electrode material [31,32]. Although metal coating and insulation can be processed in batches, the FIB step remains a serial process and each AFM-SECM probe must be individually processed. The FIB milling process can be adapted to produce ring electrodes [60] and electrodes of sub-micron [61] and nanoscopic dimensions [38]. AFM-SECM probes with different electrode materials and electrode shape located at the base of the non-conductive AFM tip are shown in **Figure 7**.

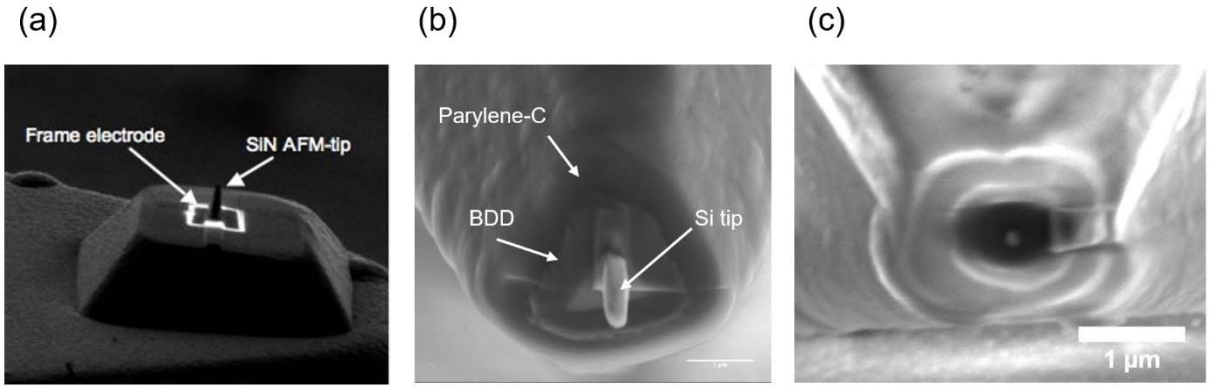

Figure 7. (a) SEM image of an integrated frame sub-microelectrode with an edge length of 800 nm and a tip height of 300 nm. Unpublished data; b) integrated ring BDD electrode, insulated with Parylene C (unpublished data). c) Front view of an AFM-SECM probe showing the insulating AFM tip (length approx. 200 nm) located next to the recessed disc nanoelectrode with radius of 50 nm. Adapted from P. Knittel at al., *Faraday Discuss.* 193, 353–369 (2016). Copyright 2016 Royal Chemical Society.

Also, top milling rather than side milling steps has been evaluated by Kranz and co-workers [40] to minimize the time-consuming FIB steps and to evaluate the potential for automated FIB milling routines using advanced software for patterning complex structures. The distance between the electrode and the surface is defined by the length of the re-shaped AFM tip, which follows the topography of the sample in constant force mode. Thus, with the tip imaging in contact mode, the electrode is maintained at a constant distance from the surface and is protected from potential contamination issues associated with the electrode making intimate contact with the surface. As with SECM, the spatial resolution of this type of electrochemical probe will depend on the electrode size and its distance from the surface. The force constants of these probes are in the range of 0.1 to 1N/m for silicon nitride cantilevers depending on the

insulation material [58,62]. The silicon nitride AFM-SECM probes have been used in dynamic mode AFM to minimize frictional forces associated with contact mode imaging when imaging soft samples. [63] These probes have also been used for PeakForce Tapping™ imaging, providing local electrochemical and nanomechanical information such as Young' modulus or adhesion forces [38,58,64]. Given the small oscillation amplitudes employed during dynamic operation, the current flowing at the electrode is very similar to that obtained with the tip operated in contact mode. These probes have been used e.g., for mapping biosensor activity [63,65] and for imaging soft modified electrodes [58,64].

Using FIB, also "L-shaped" AFM-SECM probes were processed bearing the electrode next to the AFM tip at the plateau of the tip [33]. Silicon cantilevers were coated with a thin Pt layer (25 nm) and subsequently insulated with Parylene C. The electrode was exposed via a triangular FIB milling step, such that the insulation layer was removed to expose the electrode and leave the edge of the coating that serves as AFM tip. In a follow-up study, a bundle of carbon nanotubes consisting of entangled multiple SWNTs was formed by dielectrophoresis and at the same time attached to a metallized AFM tip (i.e., no further bonding steps were required) [66]. In dependence of the electric potential frequency and amplitude, CNT bundles with diameters of 300-400 nm were attached to the AFM tip. The whole cantilever with the modified tip and the chip, after making electrical contact, was the insulated with Parylene C (approx. 400 nm) and either a disc electrode or a L-shaped AFM-SECM probe was exposed forming a Parylene C-AFM tip (diameter: 300–400 nm and a height of 300–400 nm). The functionality of the L-shaped probes was demonstrated by imaging the morphology and SECM feedback response of A CNT network deposited between two gold contacts [33,66].

Conical gold or BDD electrodes as the imaging tip have been fabricated by combined FIB-milling and reactive ion etching (RIE) process steps [30]. The silicon AFM probe is first coated with titanium/gold/titanium or BDD layer and then the entire cantilever was insulated with

silicon nitride prior a sacrificial chromium layer is deposited. The projective chromium layer allows selective RIE etching, which removes the silicon nitride but stops at the gold or BDD layer, respectively. With a single FIB processing step, the Cr cap is removed, exposing a small area of the silicon nitride layer, which is in a subsequent step removed by RIE. Conical Au- and BDD electrodes with tip curvature radii of 150 to 200 nm and heights of the conical electrodes in a range of 250-300 nm were obtained, after removal of the protective chromium layer (wet etching). The electrochemical characterization via cyclic voltammetry revealed defects in the insulation layer as well as some contaminations from titanium oxide (TiO_x) blocking the gold electrode. The fabrication process was later improved in respect to the insulation by adding a second 50 nm zirconium oxide (ZrO_2) or aluminum oxide (Al_2O_3) layer. Alternatively, using electrophoretic paint after electrical wiring facilitated obtaining pinhole-free insulation while also coating the electrical contact [34]. These probes were used to investigate gold nanocontacts between the AFM-SECM probe and a gold bead crystal in sulfuric acid.

Commercially available AFM probes have also been employed by other researchers, however, less sophisticated techniques than FIB have been used to reveal and define the electrode, positioned here in the vicinity of the tip apex. Commercial Pt/Ir, Pt or Au-coated AFM probes were insulated with either Parylene C [28,35] or a photoresist layer [26] and then the conductive apex of the tip was exposed using either mechanical grinding [28,35] or UV light, exposed through a mask [26]. Conductive carbon-coated AFM probes were fabricated from silicon AFM probes modified with Parylene C, which was pyrolyzed at 900° C in inert N_2 atmosphere [67] However, a drawback of using these approaches may be the inability to produce electrodes of reproducible dimensions and electrode materials of sufficient stability.

High-aspect AFM-SECM probes have been fabricated based on single walled carbon nanotubes (SWNTs) attached to AFM tips [68] which served for metal nanowire formation and SECM-AFM probe fabrication [27]. After attaching a SWNT to the AFM tip, subsequent deposition of metal, and insulation of the metallized SWNT with an electrodeposited polymer,

the electrode was exposed using FIB revealing a nano-sized disk-shaped electrode. Although serial fabrication steps are laborious, the size of the metallic electrode can be uniquely controlled by the amount of deposited metal, i.e., disc electrodes down to ~ 10 nm can be reliably produced. Needle-type AFM probes consisting of conductive Ag_2Ga wires at the tip apex and insulated with Parylene C are nowadays available from NaugaNeedles LLC. [69] These commercial probes have been used to fabricate high-aspect ratio AFM-SECM probes [37]. In a first step, the probes were further insulated with electrophoretic paint to improve the Parylene C insulation, which may suffer during handling of the cantilevers. After insulation, the disc electrode was exposed via FIB milling. As Ag_2Ga is a rather exotic electrode material, the exposed electrode surface is modified with a Pt nanoparticle film using an electroless galvanic exchange process. AFM-SECM probes with electrode radii of around 150 nm have been fabricated with the electrode slightly protruding from the needle.

Another fabrication approach for needle-type AFM-SECM probes was achieved by electron-induced deposition (EBID) of C/Pt composite nanowires at the apex silicon AFM probes. [36]. First, a tiny, truncated platform is FIB milled at the tip apex, which is subsequently modified with a Pt/C nanowire (approx. 1 μm length) via EBID. To make contact to the nanowire and to improve the electrical resistivity, which is for Pt/C is in the order of 0.1 Ω cm, the whole cantilever was coated with a 100 – 200 nm thick gold layer deposited via evaporation. The probes were insulated with atomic layer deposition (ALD) of Al_2O_3) whereby only a layer 20 – 50 nm produced pinhole free uniforms films. The electrode was then exposed using FIB milling. As proof-of-principle, metal such as Ag and Ni were electrochemical deposited showing only modification at the exposed electrode. Although, no electrochemical imaging experiments using such probes have been presented to date.

Another FIB-based approach for fabricating conical polypyrrole (Ppy) electrodes was presented by Knittel et al. [39]. First, a small, truncated platform at the apex of gold-coated and insulated silicon nitride AFM probes were formed via FIB to expose a squared nano-sized

electrode, which was subsequently modified with a Pt/C cone using ion-beam induced deposition (IBID). The size of the deposit is defined by the size of ion beam. The conically shaped Pt/C tip was then electrochemically modified with a layer of Ppy. As these probes are intended for force spectroscopy experiments, the obtained tip curvature radius of 50-75 nm was sufficient. The radius could be improved by another FIB processing step in case imaging is intended with these probes.

Significant progress has been made in respect to improving the achievable spatial resolution in SECM and AFM-SECM. An ideal AFM-SECM probe has a high-aspect ratio, and a tip curvature radius of only a few nanometers along with a nanoscopic electrode either at the tip apex or located below the tip apex. However, for force spectroscopy measurements at soft samples micro-meter sized colloidal probes [70,71] are advantageous, as extremely high pressures may be exerted to a soft sample if sharp AFM probes with nanometer-sized tip curvature radii are employed. Typically, micro-sized silica spheres are glued onto tipless AFM cantilevers to increase the contact area between the probe and the sample, thereby decreasing the mechanical pressure on the investigated sample. Knittel et al. introduced colloidal AFM-SECM probes for electrochemical force spectroscopy measurements [72]. A micro-sized disc electrode is milled at the very end of the cantilever into a gold-coated and insulated, tipless silicon nitride cantilever. A gold-coated colloid is then glued to this disc electrode making electrical contact to the conductive sphere. Such colloidal AFM-SECM probes have been modified with polymers such as PEDOT [72] (see **Figure 8**) or polydopamine [73] for adhesion measurements to study the effect of electrical signals on cellular and molecular interactions.

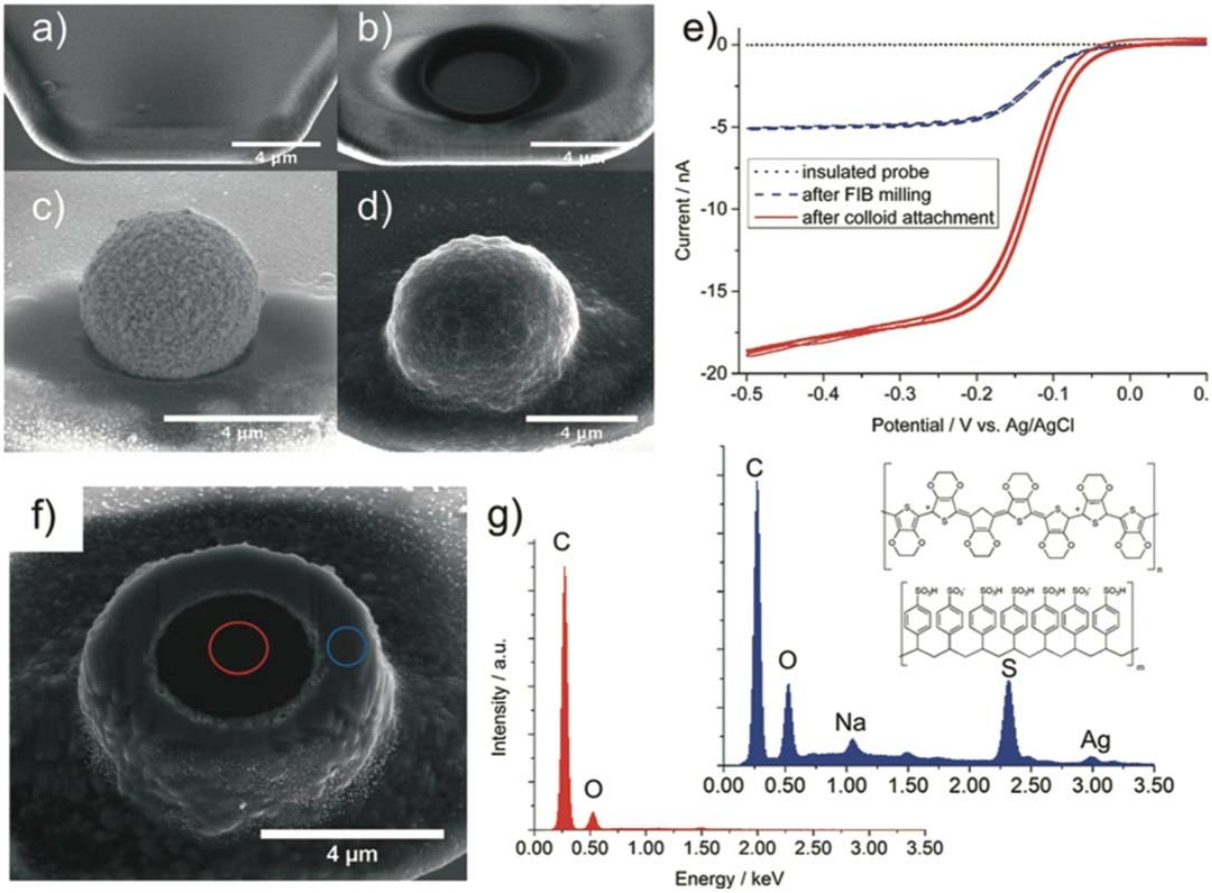

Figure 8. Fabrication of the PEDOT:PSS-coated conductive colloidal AFM-SECM probe. (a–d) SEM images of the main fabrication steps (insulation, milling, colloid attachment and polymer deposition). (e) Electrochemical characterization after each step via CV in 10 mM $[Ru(NH_3)_6]Cl_3$/0.1 M KCl (3 consecutive cycles are shown, scan rate: 100 mV s^{-1}). (f) SEM image showing a cross section of the modified colloidal probe shown in (e); (g) EDX spectra recorded at the marked spots in f (red: core of the polystyrene sphere, blue: PEDOT:PSS, inset structure of PEDOT:PSS). Reproduced with permission from P. Knittel et al., *Nanoscale* 8, 4475–448 (2016). Copyright 2016 Royal Society of Chemistry.

Also, colloidal BDD-AFM-SECM probes have been fabricated using the same approach [73]. The forces constants of these physically robust and electrochemically unique AFM-SECM probes are quite low with values in the range of 0.85 +/- 0.04 N/m compared to other commercially available diamond-coated AFM probes, as silicon nitride cantilevers with a nominal force constant of 0.06 N/m were used to fabricate such probes. The authors showed that the very same probe can be used for electrochemical force spectroscopy, conductive AFM mappings at flat samples and AFM-SECM measurements. Although, the concept is interesting due to an extremely robust AFM-SECM electrode and which chemical properties can be modified by the surface termination of BDD (e.g., hydrogen-terminated, or oxygen-terminated),

they only have quite limited use for high-resolution imaging given the limited achievable lateral resolution.

Independent of the fabrication process, AFM-SECM probes with a design format *i.e.,* where the electrode is also in the same location as the apex of the imaging tip, can also be used in conductive AFM mode (c-AFM) *i.e.,* to directly measure the current that flows through a substrate in air when a voltage is applied between the tip and the substrate. In this way the electrical properties of the substrate, if (semi)-conducting can also be spatially quantified and may be correlated with the electrochemical response [74,75].

1.3. Commercially available AFM-SECM probes

The opportunity to reproducibly microfabricate AFM cantilevers at the wafer-scale has in addition attributed to the popularity of AFM. Although, attempts to microfabricate AFM probes with integrated electrodes have been made in the 1990ties [25], the complexity of microfabricating such probes with integrated defined sub-micro- or nanoelectrodes, ensuring excellent insulation of the entire cantilever and chip is quite costly and requires a high demand by customers to be commercially attractive. Many of the fabrication approaches described above using serial steps such as FIB modification are expensive, and hence may be of limited use for mass production.

Nanonics Imaging Ltd. (Israel) already offered in 2002 glass-insulated, cantilever-shaped Pt probes with electrodes as small as 50 nm [76]. These probes have been used with their tuning-fork-based AFM. NaugaNeedles LLC., founded in 2007 offers needle-type AFM-SECM probes, with conductive Ag_2Ga wires selectively grown at the apex of AFM probes [69]. Needles with lengths from 1 – 100 μm and diameters from 25 to 100 nm are produced via an Ag-coated AFM probe that is immersed and retracted from liquid gallium. After insulation with Parylene C, the insulation layer is removed at the tip apex and modified with Pt resulting in protruding electrodes with dimensions of approx. 20-100 nm in diameter. For a short time,

Keysight Technologies - before closing down its AFM division - has offered AFM-SECM probes with frame electrodes as initially introduced by Kranz and co-workers [2]. Pre-mounted on a carrier to ensure electrical connection to a preamplifier located in the AFM cantilever mount, these probes were convenient to use. Scuba Probes, recently acquired by Nanosurf, a Swiss AFM company, has developed an AFM-SECM probe based on commercial triangular AFM probes coated with a thin Pt layer [77]. The probe is pre-mounted at a flexible handle where the electrical contact is made to the chip. The whole assembly is then insulated prior a conical Pt electrode is exposed by laser cutting or FIB milling. The advantage of this approach is a well-sealed electrical contact suitable for measurements in organic solvent. Bruker (Camarillo, CA) offers AFM probes with conical Pt electrodes at the tip apex, which are marketed and developed for "PeakForce Tapping SECM [78,79]. These batch-fabricated AFM-SECM probes as shown in **Figure 9** have dimensions of around 200 nm in tip height and a tip curvature radius of approx. 25 nm and are pre-mounted in a glass block, which readily fits into the PeakForce Tapping SECM module of the Bruker AFM instruments.

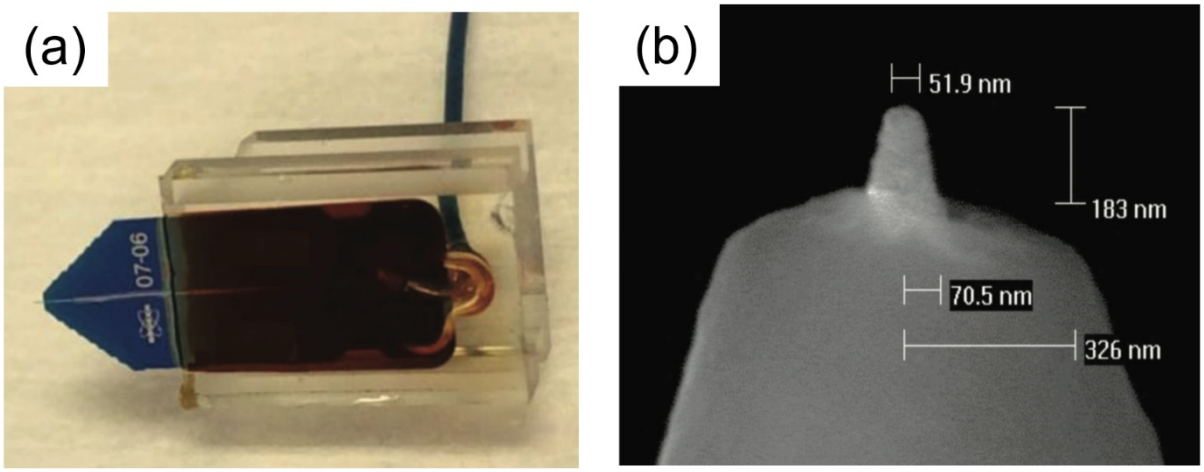

Figure 9. (a) A pre-mounted SECM nanoelectrode probe with the cantilever on the left. (b) An exposed Pt-coated tip apex with ~50 nm end-tip diameter and ~200 nm tip height (other than the tip apex, the probe is fully insulated with SiO_2 and other dielectric sub-layers). Reproduced with permission from Z. Huang et al., *Micros. Today* 24, 18–25 (2016) Copyright 2016 Microscopy Society of America.

Several factors may limit the widespread use of commercial AFM-SECM probes. Regardless of the approach or fabrication process, the commercial AFM-SECM probes are still quite expensive compared to standard AFM probes. For example, contamination of the tip or wear of

the tip during imaging, which may affect the electrochemical response of probes with the electrode located at the tip apex may limit the time such probes can be used. The availability of commercial AFM-SECM probes, which can be used with any AFM instrument is currently also still limited. If the electrical contact of the AFM-SECM probe is not already pre-encapsulated, sealing the contact located at the cantilever chip may be challenging, specifically, when working in non-aqueous solutions.

1.4 Modeling of SECM-AFM probe responses

Several authors have used numerical simulations to quantify the electrochemical response of the integrated electrode and compare this to the values measured experimentally. Modeling the response of an AFM-SECM tip is more complicated than for the traditional disk shaped SECM tip, due to the lack of axial symmetry and the need to move to 3D. Skylar et al. *[80]* used the boundary element method (BEM) to model the electrode response of the sub-micrometer frame electrodes, introduced by Kranz and co-workers [2]. The AFM tip in the center of the frame electrode and it could be confirmed by the theoretically obtained values that the presence of the tip did not alter the current-distance response, compared to the case of no tip present, when approaching infinite surfaces with associated, zero, finite and diffusion limited electron transfer rate constants. The tip was also found to have no effect on the current response when recording the feedback current as the tip scanned over gold islands, more than ten times larger the dimensions of the integrated frame electrode. Experimental currents were found to agree well with those simulated numerically. Wittstock and colleagues also used the BEM numerical simulation method to predict useful AFM-SECM tip and electrode geometries before time, effort and cost was invested in microfabrication [48].

Finite element method (FEM) simulations were used to predict the current response of the triangular-shaped electrodes defined by electron beam lithography at the apex of the AFM tip [45,46] and the diffusion-limited current response of the tip approaching insulating and

conducting surfaces. It was shown that the tip does not significantly perturb the diffusion field of a reactive site on the surface and thus could be used in substrate generation – tip collection (SG-TC) mode. Further experimental and theoretical studies showed that this tip design, compared to V-shaped silicon nitride probes and rectangular silicon AFM probe [81], was the least physically invasive for measuring reactive site diffusion profiles.

Finite element simulations were also used to calculate the diffusion controlled limited current for conical AFM-SECM probes with H ratios (H = tip height/ tip radius) of 1-5 and RG values from 1.1.- 100, which provided an excellent fit [82]. The effect of defects in tip geometry, for example off-centering of the tip, which had little effect in the current response, but also defects in the insulation (e.g., forming a crater around the electrode) were investigated. The latter resulted in a significant deviation of the current response. Numerical simulation of the diffusion behavior towards recessed AFM-SECM probes, obtained via advanced FIB top-milling steps, matched well the electrochemical data [40]. Recently, Mirabal and Barton [83] used FEM simulations to model the influence of the presence of the AFM-SECM tip (with the electrode located at the AFM tip; conical electrode) to identify possible artifacts in experimental data for *operando* studies at catalytically active sites such as nanoparticles. The authors could show by comparison of their simulation data with experimental data that the *in-situ* response for surface sites similar in size to the SECM tip can significantly deviate from operando concentration fields.

1.5 Instrumentation and Imaging Modes

1.5.1 Commercially available SECM add-on modules for AFM

The steadily increasing interest in hybrid AFM-SECM is evidenced by the fact that AFM manufacturer offer (i.e., some went out of business, such as Windsor Scientific, others shut down their AFM division such as Keysight Technologies) SECM as an “add-on” module for AFM instruments. The SECM module is usually composed of an improved electrochemical cell

with a four-electrode configuration made of PEEK or any other solvent resistant material, a specially designed AFM cantilever holder to mount the AFM-SECM probe allowing to establish electrical contact, appropriate shielding for sufficient signal-to-noise of the current signals, which are typically in the nA-fA range, and a bi-potentiostat. To date, most SECM modules that are commercially offered rely on external commercial bi-potentiostats also used for conventional SECM measurements, yet also custom bi-potentiostats with high sensitivity and bandwidth of approx. 10-20 kHz have been reported [16].

A challenge compared to other hybrid techniques is the fact that the electrical contact of the AFM-SECM probe requires thorough insulation, as the contact is usually immersed in the electrolyte solution. Performing experiments at extreme pH values or organic solvents over longer periods of times (e.g., in energy related research) remain challenging in maintaining a perfect sealing. Some companies offer pre-mounted AFM-SECM probes like the Bruker probes (e.g., **Figure 9**). In recent years, resins appeared on the market that can be applied by spray coating or brush sealing and withstand exceedingly harsh conditions and are suitable for sealing. Once their suitability for insulating/sealing AFM-SECM is proven along with reproducible deposition procedures, a new generation of probes will certainly appear as commercial products.

1.5.2 AFM modes

In the early years of AFM-SECM, integrating an electrode into the AFM tip was an effective way to use the cantilever deflection in constant force mode for maintaining a constant distance between the AFM-SECM tip electrode and the sample surface. In the case where the electrode is located at a certain distance below the AFM tip apex, the distance of the electrode to the sample is maintained by the length of the re-shaped AFM tip (e.g., as shown in **Figure 6-7**) such that topography and electrochemical response can be recorded in a single scan. If the electrode is located at the tip apex (as shown e.g., in **Figure 1 -5**) and conductive samples (e.g.,

an electrode), are imaged, the sample is scanned twice in “lift mode”, to avoid short circuiting. In a first scan the topography is recorded and stored and then the tip is lifted by a certain distance (i.e., several tens of nanometers) to record the electrochemical information in constant distance following topography via the stored AFM information.

Dynamic AFM-SECM imaging was initially shown by Kueng et al. [63] to map the enzyme activity of glucose oxidase, which was entrapped in spots of a soft polymeric matrix. Due to the extremely soft nature of the polymeric spots, imaging of the topography could only be performed in dynamic mode eliminating friction forces associated with contact mode imaging. Given the very small oscillation amplitudes employed during oscillation of the AFM-SECM probe, the current flowing at the electrode is very similar to that obtained with the tip operated in contact mode. “*Molecule touching”* (Mt)/AFM-SECM or “*tip-attached redox molecule*” tarm/AFM-SECM, experiments developed by Demaille and colleagues [16,84,93–95,85–92], are all performed in AFM dynamic mode (AFM Tapping^{TM} mode) as discussed later in this chapter. Significant improvements have been made in respect to AFM electronics and hardware, e.g., the data acquisition speed has been significantly improved. With these improvements, quantitative nanomechanical mappings (e.g., adhesion, elasticity, and energy dissipation maps) can now be recorded simultaneously with topography. For example, Bruker introduced PeakForce Tapping^{TM} (PFT) [96], in which the cantilever is oscillated off resonance at lower frequency than the resonance frequency. In Peakforce Tapping, the maximum interaction force (peak force) is sensitively controlled at each pixel and more importantly, a force-distance curve is recorded at each pixel which can be evaluated applying appropriate model (e.g., DMT model [97]). In PeakForce Tapping SECM, additionally to the nanomechanical information, electrochemical processes at the sample can be studied. A first example of PeakForce Tapping using AFM-SECM probes was demonstrated by Knittel et al. [58], using non-commercial AFM-SECM probes with an frame electrode. In this study, also the influence of the oscillation amplitude for obtaining maximum current contrast between

conductive and insulating substrate was investigated for a fixed AFM-SECM electrode size. The oscillation amplitudes in PeakForce Tapping are usually in the range of <100 nm but also higher amplitudes might be used, so that the effect of the amplitude on the current contrast has to be taken into account in particular for nanoelectrodes, in case when the electrode is not located at the tip apex [38] or the sample is not imaged in lift mode with the tip retracted and the oscillation disabled. PeakForce Tapping SECM has been reported for example in material science and energy related research [38,58,64,98–100], as described in detail in **section 1.6**.

AFM-SECM measurements in non-contact AFM (FM-AFM) using quartz tuning fork [101] require that the force sensor exhibits high stiffness ($k = 10^3$ to 10^4 N/m) to maintain small oscillation amplitudes (< 1nm) and to avoid 'jump-to-contact', as the cantilever is oscillated a few nanometers above the sample surface. So far, only a few reports have been published, using non-contact AFM with the SECM probe attached to a tuning fork [24,102–105] e.g., for mapping catalytic active materials [103–105].

1.5.3 SECM modes used in AFM-SECM

In respect to SECM modes, almost all established modes including G/C mode, feedback mode and also direct mode, (the AFM-SECM probe serves as the counter electrode) and recently also redox competition mode have been used in AFM-SECM studies. Alternating current (AC)-AFM-SECM mode has been demonstrated at model samples, mapping the magnitude of the tip current and the phase angle in a redox mediator free solution at low electrolyte concentration (1mM KCl) [106,107]. AFM-SECM probes with micro-sized Pt electrodes located below the non-conductive AFM tip were used in AC-AFM-SECM to achieve sufficient signal contrast.

Demaille and co-workers introduced an AFM-SECM imaging mode, which is based on tethering the redox mediator either to the sample surface, this mode was termed '*molecule touching'* (Mt)/AFM-SECM [84,86], or to the AFM-SECM probe, a mode termed '*tip-attached*

redox molecule' tarm/AFM-SECM [16]; the principles of these SECM modes with confined redox mediator molecules are schematically shown in **Figure 10.**

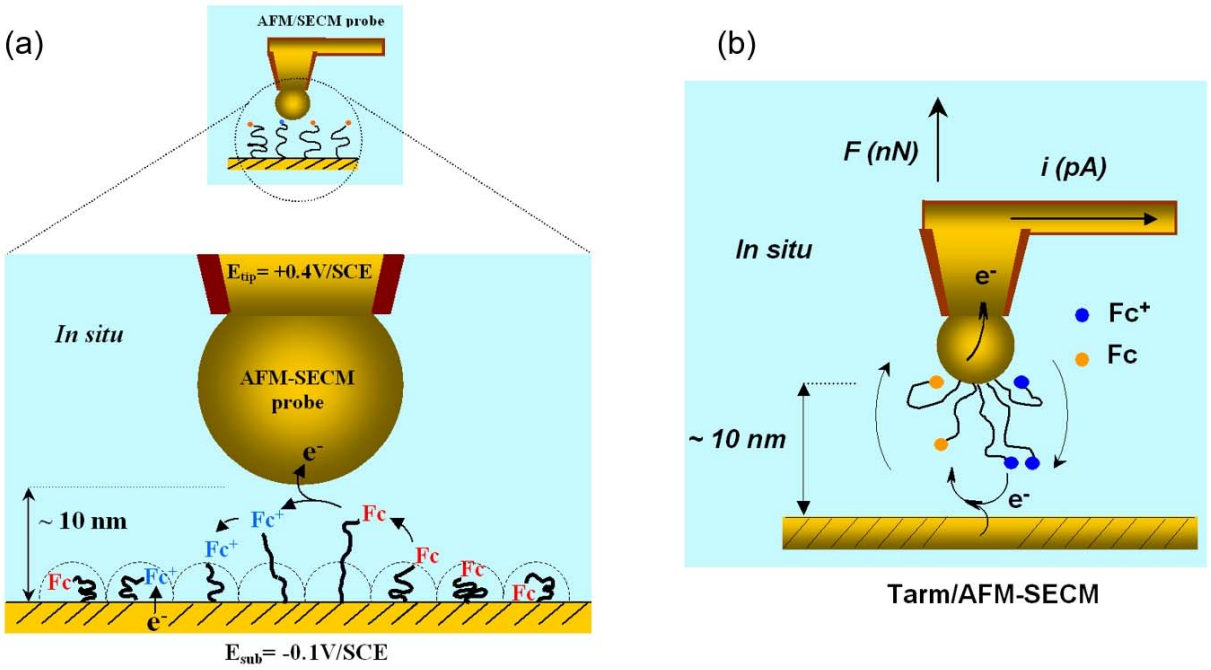

Figure 10. a) Direct electrochemical contact between an incoming AFM-SECM probe and the redox Fc heads of nanometer-sized, flexible chains (such as PEG or DNA), end-grafted onto an electrode substrate. The Fc heads are alternatively oxidized at the tip and reduced back at the substrate. Adapted from J. Abbou et al. J. Am. Chem. Soc. 126, 10095-10108 (2004). Copyright 2004 American Chemical Society b) Working principle of Tarm/AFM-SECM microscopy. The redox mediator, ferrocene (Fc), is attached to the AFM-SECM probe via a nanometer-sized, linear and flexible polymer chain (PEG). For clarity, the tip is not drawn to scale. The chains are pictured in the mushroom conformation. Adapted with permission from A. Anne et al., *ACS Nano* 3, 2927–2940 (2009). Copyright 2009 American Chemical Society.

Although, these imaging modes require a labeling step to attach the redox mediator (e.g., ferrocene) at the gold electrode via a flexible chain (e.g., PEG chain), high resolution imaging correlating the topographical and electrochemical information was obtained, as the resolution achievable in both - topography and electrochemistry - are almost on the same order of magnitude. Serial recording of the information like in lift mode is omitted. In (Mt)/AFM-SECM, the tip current is generated by the confined redox cycling of the Fc molecules at the PEG chains, which are alternatively oxidized at the tip and re-reduced at the substrate or vice versa. Taking advantage of the high-sensitive force detection, the AFM-SECM probe can be

positioned with sub-nanometer precision that allows controlled interactions between the polymer chains and the probe within the end-grafted layers. Initially flexible linear polyethylene glycol (PEG_{3400}) chains were grafted onto a gold substrate with ferrocene as the end group and with an elongated chain length of about 30 nm defining the hemispherical diffusion volume [84]. Thereby, one of the limitations in feedback mode SECM that sufficient turnover rates of the redox-active molecules are required for contrast in the electrochemical response [108] is circumvented, as the diffusional dispersion is confined. In addition, although the tip apex of AFM-SECM probe is the gold electrode, topography and current image can be recorded in a single scan, also at conductive samples using dynamic mode and the tethered redox molecules approach. Demaille and colleagues have successfully used the (Mt)/AFM-SECM in dynamic mode AFM for mainly high-resolution electrochemical mapping of biological relevant samples as discussed in detail **section 1.6.6.**

1.6 Application Areas of AFM-SECM

1.6.1 Imaging Reactive Sites on a Surface

While nowadays more problem-focused applications of AFM-SECM are emerging, to date many AFM-SECM studies are still targeting on probe fabrication. Usually, the functionality of the AFM-SECM probes is demonstrated by imaging model samples containing conductive and non-conductive areas. Model samples typically comprise conducting microbands or micrometer sized electrodes. Imaging is either carried out in feedback mode or SG-TC mode in combination with contact, dynamic or non-contact mode AFM. An example for such a model sample that goes beyond simple topographical mapping and electrochemical imaging is shown in **Figure 11.**

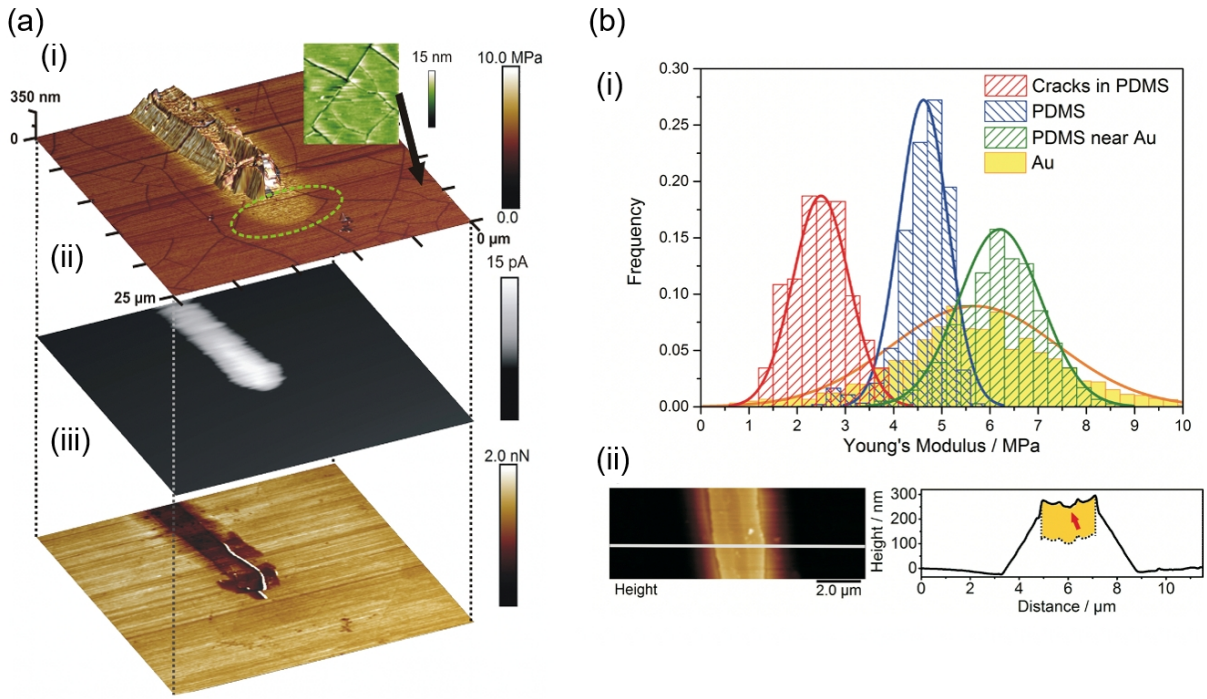

Figure 11. a) QNM-AFM-SECM measurement of a gold electrode patterned onto PDMS recorded in 2.5 mM $Fc(MeOH)_2$ / 0.1 M KCl. Peak force: 2 nN, amplitude: 80 nm. (i) 3D topography of the structure overlaid with the Young's modulus (calculated with a DMT fit, green mark shows increased stiffness of the PDMS surrounding the gold pattern, inset shows topography of the cracked PDMS); (ii) faradaic current image obtained with the AFM-SECM probe biased at 0.5 V vs. Ag/AgCl, and (iii) tip-sample adhesion image. b) (i) Histograms showing the different Young's modulus recorded on the patterned PDMS substrate. Cracks on the surface with 2.5 ± 0.6 MPa (N=200) (red), the PDMS substrate with 4.6 ± 0.5 MPa (N=12500) (blue), the PDMS near the gold structure with 6.2 ± 0.9 MPa (N=4400) (green), and the gold structure with 5.6 ± 1.7 MPa (N=2300) (yellow). The sputtered metal height is indicated in the profile in yellow, the red arrow indicates a gap in the center part of the structure Reproduced with permission from P. Knittel et al., *Anal. Chem.* 88, 6174–6178 (2016). Copyright 2016 American Chemical Society.

PeakForce Tapping SECM measurements were recorded at a soft poly(dimethylsiloxane) (PDMS) substrate that was modified with an evaporated gold microstructure [58]. While recording a single image, topographical, nanomechanical properties such as Young's modulus and adhesion as well as the feedback mode current was obtained. To improve the adhesion of the gold and photoresist for microfabrication steps, PDMS was treated with an oxygen plasma prior to the gold evaporation. This plasma treatment step leads to a hydrophilic surface layer at the PDMS and cracks, which are clearly evident in the topographical image (green inset in **Figure 11a**) (i)) and reflected in the Young's modulus map. Significantly increased Young's modulus (6.2 ± 0.9 MPa) values were measured around the gold. However, the Young's

modulus of the PDMS within the cracks, which were 2−5 nm deep and 150−250 nm wide, revealed values of 2.5 ± 0.6 MPa that agree well with the expected values for 10:1 PDMS reported in the literature. The adhesion maps showed higher adhesion at the PDMS compared to the gold strip which may be related to difference in the van der Waals interaction and the fact that the AFM tip may penetrate more into the softer substrate. The shown SECM data are not particular exciting as a sample with mixed conducting and insulating areas was imaged in feedback mode. However, multiple sets of information were obtained while imaging the sample, which is highly relevant for *in situ* studies of interfaces where morphology changes are associated with changes of the physical and chemical properties.

There have been many applications described where AFM-SECM has been used to investigate structure-activity relationships important in the material sciences. Macpherson et al. described the investigation the electrochemical and electrical properties of an industrially important dimensionally stable electrode; Ti/TiO_2/Pt [74,109] The electrode was prepared by the galvanostatic oxidation of titanium to form a porous, micrometer-thick layer, followed by the galvanostatic deposition of Pt. The surface was interrogated with the same probe first in air using conductive AFM, which revealed that not all of spherically shaped Pt deposits were ohmically contacted to the underlying titanium. The corresponding SECM-AFM maps of surface structures and electroactivity (in SG-TC mode) also confirmed this.

Wittstock and co-workers investigated the topography and electrochemical activity of the biphasic alloy Ti-6Al-4V in feedback mode SECM with microfabricated AFM-SECM probes [47,48] as shown in **Figure 6**. Although the topographical maps are recorded with the edge of the insulation, a comparable topographical resolution to imaging with conventional AFM probes was obtained. In the simultaneously recorded SECM image, current variations in the range of 0.1 pA were recorded at phase change boundaries in the alloy, which were also associated with changes in surface height. Given the low heterogeneous electron transfer rate constants associated with the two phases in the alloy, the current variations were associated

with changes in the separation between the tip and the substrate only. Due to the geometry of the AFM-SECM probe, it was not possible to image the sub-structure of the phases. This study highlighted a drawback of using very small electrodes for the measurement of slow electron transfer kinetics, a problem Wittstock and colleagues addressed in depth for feedback mode SECM [108].

Besides the microstructures containing conductive and insulating areas, highly orientated pyrolytic graphite (HOPG) and carbon-based materials have been studied by AFM-SECM. For example, Frederix et al. showed high-resolution topography and current images of HOPG using microfabricated AFM-SECM probes with conical Pt tips [53]. The obtained current image corresponded well with the topography revealing higher currents at the step edges, which the authors explained with an enhanced electron transfer rate compared to the basal plane. In fact, the heterogeneous electron transfer constant for $Ru(NH_3)_6^{3+}$ at step edges was approx. 100 times faster than at basal planes, which is in contradiction to recent studies that indicated that there might be no significant difference in respect to electron transfer between basal plane and steps in HOPG. Interestingly, although with this design the apex of the tip is exposed metal, no short circuit current was observed upon scanning the conducting HOPG surface in contact mode. The authors attributed this to tip contamination. Wain et al. [51] demonstrated the imaging capabilities of their batch fabricated AFM-SECM probes mapping graphene and isolated graphite flakes, whereby the electrochemical image was recorded in lift mode. Both, topographical and current images show high resolution maps of the features (e.g., step edges), clearly revealing heterogeneities in the electroactivity which - in contrast to the studies presented by Frederix et al. - did not correlate to topographical features (**Figure 12**).

(a)

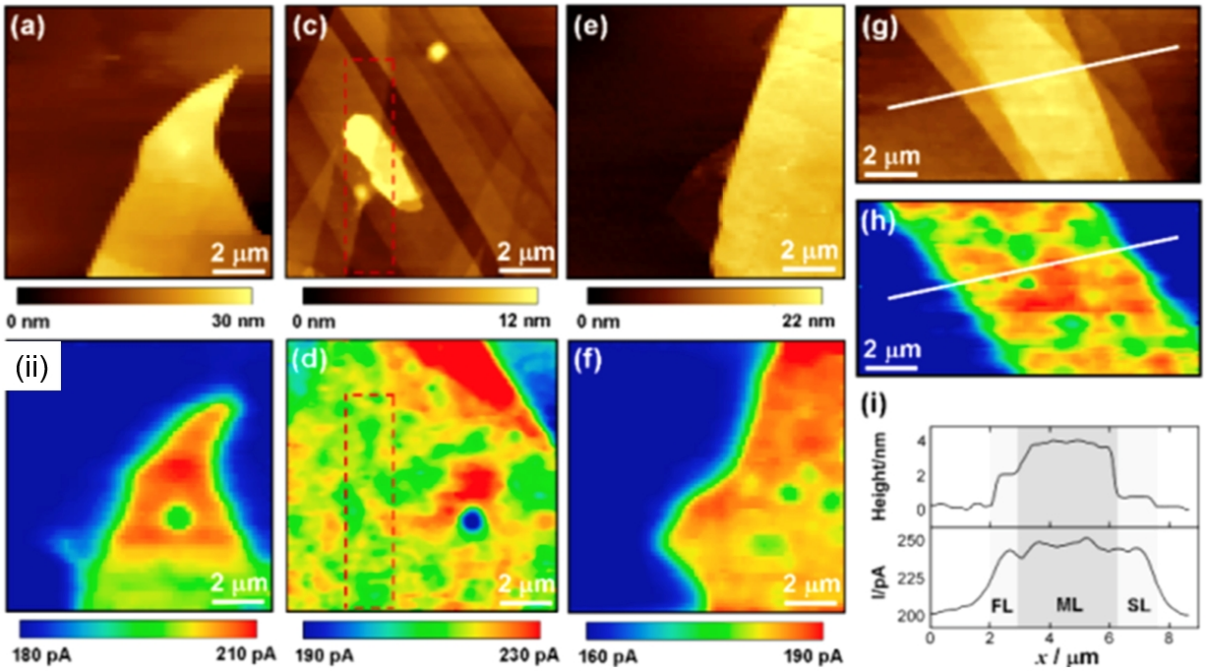

Figure 12. Feedback mode SECM-AFM images of exfoliated graphene/graphite flakes immersed in 1 mM FcMeOH/0.1 M KNO_3 solution: Topography is shown in (a), (c), (e), and (g) and the corresponding electrochemical scans are depicted in (b), (d), (f), and (h), respectively. Line scan profiles for parts (g) and (h) are shown in (i) (shaded areas highlight regions of different graphene thickness: single-layer (SL), multilayer (ML), and few-layer (FL)). Tip bias 0.3 V vs Ag, line scan frequency 0.5 Hz, lift height 150 nm, bulk tip current typically ~200 pA. Reproduced with permission from A. J. Wain et al., *Anal. Chem*. 86, 5143–5149 (2014). Copyright 2014 American Chemical Society.

Consistency in electrochemical data across length and time scales remains still challenging in nanoscale electrochemistry and will benefit from statistical analysis of repeated experiments.

There is a significant body of literature on the doping of carbon material with nitrogen, sulfur, etc. to obtain noble-metal-free catalyst for oxygen reduction reaction [110]. Schechter and co-workers studied iron-nitrogen doping of HOPG towards the ORR in 0.1 M perchloric acid using a commercially available SECM module from Nanonics Imaging Ltd. [105]. Measurements were performed in non-contact mode at a tip-sample distance of approx. 4 nm with glass-sealed AFM-SECM probes of the protruding Pt (diameter of 50 nm). The AFM-SECM tip was either used as counter electrode and the ORR substrate current was recorded, or in a subsequent scan, the AFM-SECM probe was biased at 0.75 V vs. Ag/AgCl to detect hydrogen peroxide (H_2O_2) as intermediate product of the two-electron oxygen reduction

pathway in generator-collector mode. **Figure 13** shows such maps with topography and ORR current measured in a single map, whereas the H_2O_2 map was obtained in a subsequent experiment recorded at the same location.

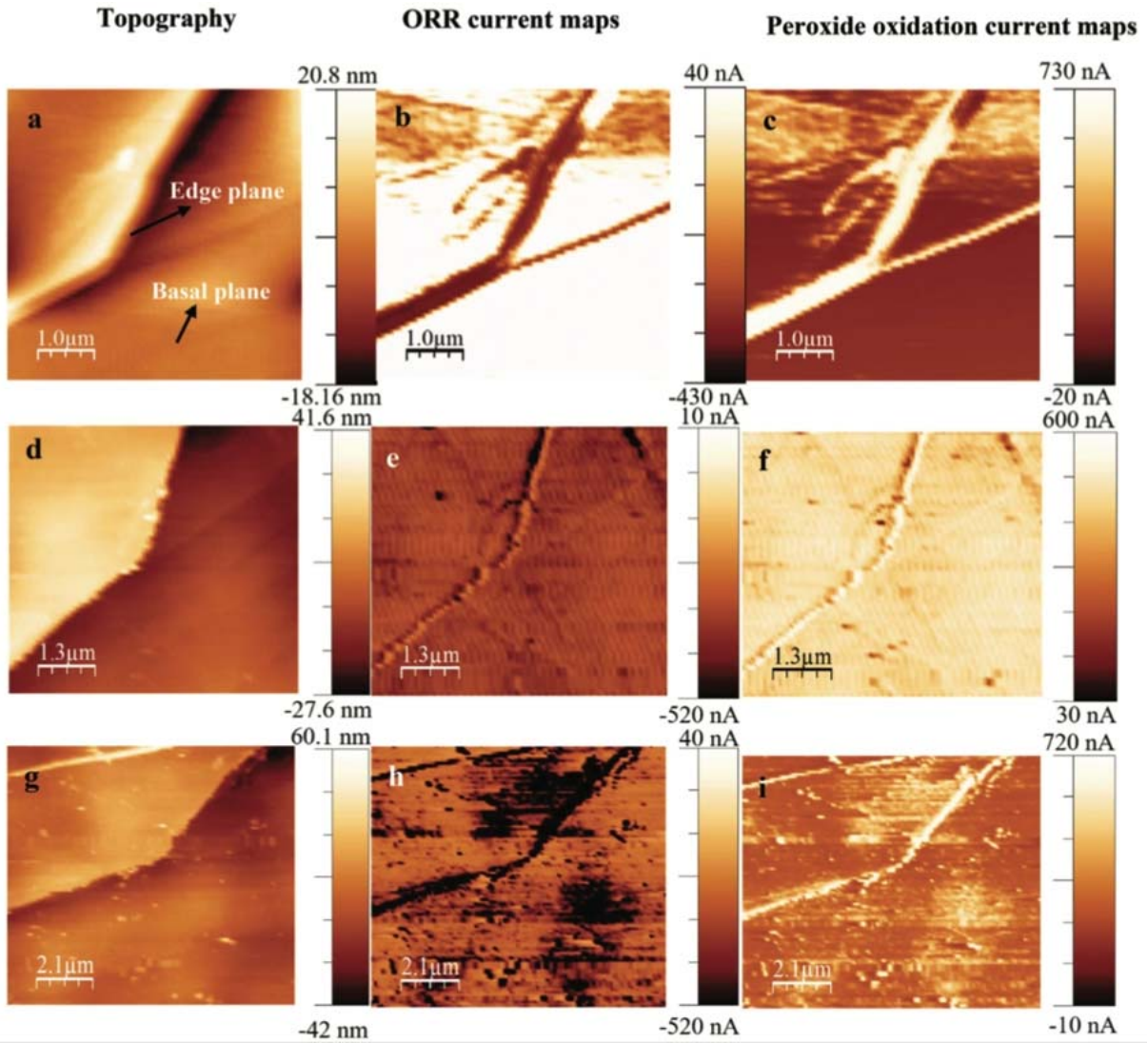

Figure 13. AFM topography scan, oxygen reduction and peroxide oxidation current mapping images (in this order) of HOPG (a, b, and c), N-HOPG (d, e, and f), and Fe–N-HOPG (g, h, and i). The applied substrate potentials for the oxygen reduction current mapping are 0.68 V (HOPG and N-HOPG) and 0.7 V (Fe–N-HOPG). The applied tip potential for the hydrogen peroxide oxidation current mapping is 1.2 V. The SECM-AFM tip scan rate used for the current-mapping experiments is 15 ms per point; (1 ms per point = 4 nm ms^{-1}). Reproduced with permission from S. Kolagatla et al., *Nanoscale* 10, 6962–6970 (2018). Copyright 2018 Royal Society of Chemistry.

Comparing the maps of the Fe-N doped HOPG with HOPG and HOPG solely doped with nitrogen, it was concluded that the catalytical activity towards ORR in acidic conditions is associated with the iron-coordinated nitrogen sites, which are predominantly located at

structural defects of HOPG. The authors report a spatial resolution for the current maps of 50 nm. Interestingly, the H_2O_2 current mapped with the nanoscopic probe showed extremely high currents for bare and doped samples of up to 730 nA.

1.6.2 Corrosion studies

AFM-SECM is highly suitable for studying corrosion, as the electrochemical processes in corrosion are in most cases associated with morphological changes. Davoodi and colleagues have used AFM-SECM to investigate localized corrosion processes [19–23,111]. Initial studies focused on the aluminum alloy AA1050. Dissolution was initiated by anodically polarizing the sample in a solution containing chloride ions (NaCl, 10 mM) and the redox mediator, I_3^- [21]. I_3^- was reduced to I^- at sites where the aluminum alloy started corroding and the AFM-SECM tip was biased at a potential to detect I^-. This way, it was possible to correlate the evolving morphology of the corroding surface with redox activity.

Further studies of the group were focused on the corrosion behavior of aluminum alloys using *in-situ* AFM, Kelvin probe microscopy and AFM-SECM to examine and interpret the localized corrosion behavior [20]. It was found that the Al-Mn-Sr-Zr alloy contained a smaller number of intermetallics with larger Volta differences, compared to the EN AW-3003 alloy. This correlated well with the SECM-AFM images which showed that the EN AW-3003 allow was significantly more corrosion active, resulting in higher material loss during dissolution.

More detailed work on the EN AW-3003 alloy was carried out with the sample held under both cathodic and anodic control [22,23].

Souto, Kranz and co-workers used AFM-SECM to induce pitting corrosion [112,113], for dissolution studies of copper crystals deposited on gold [114], and for recording electrochemical and morphological changes during the dissolution of pure copper [115]. Single corrosion pits in a nitrite/chloride containing solution were induced on a passivated iron sample by generating nitric acid at the AFM-SECM tip that locally removes the passivating layer, inducing fast corrosion of the substrate in the presence of chloride anions [112]. With the

electrode located below the apex of the re-shaped silicon nitride tip, which tip radius is comparable to commercial AFM probes, the morphology of the formed pits was investigated in-situ with the same AFM-SECM probe. In a follow up study, the pit size and depth were studied in dependence of the AFM-SECM electrode size, the duration of the nitric acid generation and the mode (static or scanning the probe) [113]. The smallest pits that could be produced were in the range of 1.2 – 2.7 μm, which is related to the size of the AFM-SECM electrode the distance to the surface (defined by the re-shaped AFM-tip). Although only micro-sized pits could be obtained with this AFM-SECM probe design, the pits could be directly imaged. The same research groups presented the semi-quantitative mapping of copper (II) ion release during surface corrosion of copper along with recording morphological changes induced by the dissolution/corrosion process. In a first approach, as model system, a gold sample modified with copper crystal modified was anodically swept from -0.3 V to +0.5 V vs. Ag/AgCl with a sweep rate of 1 mV/s in 0.5 M NaCl solution, while the changes in morphology were recorded. The AFM-SECM probe was biased -0.3 V vs Ag/AgCl to re-reduce the released copper (II) ions at the AFM-SECM probe. Significant release of copper (II) ions was observed at potential higher than -0.15 V; however, features in the electrochemical image could not be resolved at higher potentials due to the saturation of the preamplifier. To determine the amount of the released copper (II) ions, the AFM-SECM probe had to be retracted from the sample surface to the bulk of the solution and the copper deposited at the frame electrode was re-oxidized during linear sweep voltammetry, evaluating the peak current. Calibration of the AFM-SECM probe in copper (II) ion solution prior to the measurements, allowed for a semi-quantification of the released copper (II) ions. Under similar experimental conditions, the release of copper (II) ions and the morphological changes at pure copper samples was studied. Although, at higher overpotentials, morphological changes were clearly evolving, the information achievable from the SECM data are limited by the sensitivity of the preamplifier. An in-depth study of pure copper corrosion in acidic conditions revealed that corrosion products

(crystals) appeared at a substrate potential of -0.16 V vs Ag/AgCl, which locally blocked the release of copper (II) resulting in zero current values recorded over those spots in the corresponding SECM images [115]. It was hypothesized that these precipitates are poorly adhering copper salts. The correlation of the electrochemical data with the topographical maps and their interpretation are challenging, given experimental factors such as limitations recording the electrochemical signal, contributions from convection due to scanning and possible saturation of the copper deposition onto the frame electrode.

1.6.3 Nanoparticle modified substrates

SECM and hybrid SECM studies have emerged not only for imaging nanoparticles down to the single nanoparticle level, but also to provide information in respect to the electrocatalytic activity. Kranz and co-workers used their AFM-SECM probe design to visualize the nanomechanical and electrochemical properties of gold nanoparticles, either electrochemically deposited onto conductive soft PDMS electrodes [64] or of gold nanostars transferred onto a PDMS substrate [38]. Pulsed electrochemical deposition was applied to control the seeding and growth process of stabilizer-free, spherical gold nanoparticles. Thereby, particles with an average size of 76 +/- 5 nm were deposited onto the conductive carbon-PDMS electrodes, which were obtained by mixing 25 wt % carbon black with a ratio of 10 :1 (base polymer : curing agent) PDMS. A non-uniform distribution of carbon within the PDMS forming agglomerates is clearly evident in the Young's modulus map, and in the feedback mode SECM image. The Au nanoparticles are preferentially deposited at such carbon agglomerates, which make their identification in the SECM image challenging as individual nanoparticles cannot be resolved given the size of the AFM tip-integrated frame electrode (frame length around 800 nm) and the distance of the AFM-SECM electrode to the sample surface, leading to overlapping diffusional profiles in feedback mode SECM. The authors additionally used conductive-AFM, SEM analysis, and approach curves recorded at different areas of the substrate with statistical

analysis, which in summary lead to a thorough characterization of the gold NP-modified soft electrode but at the same time showed the limitations using sub-micron sized electrode for characterizing nanomaterials. Knittel et al. [38] also used PeakForce SECM to characterize gold nanostars (i.e., high aspect ratio aspects nano objects with cores of around 10 nm and spikes up to 30 nm in length) deposited onto soft PDMS substrates. For these studies, AFM-SECM probes with nanodisc electrodes similar to the design of Wittstock and colleagues [47] were used. The nanostar sample is quite challenging in respect to AFM characterization giving the shape of the gold nanostars, but also for SECM, leading to artifacts – an issue that is well-known and described in the AFM community, but less frequently addressed in the SECM literature [116].

In the AFM but also SECM literature, frequently a clear statement of post-data treatment procedures is absent. In respect to the Au nanostar characterization, the physical properties such as adhesion and Young's modulus were correlated to the electrochemical data, including studies at the single gold nanostar level. This contribution clearly points at associated challenges. For the topographical image, a high-aspect ratio AFM tip would be beneficial, for mapping nanomechanical properties of soft materials colloidal probes as described in **section 1.5.2** would reduce artifacts related to the penetration depth into the soft material. In respect to electrochemical imaging, nanoelectrodes with a reliable and accurate position at a defined nanometer-range from the sample surface are required. As shown in the images and discussed in the contribution, the obtained multiple parameter maps show artifacts resulting from a compromise when optimizing the topographical resolution and minimizing the artifacts in the nanomechanical and electrochemical information.

Jiang et al. [98] used commercial AFM-SECM probes from Bruker Inc. and the PeakForce SECM module along with conductive AFM to study interfacial properties of p-Si and p^+-Si photoelectrodes, modified by well dispersed Pt NPs (diameter range from 20-150 nm). For photocatalytic activity, the catalyst nanoparticles require mechanically stability and good

contact to the underlying semiconductor electrode. The authors used conductive AFM, current-voltage (I-V) measurements at single particles, and AFM-SECM measurements to investigate the electrochemical performance of the Pt NP-modified p-Si and p^+-Si electrodes. The obtained contact currents showed significant differences in the contact currents up to a factor of 1000, although in air the particles were well attached to the electrode. The dispersed Pt nanoparticles showed significant weaker adhesion in electrolyte solution and could only be imaged using very low force settings (700 pN), which could be maintained using PeakForce Tapping. The authors compared the feedback current of the SECM data recorded with ($Ru(NH_3)_6^{3+}$) as redox mediator in lift mode and current values obtained in contact with the sample at areas without Pt NPs and at Pt-NPs. Based on these measurements, they concluded that a substantial fraction of the mapped nanoparticles had poor electrical contact to the underlying substrate. Only one sample area was investigated.

Schechter and co-workers used commercial AFM-SECM probes from Nanonics Imaging Ltd. (Pt nanoelectrode sealed in glass), e.g., to deposit Pt nanoparticles on HOPG from aqueous hexachloroplatinate solution using the AFM-SECM probe as counter electrode in direct mode SECM and non-contact mode AFM with a maintained tip-sample distance of 4-8 nm [102]. The depositions were evaluated in respect to the hexachloroplatinate concentration, the deposition mode (static or scanning), the scan rate of the tip and the deposition time by recording topographical images. In dependence of the deposition conditions, the authors report that the deposited Pt particles are dragged by the tip to the edge of the scanned area. Overall, a quite broad distribution in respect to diameter and height was obtained. In a follow up study, they investigated ORR and H_2O_2 evolution as a side product of ORR at catalytically active surfaces like HOPG and dispersed Pt nanoparticles on glassy carbon [104]. The Pt particles were deposited as previously described by the authors [102]. In this study, the authors aimed at simultaneously mapping topography, ORR currents and H_2O_2 currents. For that purpose, a thin gold coating was deposited onto the glass sheath of the AFM-SECM probe, which was then

used as second electrode with macroscopic dimensions, although the immersed area for the working electrode 2 was not specified. With the second working electrode mapping H_2O_2 with high current collection efficiency to in close proximity to the active sites was targeted. The ORR current maps indicated that only around 50% of the Pt particle surface contributed to the ORR. Observing high H_2O_2 oxidation currents at the Pt particles, the authors concluded that the ORR follows the two-electron pathway rather than the four-electron reduction of oxygen directly to water. Due to the nanoscale distance, reported with 4-8 nm, of the AFM-SECM probe to the sample surface, high lateral resolution was achieved in the electrochemical maps in contrast to the topography image of the Pt particles, which shows lower resolution and artifacts that may be associated with a large curvature radius of the protruding Pt electrode.

Huang et al. [91] used dynamic mode AFM and Mt/AFM-SECM to study PEGylated gold nanoparticles. Arrays of citrate-stabilized gold nanoparticles (AuNPs) were casted onto a gold substrate that was modified with an amino-undecane thiol self-assembled monolayer to suppress direct electron transfer from the macroscopic gold surface towards the solution. As the AuNPs still could exchange electrons with the underlying modified gold substrate, they acted as individual nanoelectrodes. The high-resolution topographical and electrochemical images revealed individual nanoparticles with a height of approx. 10-20 nm and a width of around 80 nm, which is related to tip-convolution artifact as the tip curvature radius of the AFM-SECM tip was around 100 nm. In the presented studies, the authors determined that 70%-80% of the particles investigated gave an electrochemical response. Combining the results from the macroscopic CV experiments with the electrochemical response of individual nanoparticles, the authors determined the number of Fc-PEG chains per nanoparticle, which resulted in a broad distribution of 200–900 chains per particle and 20% of the particles lacking Fc-PEG chains, which might be explained by contamination of the surface and hence attenuate the modification with the PEG chain. AFM-SECM probes with smaller tip curvature radii in the order of the size of the nanoparticles allowed the visualization of the PEG corona and the core size of the

nanoparticles at the single particle level, through the evaluation of the simultaneously obtained topographical and electrochemical data. Although not all observations in this study could be fully clarified, the presented data in combination with statistical analysis clearly show the excellent potential of Mt/AFM-SECM for providing fundamental insight in nanoparticle modification at the single particle level.

In a similar study, Demaille and co-workers presented Mt/AFM-SECM measurements of a dense nanodot array, as shown in **Figure 14** [88].

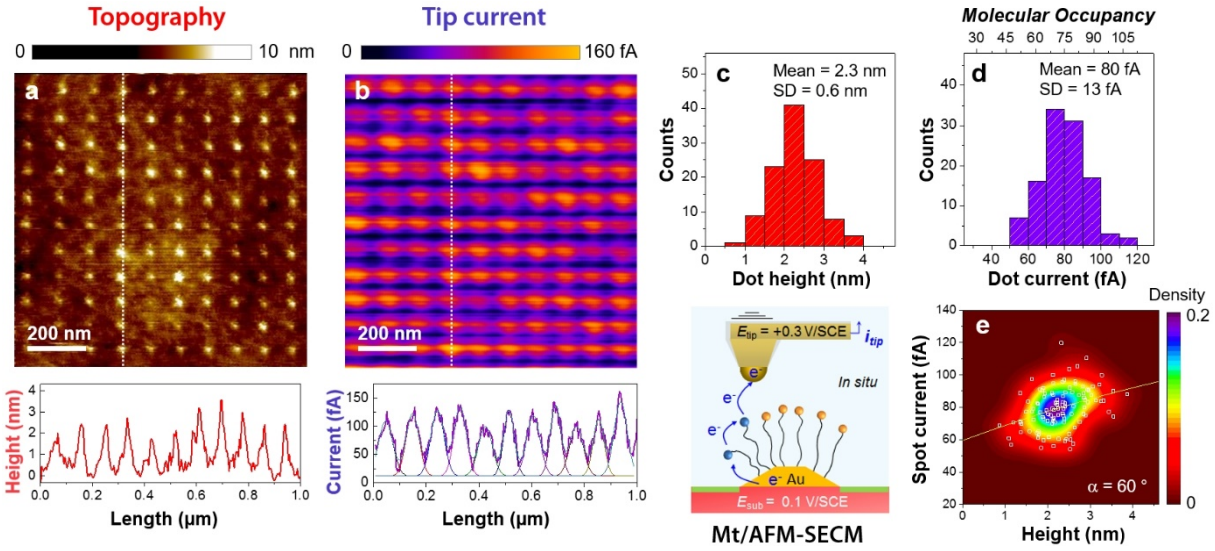

Figure 14. Mt/AFM-SECM in situ imaging of a Fc-PEGylated nanodot array. Simultaneously acquired topography (a) and tip current (b) images. Cross sections of the images taken along the column of nanodots indicated by a vertical white dotted line are also shown. (c, d) Histograms of the nanodot height and spot current values. (e) Cross correlation plot showing the spot current of the nanodots as a function of their respective height. The yellow line is calculated using eq S3 with the best fit value α = 60°. Reproduced with permission from K. Chennit et al., *Anal. Chem.* 89, 11061–11069 (2017). Copyright 2017 American Chemical Society.

A dense nanodot array consisting of single gold nanodots with a diameter of approx. 15 nm, a height of 2-3 nm and a pitch size of 100 nm was produced by electron beam-lithography, wet-etching and thermal treatment on a highly n-doped Si substrate. The nanodot array was the modified in a subsequent step with Fc-PEG chains. The topographical and electrochemical images match well, with all nanodots showing an electrochemical response with an average spot current of 80 fA and a relative standard deviation of 18%. The number of Fc-PEG chains

per nanodot was evaluated and resulted in few tens of redox-labeled macromolecules immobilized on individual nanodots.

1.6.4 Surface patterning

Using AFM-SECM for patterning surfaces has the advantage that smaller patterns may be achieved, but more importantly, that depositions or dissolution processes leading to surface modifications can be directly imaged in real-time, although there is only a limited number of reports using AFM-SECM for surface modifications. Nishizawa and co-workers demonstrated that AFM-SECM is suitable to pattern surfaces modified with biomolecules [28,117]. AFM-SECM probes with the electrode located at the apex of the AFM tip were used for patterning, which had a rather large blunt tip (approx. 0.5 μm), as the electrode was exposed by mechanical grinding. Applying a voltage pulse (1.5 V) to the AFM-SECM probe, hypobromous (HBrO) acid was generated in HBr solution, which locally removed heparin form a PEI/heparin coated glass surface in the vicinity of the electrode. After the electrochemical patterning step, the substrate was immersed in a solution containing fluorescently labelled fibronectin and the generated patterns were visualized by fluorescence microscopy [28]. The resulting size of the fibronectin patterns was found to be in the order of 2 μm. In a follow up study, the authors used the same approach to generate patterns in the vicinity of cells to direct cell growth [117].

Charlier et al. used hand-fabricated AFM-SECM probes to electrochemically induce patterning of grafting of a non-conductive polyacrylic film onto gold surfaces [90]. Electrochemical grafting of vinyl monomers was carried-out from an aqueous solution containing acrylic acid monomers and nitrobenzene diazonium tetrafluoroborate (NBD). The gold substrate was biased cathodically to electrochemically generate nitrophenylene radicals from NBD, which assembled onto the surface and served as an initiator for the radical polymerization of vinylic monomers. The AFM-SECM probe was used as a counter electrode (direct mode SECM). Patterning was carried out using the AFM-SECM probe retracted approx. 5 μm from the

substrate surface. Spatial movement of the probe resulted in nanopatterning of the surface with lines ~ 200 nm wide and 35 nm thick, of electrografted polymer. Imaging of the deposited polymer pattern was realized *ex-situ* using conventional AFM probes in tapping mode. A similar approach using the AFM-SECM probe as the counter electrode was demonstrated by "writing" lines of nano-electrografted vinylic monomers with a film thickness of approx. 40 nm [89]. Izquierdo et al. used AFM-SECM in GC mode to form corrosion pits on iron surfaces [112,113], as described in **section 1.6.2**

1.6.5 Imaging membrane transport processes

The transport of chemical species across synthetic and biological membranes is of great interest in many areas, ranging from, for example, separation, membrane-supported reactions and gas permeation, to life science applications, such as transdermal drug delivery. Membrane transport through synthetic membranes is also a popular example in AFM-SECM studies to demonstrate the dual functionality of AFM-SECM probes [1,35,45,118,119]. Pores are readily identified topographically with high spatial resolution, while transport through an individual pore can be mapped simultaneously by measuring the current signal. The only requirement for the measurement is that the molecule transporting through the membrane has an associated electrochemical signature *e.g.,* is redox active or can be detected indirectly via electrochemical means. Through simulation this signal can then be converted into a quantifiable rate of mass transfer.

The membrane usually functions as a separator between a donor (containing the species of interest) and a receptor compartment. Transport across the membrane can occur via diffusion, migration, or convection, although using AFM-SECM only the first two transport modes have been studied.

Diffusion through the pores of a track-etched membrane was the first example demonstrating the functionality of hand fabricated AFM-SECM tip (shown in **Figure 1A**)) driving through the

concentration gradient $Fe(CN)_6^{4-}$ across a low pore density, track-etched polyethylene terephthalate membrane, with pores in the range of 0.5 – 1.5 μm (diameter) [1]. The tip current thus has contributions from diffusion and migration under the experimental conditions employed. Experimentally, the AFM-SECM tip currents were found to vary significantly between different pores, but correlated well with pore diameter, which could be accurately characterized by the topographical image. Macpherson and Unwin used Pt-coated commercial AFM cantilevers to record topographical images of a hydrated polycarbonate membrane with 100 nm (diameter) pores and at the same time record the electrochemical signal of the electrolyte filled pores that contained $IrCl_6^{3-}$ as redox active species [118]. In this case, the resolution of the current image was defined by the part of the Pt coated tip that penetrates the pore AFM-SECM. Also, Baker and coworkers demonstrated the functionality of their AFM-SECM probes by mapping the diffusion of $Ru(NH_3)_6^{3+}$ through a porous poly(imide) membrane with highly uniform size distribution of well-defined micro-sized pores as shown in **Figure 15** [35].

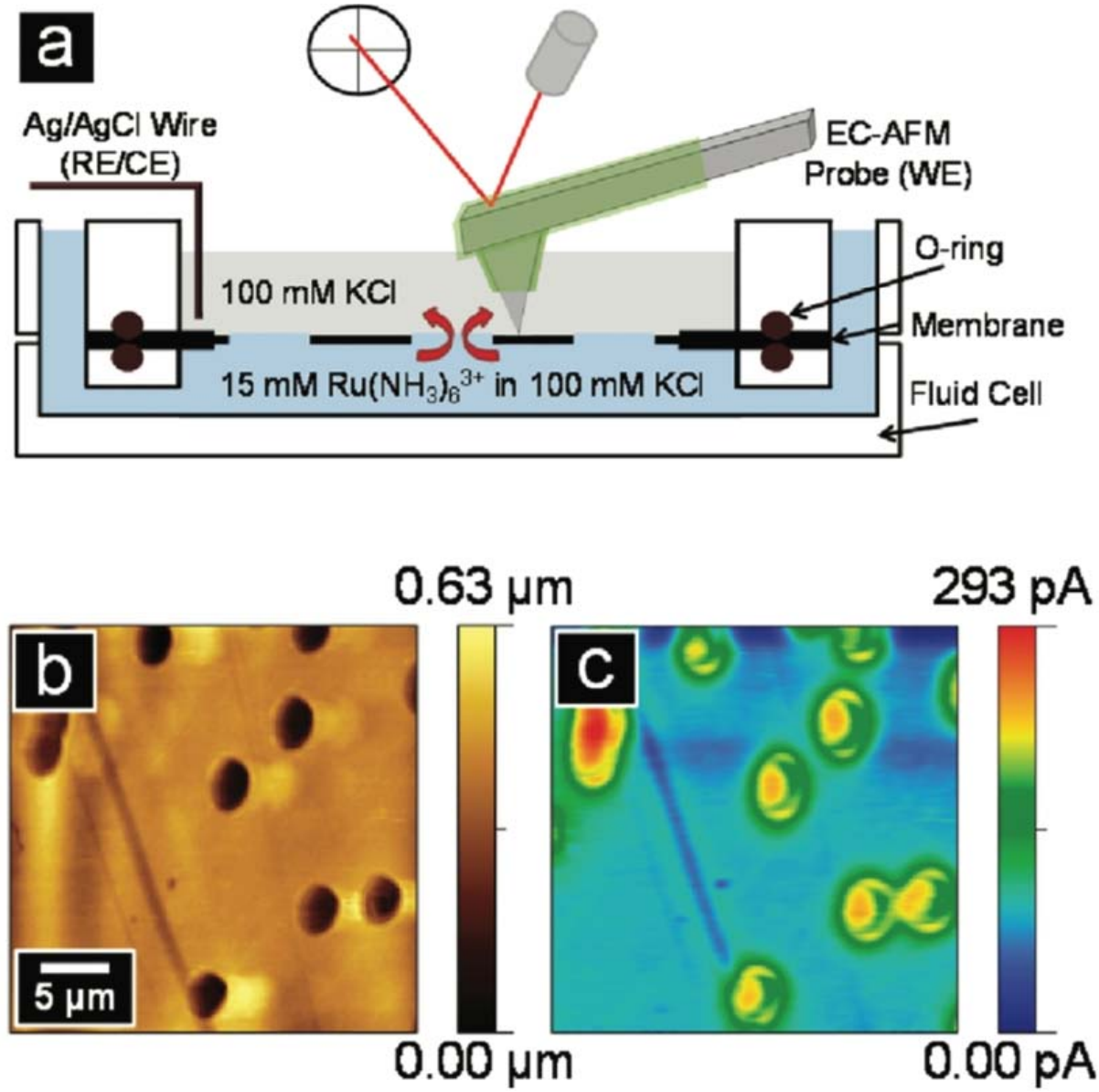

Figure 15. a) Scheme for SECM-AFM transport experiment with poly(imide) membranes and an asymmetric concentration gradient. (b) Topographic image of a porous poly(imide) membrane and (c) the corresponding electrochemical image from reduction of $Ru(NH_6)^{3+}$. Reproduced with permission from M. A. Derylo et al., *Langmuir* 27, 13925–13930 (2011). Copyright 2011 American Chemical Society.

Kueng et al. investigated the diffusion-controlled transport of glucose through a porous polycarbonate membrane, containing pores of size ~ 200 nm [120]. For these experiments the frame electrode of the AFM-SECM tip was modified with glucose oxidase (GOx) that was immobilized at the surface of the integrated frame electrode by electrochemically induced entrapment of the enzyme in electrophoretic paint. If the AFM-SECM tip was located over the pores during imaging the membrane, glucose diffusing through the pores was oxidized in the enzyme-catalyzed reaction and H_2O_2, as side product, was electrochemically detected at the

AFM-SECM frame electrode. The current measured could be accurately quantified in terms of a local glucose concentration and was found to be in good agreement with that predicted for radial diffusion of glucose away from the pore opening. In a collaborative study, the research groups of Arrigan, Gregoire, and Kranz investigated the diffusion profiles in dependence of the pore distance in nano-pore arrays between two immiscible electrolyte solutions forming a liquid/liquid interface (nano-ITIES [121]) [119]. It has been shown in previous studies [122] that the measured currents were lower than the theoretically derived currents using the common design criterion that $r_c > 20r_a$ (r_c, center-to-center distance; r_a, disc electrode radius) established for microelectrode arrays. The authors used FIB to fabricate nanoarrays with different r_c/r_a ratios in silicon nitride (SiN) membranes (50 nm thick) with 100 pores (pore radii (r_a): 86 ± 6 nm) in a hexagonal arrangement. The diffusion profiles were investigated with deposition of silica induced by surfactant diffusion at the nanoITIES and by imaging the diffusion profiles of $Ru(NH_3)_6^{3+}$ through the pores using an AFM-SECM-probe with a conical conductive Pt/C tip. For the narrow-spaced pores (r_c/r_a: 21 ± 2), the whole array is covered by the silica deposit due to the overlapping diffusion profiles at the individual pores, which is also evident in the AFM-SECM images shown in **Figure 16**.

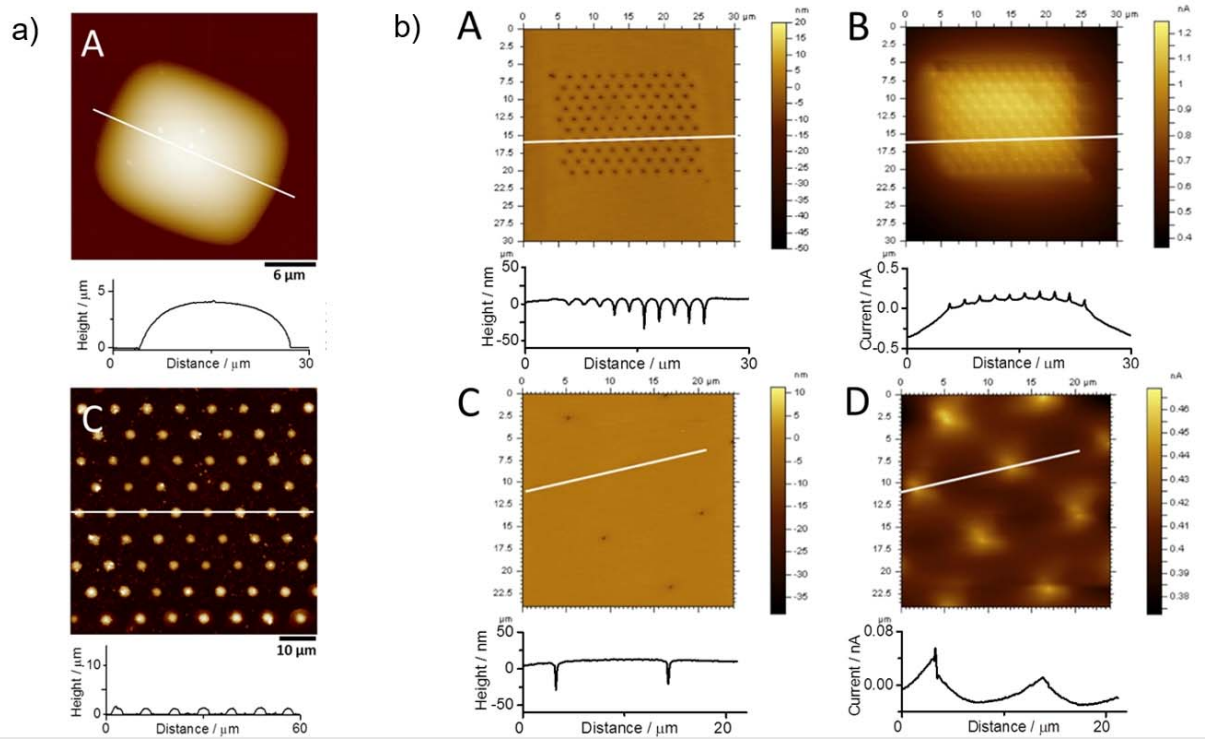

Figure 16. a) AFM height images of the silica-modified nanopore arrays with r_c/r_a of 21 ± 2 (A) and 91 ± 7 (D) obtained by calcination. The corresponding height vs distance profiles marked by the white lines are shown below. b) AFM height (A, C) and electrochemical current (B, D) images of unmodified nanopore arrays with r_c/r_a of 21 ± 2 (A, B) and 91 ± 7 (C, D), recorded with a Pt/C AFM-SECM probe. Faradaic current resulted from the reduction of $Ru(NH_3)_6^{3+}$ diffusing through the nanopores. The corresponding height or current signal vs distance along the white lines is illustrated below each image. Adapted with permission from Y. Liu et al., *Anal. Chem*. 88, 6689–6695 (2016). Copyright 2016 American Chemical Society.

The topography image clearly reflects the hexagonal arrangement of the individual pores, while the current image shows an increased current value over the whole array with a decreasing current gradient towards the edges. The individual pores are only visible as current spikes in the cross-sectional profile as the conical Pt/C tip (tip curvature radius: 20 nm) penetrates the pores, where the concentration of the redox mediator is higher compared to the upper compartment, which is initially filled with electrolyte solution. Only a few pores in the current images seems to be blocked visible by decreased currents over such pores. Increasing the distance of the pores to a r_c/r_a ratio of 91 ± 7, both the silica deposition and the current image clearly indicate the independent diffusion zones around the individual pores.

1.6.6. Biological related studies

AFM as well as SECM and their hybrid techniques have a long tradition in studying biologically/biomedically relevant systems. Early studies were predominantly focused on studying enzyme activity. Kranz and co-workers imaged the enzyme activity of patterned enzyme-containing spots. Glucose oxidase was immobilized in a soft polymer matrix that was electrochemically deposited in presence of the enzyme at pores with a periodic microstructure [63]. In presence of glucose, the SECM-AFM tip electrode detected H_2O_2, which is the electroactive byproduct of the GOx catalyzed reaction of glucose with oxygen. This was one of the early dynamic mode AFM-SECM measurements, as the soft polymer spots could not be imaged in contact mode and even in dynamic mode, some artifacts like stripes are visible. The topographic image in presence of glucose corresponds well with the current image, clearly showing high currents due to the enzymatically produced H_2O_2 concentration above the GOx-containing spots. A similar experiment at micropatterned enzyme spots was shown by the same group using horseradish peroxidase, which was covalently immobilized via a self-assembled monolayer at micro-structured gold pattern [65]. In the presence of H_2O_2 and hydroxyl methyl ferrocene (FMA), horseradish peroxidase catalysis resulted in the formation of water and FMA^+. The latter was electrochemically detected at the AFM-SECM tip electrode. In this case the AFM-SECM mappings were recorded in contact mode AFM and feedback mode SECM visualizing redox enzyme activity correlated with substrate topography.

Hirata et al. used a similar approach to map the topography and redox activity of glucose oxidase immobilized on poly-L-lysine and poly(4-styrenesulfonate) using HOPG as substrate [26]. In the presence of glucose, variation in current activity was seen over the enzymatic film, however when the HOPG was biased at a potential to oxidize H_2O_2, the current detected at the AFM-SECM electrode was significantly reduced. As already described in **section 1.6.5**, the electrode of the AFM-SECM probe, ideally with a design that omits contact between the

electrode and the surface, can be modified with an enzyme containing film, e.g., enclosing GOx [120].

Demaille and colleagues used Mt/AFM-SECM for imaging biological nano objects with high topographical and electrochemical resolution [87,92–95]. In their initial studies, the conformation and motional dynamics of end-grafted DNA oligonucleotides was studied on the basis of force and current approach curves, as discussed in detail in **section 1.6.7** [95].

In a subsequent study, the same group introduced the idea of using redox-immuno-marking to render any protein visible in Mt/AFM-SECM imaging. As a proof of concept, regular arrays of mouse IgG (used as a model non-redox protein to locate) was formed on a gold substrate using bead lithography. [87] Subsequently, the immobilized IgGs were redox-immunomarked by making use of Fc-PEG-labeled antimouse antibodies, and then imaged in tapping mode Mt/AFM-SECM. The topography and current images revealed individual antigen/antibody dots, with a width of approx. 300 nm and a height of around 12 nm. Control experiments, such as recording scans varying the substrate or tip potential, confirmed that the current image of the dots resulted from the detection of the Fc heads by the probe, and thus evidenced the specific on-surface formation of the antigen/redox-labeled-antibody immune-complex.

Nault et al. used Mt/AFM-SECM in combination with redox-immuno-marking to identify the protein distribution on individual virus particles [92]. They studied rod-shaped potyvirus particles, namely the lettuce mosaic virus (LMV) and potato virus A (PVA), which have a length of approx. 700-900 nm and a diameter of 10-15 nm. In this remarkable work, two virus proteins were marked in separate experiments: the coat protein CP and the protein VPg, existing as a single copy located at the extremity of the rod-shaped viral particles. For the selective redox-immuno labelling of these proteins, anti-CP- or anti-VPg-rabbit immunoglobulin gamma (IgG) were used as primary antibodies and anti-rabbit IgG labeled with Fc- PEG_{3400} chains as secondary antibodies. To avoid non-specific binding, the substrate

was modified with a PEG/BSA layer. The modified viruses were imaged with Mt/AFM-SECM. The Mt/AFM-SECM images reproduced in **Figure 17** reveal 5 CP-marked virus particles with the expected rod like shape and dimensions of 900 nm in length (see **Figure 17d**)), approx. 85 nm in diameter and 5-6 nm in height.

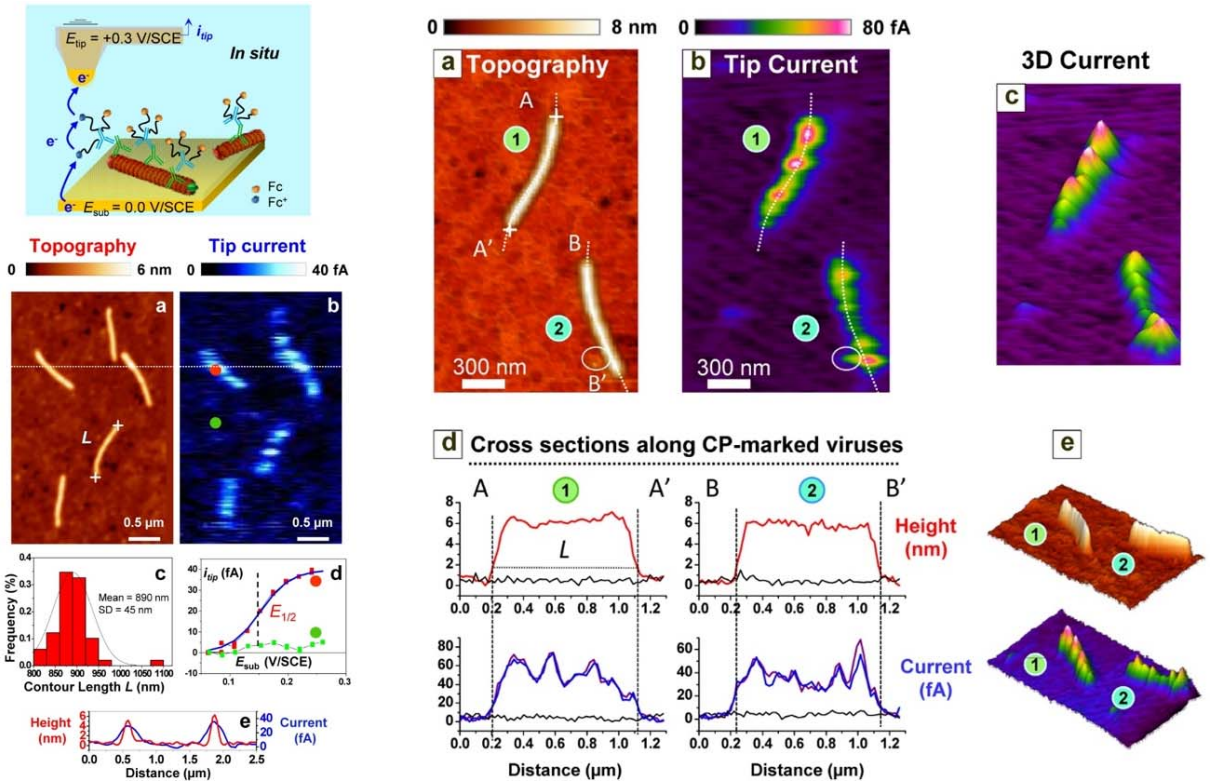

Figure 17. Left : *In-situ* Mt/AFM-SECM tapping mode imaging of CP-marked LMV particles immobilized on a gold substrate. Top: Scheme of the redox cycling of the Fc heads borne by the Fc-PEGylated antibodies generating the tip current. Bottom: Simultaneously acquired topography (a) and tip current (b) images. The histogram in (c) shows the distribution of the contour length L of the virus particles as measured in (a). Shown in (d) is the dependence of the tip current i_{tip} with the substrate potential E_{sub}, with i_{tip} being measured either above a virus particle (red dot in (b) and (d)) or away from the viruses (green dot in (b) and (d)). Cross sections of the topography and current images along the dotted lines shown in (a) and (b) are plotted in (e), respectively, as red and blue traces. Tip potential for imaging E_{tip} = 0.3 V/SCE and substrate potential E_{sub} = 0.0 V/SCE. Imaging medium: 10 mM pH 7.4 phosphate buffer. The tip current image was first order flattened. Right: *In-situ* Mt/AFM-SECM tapping mode imaging of CP-marked LMV particles immobilized on a gold substrate. Simultaneously acquired topography (a) and raw tip current (b) images. The tip current image is also presented in a 3D format in (c) to better show the string of current spots "borne" by the viruses. (d) Cross sections of the topography and current images taken along the viruses labeled (1) and (2) in (a) and (b). Curves in red are cross sections of the topography image (a); curves in blue and purple are cross sections of the trace (b) and retrace (not shown) current images, respectively. Cross sections taken away from the viruses are also shown as dark curves. (e) 3D tilted views of the topography and current images; E_{tip} = 0.3 V/SCE, E_{sub} = 0.0 V/SCE. Imaging medium: 10 mM pH 7.4 phosphate buffer. Adapted with permission from L. Nault et al., *ACS Nano*. 9, 4911–4924 (2015). Copyright 2015 American Chemical Society.

The deviations in height and diameter from literature values were attributed to artifacts known when imaging soft samples, as well as convolution of tip geometry when imaging nanoscale objects. The simultaneously recorded current image reveals current spots, which exactly match the locations of the viruses in the topography image. The number of current spots varied from one particle to the other: a statistical analysis showed that most of the virus particles displayed 4 to 10 spots (see **Figure 17)**). This result evidenced how Mt/AFMSECM can uniquely reveal the way redox functionalization endowed to viral particles is distributed both statistically within the virus population, but also spatially over individual virions. The authors also labeled the terminal protein VPg using the same strategy. Comparing the topographical with the current image, current spots located only at one end of the virus particles were observed in this case, indicating the electrochemical detection of VPg, thus demonstrating the capability of Mt/AFM-SECM for locating *individual* copies of viral proteins.

Recently, Demaille and colleagues studied scaffolding of enzymes on virus nanoarrays [93,94,123], to evaluate the potential of such scaffolds for bioelectrocatalysis and for biosynthetic and sensing applications. Random arrays of *fd* bacteriophage particles, composed of approx. 2700 copies of a major coat protein, packed around a single-stranded circular DNA, were modified with pyrroloquinoline quinone-dependent glucose dehydrogenase (PQQ-GDH) along with co-immobilized ferrocene PEGylated antibodies on their protein shell [94]. These enzyme/redox mediator-modified virus scaffolds showed significant enhanced catalytic currents compared to non-scaffolded PQQ-GDH. In a highly interesting follow up study [85], the authors used Mt/AFM-SECM to gain insight in the correlation of location (topography) and catalytic activity (current response) at a single particle level.

The rod-shaped fd bacteriophage particles were immobilized on a silane (C11) SAM modified SiO_2 substrate and subsequently modified with the antibodies, redox-labeled proteins and enzyme as shown in **Figure 18**.

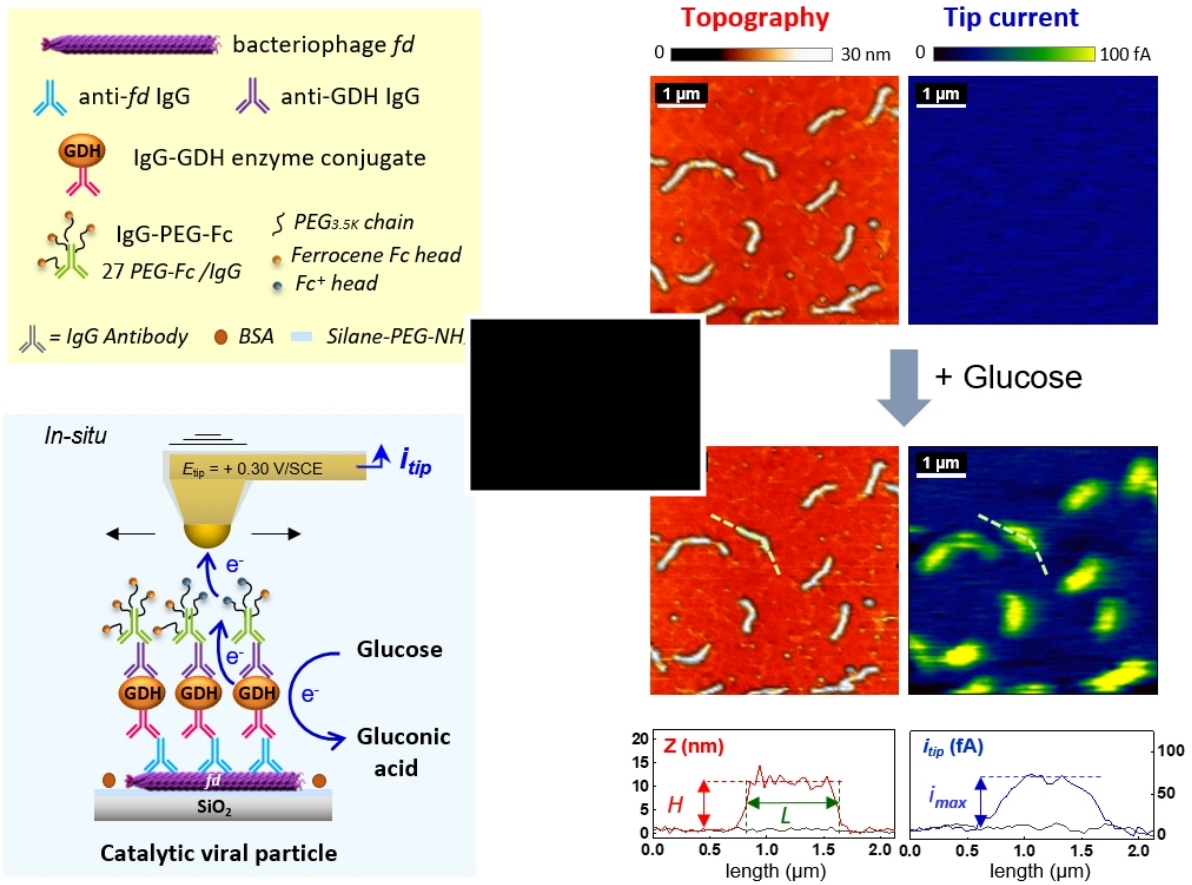

Figure 18. Left: Molecular components of the Fc-PEG / PQQ-GDH integrated system immuno-assembled onto *fd*-particles, (*i*), functional interrogation of the resulting scaffolded integrated system by a Mt/AFM-SECM tip (*ii*). Right: In-situ tapping-mode Mt/AFM-SECM imaging of a random array of Fc-PEG / PQQ-GDH immunodecorated *fd*-particles adsorbed on a SiO_2 surface. Shown are the simultaneous topography and tip current images of the very same particles, acquired in the absence (*i*) and after the addition (*ii*) of 10 mM glucose. Tip potential E_{tip} = + 0.3 V/SCE. Imaging buffer: Tris buffer pH 7.5. The correlated height and current profiles shown in (B) are image cross-sections taken along the dotted line. Reproduced with permission from T. O. Paiva et al., *ACS Catal*. 10, 7843–7856 (2020). Copyright 2020 American Chemical Society.

Mt/AFM-SECM images were recorded in absence and in presence of the co-substrate glucose. Only in the presence of glucose, and at a sufficient tip potential of +0.3 V vs. SCE, were the fd particles appearing in the current image, evidencing that the current was associated with the enzymatically catalyzed glucose oxidation reaction. All particles investigated during these studies showed that the current response peaked in the middle of the *fd* bacteriophage particles visible as catalytic "hot spots". Using the obtained high-resolution current data and assuming the particles can be considered as homogeneous 1D objects, the authors provided a quantitative model which suggested that these catalytic hotspots were related to an interplay

between charge transport by electron hopping between ferrocene moieties along the viral particles and enzymatic catalysis. Based on the statistical analysis of the biocatalytic activity across 59 individually decorated fd bacteriophage particles and the quantitative model, the authors provided an analysis of the PGG-GDH enzyme kinetics at the single *fd*-scaffold level. Although electrocatalytic data at the single nanoparticle level have been reported, this is the first comprehensive study on mapping enzymatic activity with such high resolution and providing a quantitative evaluation of the enzyme kinetics. So far, only fluorescence studies, i.e., total internal reflection fluorescence microscopy (TIRF) have been reported to map catalytic bursts from single enzyme molecules [124].

1.6.7 Electrochemical force spectroscopy

Force spectroscopy has been extensively used to study cell mechanics and cell adhesion [125] but also for quantitative determination of mechanical properties of polymers, modified surfaces, electrodes etc. Recording force distances curves while simultaneously recording SECM approach curves was first shown by MacPherson and Unwin [1,118] and by Demaille and colleagues using their hand fabricated probes [14].

Demaille and colleagues recorded simultaneously force and current approach curves upon approaching an AFM-SECM probe toward a layer of flexible linear polyethylene glycol (PEG_{3400}) chains, end-grafted onto a gold substrate, and bearing a terminal redox Ferrocene (Fc) label [84], as shown in **Figure 19**.

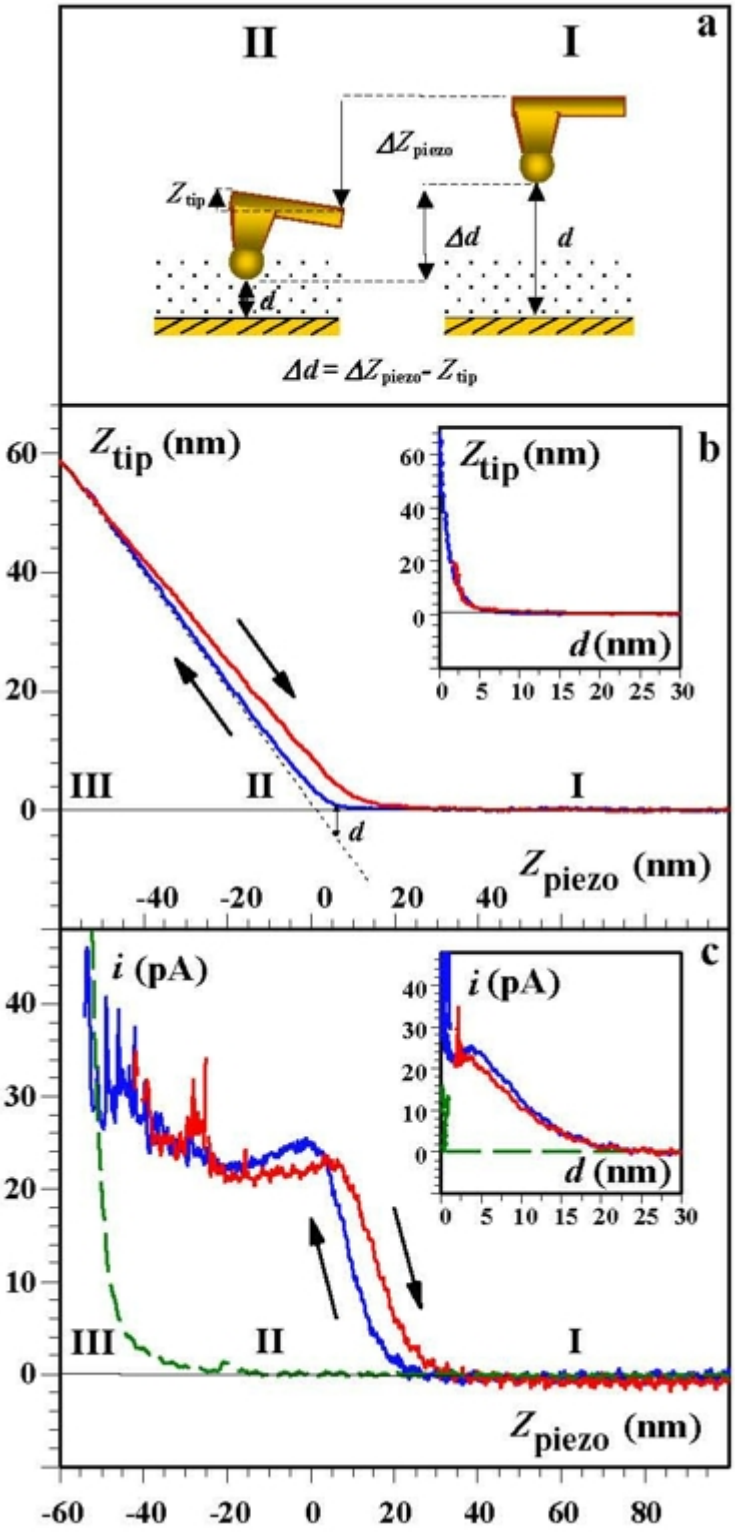

Figure 19. (a): Representative deflection behavior of a combined AFM-SECM probe partially penetrating a substrate-grafted PEG layer (represented as a dotted area). (I) The gold tip is in solution far away from the substrate and thus not deflected. (II) Upon further approach by an increment ΔZ_{piezo}, the tip is brought in contact with the layer and starts to compress it. As a result, the flexible cantilever-arm bends upward by an amount Z_{tip}. When in region III, the tip has made hard contact with the substrate. Simultaneously recorded tip-deflection (b) and tip-current (c) vs. piezo elongation Z_{piezo} curves for a gold substrate bearing redox Fc-PEG_{3400} chains (continuous lines) or Biotin-PEG_{3400} chains (dashed line in (c), the retraction curve is not represented). The dotted line in (b) is used to show graphically how the tip-to-substrate distance d is determined and how the Z_{piezo}=0 point is defined. The insets in (b) and (c)

show the respective re-plots of the curves as a function of *d* as derived as explained in the text. E_{sub} = -0.1 V/SCE; E_{tip}= +0.4 V/SCE. 1M $NaClO_4$ supporting electrolyte. Adapted with permission from J. Abbou et al., *J. Am. Chem. So*c. 126, 10095–10108 (2004). Copyright 2004 American Chemical Society.

The force curve revealed the typical compression of the elastic layer formed by the end-grafted chains, indicated by a rounded region in the force-distance curve. The current signal corresponded to detection of the Fc labels undergoing positive feedback tip-to-substrate redox cycling. The current approach curve was quantitatively analyzed using a model which described motion of the Fc head as a diffusion process retarded by the restoring force exerted by the PEG chain. This model allowed the dynamics of the end-grafted chain to be quantified in terms of an effective chain-end diffusion coefficient.

These results illustrate the capability of Mt/AFM-SECM for characterizing, *in-situ*, the dynamics of end grafted polymer chains. Moreover, as AFM-SECM allows the force and current responses associated with chain compression to be simultaneously measured, the interplay between chain conformation and dynamics and their modulation upon confinement, can be explored. Additionally, since redox cycling of the Fc head is an efficient amplification mechanism, only a small number of chains are addressed by the tip (~100-200 in **Figure 19**). Mt/AFM-SECM was also used to explore the conformation and motional dynamics of end-grafted DNA oligonucleotides [95]. Contact mode force and current approach curves were recorded at a gold surface bearing a layer of thiol-end grafted Fc-labeled $(dT)_{20}$ chains, both before and after hybridization with complementary $(dA)_{20}$ strands. The force curves recorded before and after hybridization were similar, while a ~ 4-fold decrease in the intensity of the current approach curve was observed after hybridization. It was concluded that the dominant motional mode of both single and double stranded oligonucleotides was hinge motion around the relatively long C_6-thiol anchoring spacer of the chains. Anne et al. monitored *in-situ* the enzymatic incorporation of a Fc-labeled nucleotide at the free end of oligonucleotides grafted on a gold surface [85]. Force spectroscopy was used to demonstrate grafting of unlabeled $(dT)_{20}$ – SH chains onto the gold surface. The onset of a current approach curve after the DNA layer

had been exposed to the enzyme terminal transferase in the presence of the Fc-nucleotide, revealed the efficient single base extension of the end-grafted DNA strands.

Kranz and colleagues developed colloidal AFM-SECM probes with low force constants (to ensure high sensitivity force measurements) [72,73,75] facilitating studies on the adhesion forces at electrified interfaces in dependence of the applied potential. These probes are intended for high-throughput single cell force spectroscopy measurements and single cell adhesion studies. By applying a potential to the e.g., polymer-modified colloidal AFM-SECM probe, the adhesion properties between the polymer and individual living cells can be altered. Knittel et al. showed in an initial study force spectroscopy using conical Pt/C-AFM-SECM probes, which were modified with a conductive polymer (p-toluene sulfonate doped Ppy) [39]. The electrochemical and physical properties of the conductive polypyrrole tip can be altered from a conductive (hydrophilic state) to an insulating state (hydrophobic state) by either applying positive potential (+400 mV vs Ag/AgCl) or negative potential (-400 mV vs Ag/AgCl) to the tip, respectively. During first model studies, the adhesion forces between an oxygen plasma-treated glass slide (hydrophilic substrate) and the PPy-coated AFM-SECM tip was recorded in dependence of the applied bias to the tip. For the positively biased tip-surface contact region, adhesion forces were observed which are attributed to van der Waals attraction, its interplay with the electrostatic repulsion and other contributions such as ionic binding and hydrogen bonding. If the AFM-SECM tip is biased negatively, the polymer becomes more hydrophobic and significantly less adhesion forces were observed is observed.

The quantitative evaluation of the force curves requires the precise knowledge on the contact area between the AFM probe with the sample using models such as the Hertz model or the Derjaguin-Muller-Toporov (DMT) model (Young's modulus) [126]. For soft samples, the so-called colloidal AFM probe technique [70,71] using a spherical AFM tip is advantageous, as the mechanical pressure due to a large contact area is reduced compared to sharp AFM probes,

which may substantially penetrate the soft material surfaces, resulting in a variable contact area of the AFM probe with the sample.

Kranz and colleagues used conductive colloidal AFM-SECM probes that are fabricated by attachment of a conductive colloid to an inlaid microscopic disc electrode at the end of a gold-coated and insulated tipless cantilever for electrochemical force spectroscopy. Thereby, electrical contact can be established to the colloid. Daboss et al. modified tipless silicon nitride cantilevers with boron-doped diamond colloids [75] and performed force spectroscopy in dependence of the BDD surface termination and the applied potential to the tip [75]. The force constants of these physically and chemically robust colloidal BDD-AFM-SECM probes were as low as 0.85 +/- 0.04 N/m. The authors demonstrated that the same probe can be used for different measurements without changing probe at the same sample location (e.g., conductive AFM, AFM-SECM measurements and electrochemical force spectroscopy). Of course, it should be noted that given the size of the actual BDD colloid, the achievable resolution in the SECM imaging is only comparable with conventional SECM measurements using microelectrodes.

Conductive colloidal AFM-SECM probes are an attractive alternative to conventional single-cell force spectroscopy (SCFS) measurements, where a single cell is attached to a tipless AFM cantilever and the adhesion forces of the cell with a specific substrate are quantitatively evaluated. In a collaborative effort, Higgins, Kranz and co-workers used conductive colloidal probes modified with poly(3,4-ethylenedioxythiophene) doped with polystyrene sulfonate (PEDOT:PSS) to map the adhesion forces between mouse fibroblast cells and the conductive polymer at physiological conditions in dependence of the applied probe bias [72]. PEDOT:PSS is frequently used as scaffold material, as its properties such as conductivity, stiffness, and surface morphology can be easily altered e.g., by the used dopant. Initial adhesion measurements performed on hydrophilic glass samples in 0.1 M KCl solution to screen

electrostatic interactions. The applied bias to the AFM-SECM probe, open circuit potential (OCP, -0.2 V), +0.8 V and −0.6 V vs. Ag/AgCl) resulted in a statistically significant difference in the measured adhesion forces. The lowest adhesion force was recorded for the positively biased polymer, which may be related to the ionic interactions of the negatively charged, fairly large PSS molecules with the positively charged polymer in the oxidized state. At negative bias, a maximum adhesion of to 2.13 ± 0.53 nN, similar to the measured adhesion at OCP was observed. For the negatively biased AFM-SECM probe and at OPC, also rupture forces are observed, which are related to the "pulling" and stretching of polymer chains, which is less pronounced for the oxidized PEDOT:PSS film. Electrochemical force spectroscopy measurements at living mouse fibroblast cells revealed jumps in the force curves related to membrane tethers known from interaction with membrane proteins. Statistical analysis of the data did not result in a statistically significant difference neither in maximum energy, nor in adhesion forces in respect to the bias of the colloidal probe. This may be explained by the large PSS-dopant (M_W = 70 000), resulting in the fact that the overall polymeric structure does not drastically change when applying moderate positive or negative potentials. However, the advantage of this approach is that many cells can be probed with the same modified colloidal AFM-SECM probe (in this study up to 14 cells were investigated), whereas in SCFS limited cell viability leads to low throughput.

Daboss et al. electrodeposited polydopamine (PDA) onto conductive colloidal AFM-SECM probes from basic dopamine solutions [73]. PDA films are characterized by strong adhesive and redox- and pH-switchable properties related to its multitude of functional groups (phenolic, quinone, amine, imine groups), which renders PDA ideally suited as adhesive coatings for cell immobilization and cell proliferation. The presence of the catechol/quinone groups, when the PDA film was biased at -0.3 V vs Ag/AgCl or +0.5 V vs Ag/AgCl was confirmed by FTIR microscopy. The adhesion properties of PDA in respect to the applied potential were investigated for surfaces of different wettability, such as hydrophobic or hydrophilic self-

assembled monolayers using electrochemical force spectroscopy. The force curves also confirmed that electrochemically deposited PDA films are indeed polymeric in nature, which could be derived from the observed plateaus of constant forces, with contour lengths up to 200 nm. Besides the significant differences of the obtained adhesion force in dependence of the applied potential (i.e., positively polarized PDA-modified 6.2 ± 2.2 nN and negatively polarized film 2.6 ± 1.1 nN, as depicted in **Figure 20)**, adhesion measurements were also carried out at *Pseudomonas fluorescens* bacterial cells.

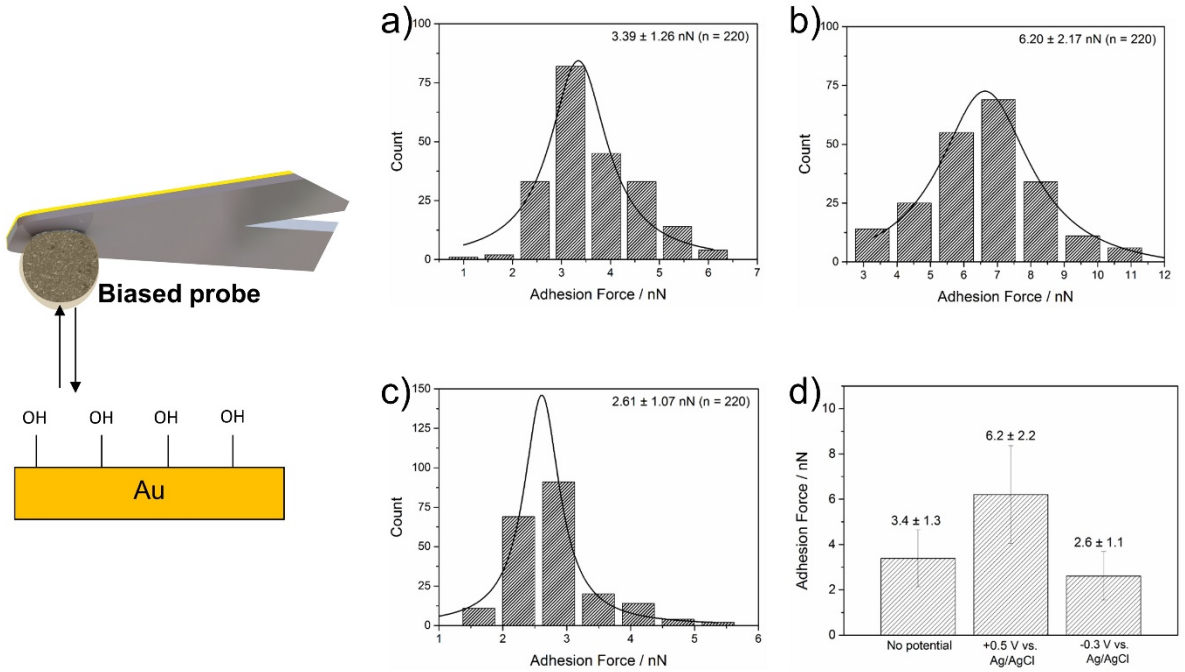

Figure 20. Schematic of the postulated redox switchable character of PDA and scheme of the PDA modified colloidal probe Electrochemical force spectroscopy on SAM-modified gold surfaces a) and b) CH3-terminated and c) and d) OH-terminated with the colloidal PDA-modified AFM-SECM probe biased at a) and c) 0.5 V vs Ag/AgCl and b) and d) −0.3 V vs Ag/AgCl. e) Bar chart of adhesion forces (n = 220). Adapted with permission from S. Daboss et al., *Anal. Chem*. 92, 8404–8413 (2020). Copyright 2020 American Chemical Society.

In dependence of the applied potential, the adhesion forces between the bacterial cells and the PDA-coated polymer, a similar trend with adhesion forces of 6.0 ± 1.1 nN (positively biased) and 1.1 ± 0.7 nN (negatively biased) were observed, clearly revealing the dependence of surface charges of the PDA film on bacterial adhesion which are attributed to strong force interaction of molecules at cell surface (i.e., polysaccharides) with the quinoids groups of the oxidized PDA film. The recorded force curves revealed also long-distance interactions (rupture features)

of flagella and fimbriae at the cell surface. Like the studies with PEDOT-coated colloidal AFM-SECM probes, these experiments showed that such probes are ideally suited for high-throughput experiments, as single cell attachment at the tipless cantilever is avoided. In addition, by tuning the properties of the polymer film, valuable insight into cell adhesion can be provided.

1.6.8 Emerging areas of applications

So far, AFM-SECM has been predominantly used in corrosion science, for studies at catalytically active surfaces, e.g., nanoparticles and for investigating biological samples. The multiple data set achievable in AFM-SECM measurements may also be highly suitable for *in-situ/operando* studies at other complex systems such as battery electrodes. To date, this potential has not yet been fully explored and only few examples were reported using AFM and SECM sequentially e.g., for investigations of solid/liquid interphase (SEI) formation at glassy carbon electrodes [127], or to study interface processes of redox flow batteries [128]. Recently, Mahankali et al. demonstrated AFM-SECM studies using commercial probes from Nanonics Imaging Ltd. (conical Pt probe with a diameter of 100 nm) in non-contact AFM mode and redox competition mode to study Li−S interfacial redox reactions at glassy carbon electrodes in solutions containing Li_2S_8 [99]. Given the abundance of sulfur, lithium−sulfur (Li−S) batteries may be a promising concept, if the current limitations of short cycle life, fast capacity fade and poor efficiency, associated with the dissolution of lithium polysulfides (LiPS), and the associated side reactions could be circumvented. The initial formation of Li_2S/Li_2S_2 particles was achieved by a nucleation process at galvanostatic discharge from OCP to 2.05 V vs Li/Li^+ followed by a growth process. AFM-SECM studies were then performed in pure electrolyte to avoid side reactions of the polysulfide-containing solution. The substrate potential was varied from 2.5 to 2.7 V vs Li/Li^+, while the AFM-SECM probe potential was kept at a constant potential of 2.6 V vs Li/Li^+. Correlating the topographical information of Li_2S/Li_2S_2 particles

at different applied potentials at the electrode with the laterally resolved information from the SECM maps, the authors could identify electrochemically active (i.e., conducting) and inactive (i.e., insulating) regions as shown in **Figure 21)**.

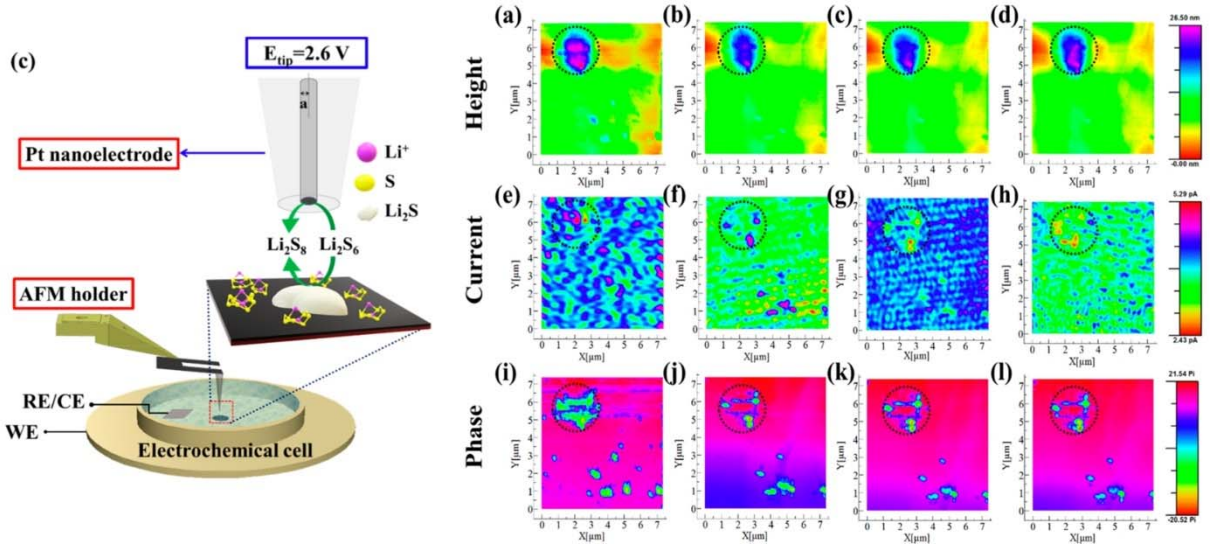

Figure 21. a) Schematic representation of SECM electrochemical cell setup and zoom-in part depicts the competitive SECM mode used for imaging of Li-S cathode surface where the substrate was biased between 2.5 to 2.7 V, and tip was biased at a constant potential of 2.6 V vs Li/Li^+. b) AFM−SECM imaging of Li_2S/Li_2S_2 on carbon surface during oxidation: simultaneous height (first row), current (second row), and phase shift (third row) mapping of Li_2S/Li_2S_2 surface. First column images (a,e,i) correspond to Li_2S/Li_2S_2 [galvanostatically deposited] on glassy carbon before oxidation; second, third, and fourth column images correspond to the Li_2S oxidation at different substrate potentials of 2.5 (b,f,j), 2.6 (c,g,k), and 2.7 V (d,h,l) vs Li/Li^+ respectively; E_{tip} = 2.6 V. Adapted with permission from Mahankali et al., *Nano Lett.* 19, 5229–5236 (2019). Copyright 2019 American Chemical Society.

Combining the measurements with ex-situ data (e.g., XPS measurements), the authors concluded that Li_2S_2 is more easily oxidized compared to the Li_2S and that formed intermediate LiPS species react with Li_2S at higher potentials leading to the deposition of insulating solid products. In addition, a size-dependent oxidation process with smaller particles being oxidized at initial stages at lower overpotential was identified.

2. COMBINED SCANNING ELECTROCHEMICAL MICROSCOPY-SCANNING TUNNELING MICROSCOPY (STM-SECM)

Electrochemical scanning tunneling microscopy (EC-STM) is a very useful technique for investigating electrochemical processes at the solid-liquid interface at extremely high (~ sub

Å to ~ nm level) *x*, *y* and *z* resolution [12]. In EC-STM the tip consists of a conventional sharpened STM tip, coated in insulator, at all but the tip apex to minimize unwanted electrochemical processes contributing to the tunneling current, during topographical imaging of the substrate. Given that this tip design has also been used by many for the fabrication of nanoelectrodes in electrochemical studies [3,11,12], it is no surprise that researchers have investigated ways forward to perform EC-STM and SECM together, with the same probe. In fact there has been some debate in the literature as to whether the current that flows when STM is carried out in a humid environment on low conductivity substrates is actually due to electrochemistry or tunneling [129,130].

Initial studies in this area were carried out by Williams and co-workers who employed a Pt-Ir wire electrolytically sharpened and insulated, in EC-STM tunneling mode, to determine the point of contact with the substrate of interest *i.e.* tip-sample separation = 0. The tip was then retracted a set distance (100 – 500 nm) and SECM SG-TC imaging carried out in a fixed plane above the sample surface [131,132]. However, given that the tip is not tracing sample topography in SECM mode, significant variations in sample topographically can result in tip crash.

This approach was employed to investigate pitting corrosion activity on stainless steel surfaces. Current spikes were observed in the SECM images which were thought to be linked to pitting precursor events and the formation of metastable pits. In most cases the local environment was unable to support continued propagation of the pits and the spiked current signal indicated re-passivation. Where pit growth was possible it was postulated that this was due to the presence of manganese sulfide inclusions in the surface [131,132].

In an interesting approach, Stimmig and researchers used the EC-STM tip to directly transfer a single Pd nanoparticle, deposited electrochemically, from the tip to a conducting substrate and then the same tip was employed to probe the electrocatalytic activity of the particle [133]. Once transferred, the EC-STM imaging mode was used to first locate the Pd

particle and then with the feedback control disabled the tip was retracted ~ 10 nm from the surface of the nanoparticle. Finally, in a solution containing 0.1 M sulfuric acid, the substrate potential was pulsed to a potential sufficient to enable proton reduction at the surface of the Pd nanoparticle (~ 2 nm – 5 nm radius), whilst the tip was held constant at a potential sufficient to detect any electrogenerated hydrogen. Current densities for the electrooxidation of hydrogen, at the Pd nanoparticles investigated in this study, were found to be two orders of magnitude greater than for a 200 nm sized particle.

Treutler and Wittstock employed Pt etched tips coated with an electrophoretic paint, of an optimized geometry, for combined ECSTM and SECM measurements [134]. After the probe was brought into tunneling contact, an ECSTM image of the substrate topography was recorded in constant current mode. The tip was then retracted a set distance (here ~ 20 nm) and an SECM feedback map of the sample recorded (with tip and substrate held under appropriate potential control) at constant distance, *i.e.,* tracing the substrate topography. In this way it was possible to record SECM maps at tip-substrate separations that were smaller than the surface roughness. This methodology was applied to a flame annealed gold substrate covered with an insulating self-assembled monolayer (SAM). The tip was used to mechanically remove zones of the SAM in selected areas, in order to pattern the sample.

Figure 22 shows an ECSTM topography map of the substrate and the corresponding SECM feedback map of the surface recorded in a solution containing the redox mediator, $Ru(NH_3)_6^{3+}$. [134] The substrate was biased at a potential to reduce $Ru(NH_3)_6^{3+}$ whilst the tip was poised at a potential to detect electrogenerated $Ru(NH_3)_6^{2+}$.

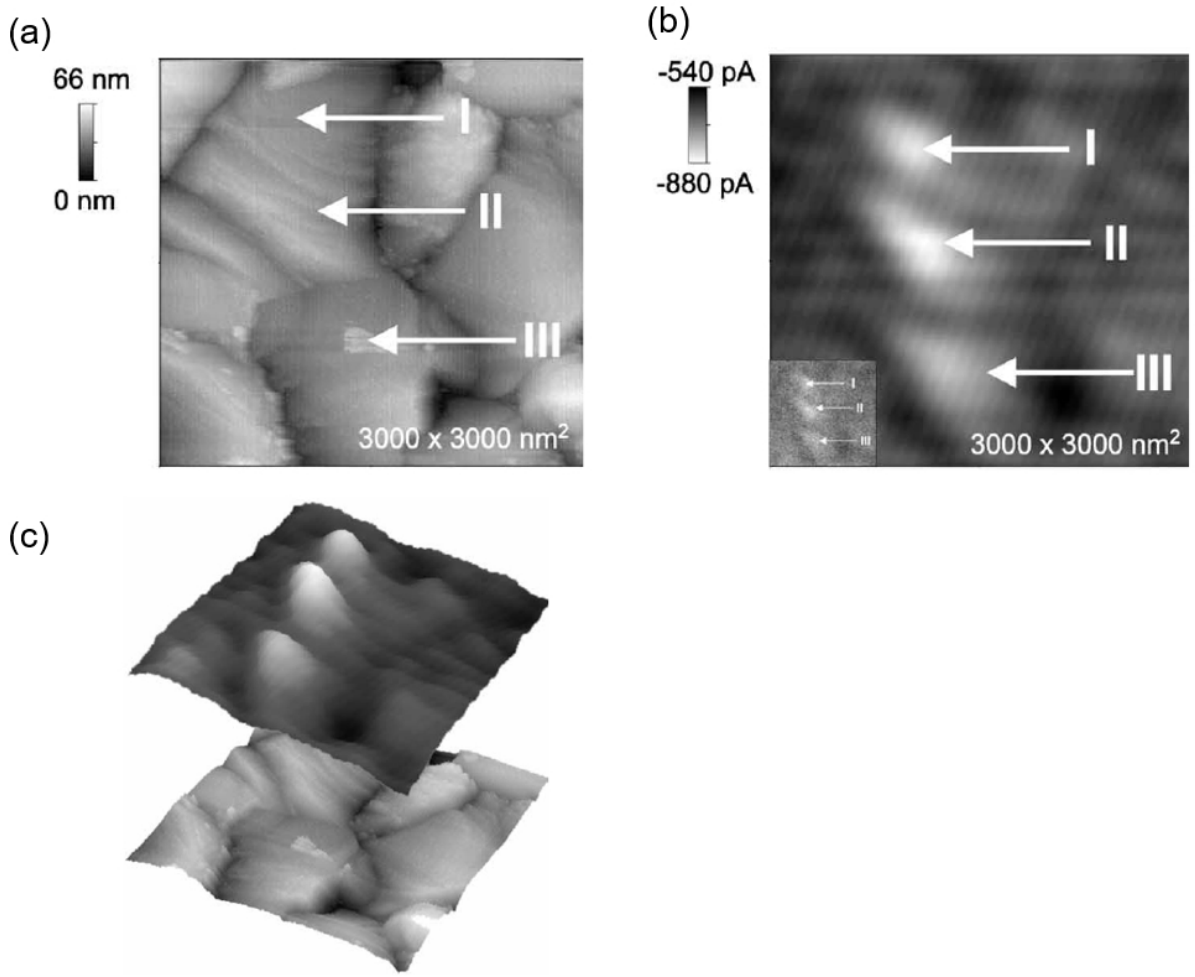

Figure 22: (a) ECSTM scan of a dodecanethiolate-covered gold electrode, E_T = -50 mV, E_S = 0 mV, tunneling current = 0.8 nA, after tip induced removal of the dodecanethiolate film; (b) quasi-simultaneous SECM scan of the same area, image frame 3000 x 3000 nm^2, 2D FFT filtered, E_T = -250 mV, E_S = 10 mV, radius of tip electrode = 69 nm, imaging distance = 20 nm, inset shows SECM data without filtering. (c) pseudo-3D representation of the measurements; top, SECM data from (b), bottom, ECSTM data from (a). Reproduced with permission from Treutler et al., *Electrochim. Acta* 48, 2923-2932 (2003). Copyright 2003 Elsevier B.V.

Figure 22a shows although the ECSTM tip was able to resolve the structure of the underlying Au substrate, at high resolution, revealing height differences of ca. 70 nm, it was not possible to reveal the areas where the insulating SAM had been mechanically removed. However, these appear to have been revealed in the SECM feedback map, **Figure 22b**, where zones of increased current are clearly evident.

Siegenthaler and co-workers integrated a pH electrode into the STM tip design so that it was possible to simultaneously combine in-situ STM studies with the ability to electrochemically generate or scavenge protons and hydroxide ions. [135] The STM tip

protruded ~ 50 μm from a cylinder structure that incorporated a microring iridium oxide (pH) electrode. The distance between the STM tip and the pH electrode was ~ 80 μm. This structure was similar to the integrated frame electrode AFM tips introduced by Kranz and colleagues (discussed in **section 1.2.3**). The concept was demonstrated by investigating the pH dependent properties of an electropolymerized polyaniline film. It was shown that decreasing the pH resulted in the thickness of the film increasing whilst increasing the pH resulted in a decrease in film conductivity.

Although a useful technique, STM-SECM has not shown as much promise or been used as widely as SECM-AFM, most likely due to the fact that the substrate topography can only be obtained using ECSTM if the sample is sufficiently conducting, given that a tunneling current must be recorded. Moreover, AFM typically can be used on much rougher surfaces than STM and obviously can be employed independent of substrate conductivity. Nevertheless, the possibility of coupling STM to SECM has been very recently reevaluated by Unwin et al. [136], with the aim of imaging the proton reduction activity of gold nanocrystals deposited onto a carbon sample. Several issues that so far limited the development of combined STM-SECM have been tackled. Nanopipette-based SECM probes displaying much less leakage current than the usual coated wire STM tips were specially designed. A "tip hopping – potential pulse" scanning pattern was implemented, where the tip was approached to every pixel of the sample. The tip was initially biased at a potential where no electrochemical process took place, so that a purely tunneling current was recorded and used to set a minimal tip-substrate separation. The tip was then withdrawn by a programmable distance, and the *sample* biased at the electrochemical potential of interest, corresponding here to proton reduction. After a short delay allowing capacitive currents decay, the tip current corresponding to the collection of H_2 was recorded. The tip was then withdrawn again before being moved to the next pixel. The requirements of repeating this process fast enough to yield acceptable imaging times, while keeping the approach speed slow enough to ensure accurate STM-based distance control, were

shown to be largely conflicting. In spite of this, synchronous topography and electrochemical current images showing H^+ reduction at the gold nanocrystals could be obtained.

It is also noteworthy that very recently, the onset of nanoscale SECM, and the ensuing reduction in achievable tip-substrate distance, has led tunneling currents to be measured jointly with SECM currents. This could be seen as an unwilling combination of STM with SECM [137].

3. DISTANCE CONTROL IN SECM

There have been many different approaches employed to control and measure the tip-substrate distance of "conventional" glass coated UME disc probes during SECM imaging. One of the most utilized at the time of writing is shear force – SECM, pioneered by Schuhmann and colleagues, although here specialized glass coated electrodes are required. However other methodologies such as alternating current SECM have been implemented with glass-insulated UMEs and important developments have seen the introduction of intermittent contact SECM (IC-SECM) by Unwin and co-workers. These techniques are described in this section.

3.1. Shear Force Scanning Electrochemical Microscopy

The idea of using the detection shear forces occurring when a vibrating local probe tip is approached towards a planar substrate, as a way of measuring and controlling the tip-substrate distance was initially developed for near-field optical microscopy (NSOM) [138]. It was found that when an optical fiber (the tip) was vibrated horizontally the amplitude of the vibration was damped as the tip approached within a few tens of nanometers from the surface. It was thus possible to use the strong distance-dependence of damping to set a desired tip-substrate distance and offer a convenient way of controlling the tip approach, avoiding crash.

This methodology was adopted by the SECM community as a means of developing constant-distance mode SECM. Two experimental strategies have been proposed and are

described in detail below: (1) specially designed flexible needle-type UMEs that can be easily vibrated upon mechanical excitation; (2) attaching SECM electrodes to an oscillating device, such as a quartz oscillator.

3.1.1 Shear Force SECM with vibrating needle UMEs

3.1.1.1 Shear Force SECM at the micron scale

The first attempt to adapt shear force detection to SECM was reported by Schuhmann's group [139]. In the original configuration, a long and flexible needle-type glass insulated disk UME, fabricated by sealing 25 μm diameter platinum wire in a pulled glass capillary (1-1.5 cm long, 100 μm outer diameter), was vibrated using an excitation piezo. The vibrational motion of the tip was monitored by focusing a laser onto the lower part of the tip and detecting the resulting diffraction pattern on a spilt photodiode, **Figure 23**.

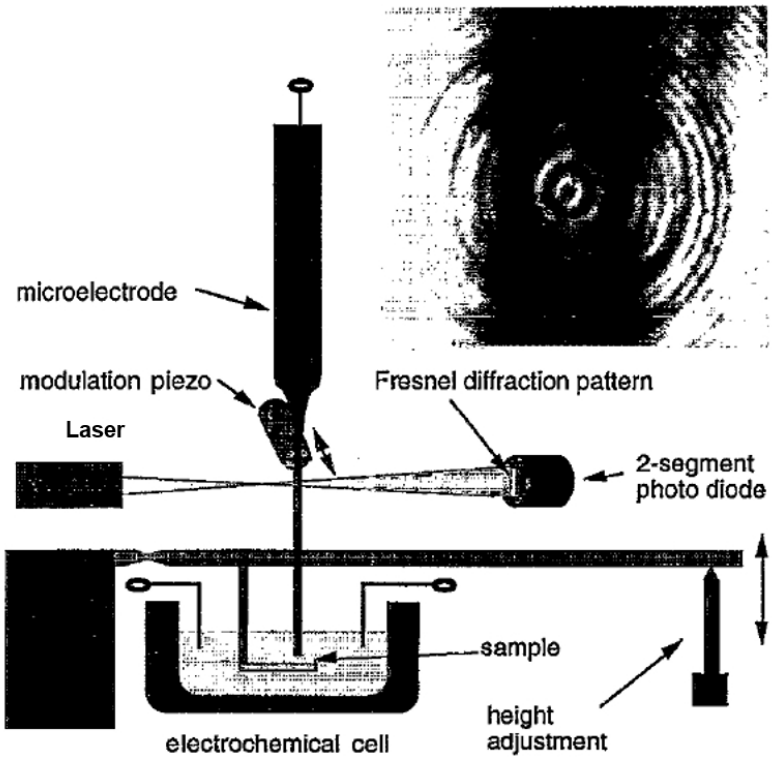

Figure 23. Instrumental set-up for shear force-based constant distance SECM. The SECM tip is a needle type microelectrode vibrated using a piezo. The tip vibration is monitored optically by diffracting a laser on the electrode body. The diffraction pattern formed on a 2-segment photodiode (upper right) is used to monitor shear force-induced damping of the tip vibration. Adapted with permission from M. Ludwig et al., *Rev. Sci. Instrum. 66*, 2857-2860 (1995). Copyright 1995 American Institute of Physics.

The tip excitation amplitude spectrum of the vibrating UME submerged into buffer solution displayed numerous peaks in the 0-20 kHz region corresponding to various modes of tip vibration. Only the lowest mode, corresponding to a frequency around 1 kHz, was sensitive to the tip-substrate sample distance. The excitation amplitude of the tip vibration was varied from 1 nm up to a few microns. The effect of vibrating the UME on the tip current recorded in a SECM configuration was investigated. It was shown that the tip current displayed a linear dependence on amplitude for large excitation amplitudes. However, by employing a low enough amplitude (< 1 μm) conditions could be found so that the tip current was not affected by the vibration.

Upon approaching the vibrating tip towards a conducting (gold) surface, the expected decay in tip amplitude, resulting from shear forces, was recorded concomitantly with an increase in tip current as a result of SECM positive feedback. However, it was observed that the decay length of the vibration approach curve was highly dependent on the stiffness of the underlying substrate material. On hard surfaces this length was ~ 1 μm, whereas on softer surfaces e.g., gold on mica, it was several tens of microns. These results indicated the non-negligible magnitude of the tip-substrate interaction forces involved, estimated to be ~ 150 μN, high enough to even bend a mica substrate. However, this initial work established the compatibility of SECM with shear force.

In a following paper Schuhmann and co-workers demonstrated that by employing a feedback loop which relied on the detection of shear forces between the vibrating UME and sample, it was possible to keep the tip-substrate distance constant (constant damping amplitude) during SECM imaging [140]. Hence it was possible to implement constant-distance mode SECM imaging, a mode free of artifacts due to sample tilt and roughness. Moreover, it was demonstrated that shear force damping of the needle-like UMEs occurred within a distance of 100 nm from the surface, meaning it was possible to hold the UME extremely close to the surface during imaging. This resulted in a much better lateral resolution compared to fixed

height imaging. Additionally, an image of the substrate topography could be reconstructed from the known adjustments of the vertical tip position imposed by the feedback loop in order to maintain a constant distance at each position of the scanned area. Hence in constant distance SECM imaging, topography and SECM current images could be simultaneously acquired.

Shear force can be used to bring any tip close to a surface and this approach has been successfully employed with non-amperometric pipette-based tips, such as miniaturized enzyme-sensors or potentiometric probes [140]. Initially, work saw the use of an enzyme-filled glass capillary tip to image a 50 μm Pt modified disk in shear force feedback mode [140]. In one application, a glucose-dehydrogenase (GLDH) filled micropipette tip was used to map the production of NAD^+, the natural cofactor of GLDH, resulting from the catalytic oxidation of NADH at the surface of the modified-Pt UME [140].

Shear force constant distance scanning potentiometry has been employed to map the dissolution of calcite crystals and shells and to map spatial variations in pH at high resolution over complex microcavity patterned substrates [141,142]. The ability to approach capillaries very close to a surface, using shear force feedback, was also used for the local deposition of silver microstructures on conducting surfaces using potential assisted ion-transfer at the tip of a micropipette [143].

Using shear force based constant distance SECM imaging to characterize the activity of single live cells was demonstrated by Schumann and colleagues [144]. Here glass needle-type SECM tips could not be used, since the significant tip-surface interactions occurring during shear force feedback caused irreversible damage to the cells. For this work, a special type of needle electrode consisting of ~ 10 μm diameter carbon fibers protruding by ~ 0.5 mm from a supporting glass capillary, were employed. The walls of the carbon fiber were insulated by deposition of an electrophoretic paint. The extremity of the fiber was cut with a scalpel to expose a disk-shaped electrode. The resulting carbon fiber UME was flexible enough for the interaction forces between the tip and the cell to be sufficiently small to allow shear force mode

to be applied to visualize the topography of individual living cells without damaging them. The carbon fiber tip could thus be positioned above a single cell and the secretion of redox-active neurotransmitters amperometrically detected at the tip. The very short gap between the cell membrane and the UME, made possible by shear force positioning, insured a 100% collection efficiency of the neurotransmitter.

The shear force constant distance-mode SECM was later mounted onto an inverted optical microscope, in a so-called “Bio-SECM” configuration, in order to study individual living cells. The Bio-SECM instrument was notably used to detect nitric oxide release and oxygen consumption [145,146], by single living cells. Note that in these works, optical readout of the distance controlling shear-forces (SFs) was used, and that specific implementation of such a setup for single cell imaging has been reviewed in literature [147]. Later on, the shear force setup was modified by replacing the optical detection system, used to monitor the tip vibrating motion, by piezoelectric elements, typically comprising an excitation dither piezo, and a receiver piezo [148]. Electrical detection of the tip vibration was shown to be much easier and more convenient than optical detection, partly because the delicate laser alignment on the tip was made unnecessary.

Further developments to shear force SECM have seen the implementation of high resolution constant-distance mode alternating current electrochemical microscopy (AC-SECM), which was used for the visualization of corrosion pits on stainless steel samples [106,149].

Over the last decade, a large amount of work aiming at making shear force regulated SECM a more reproducible and robust technique has been published. Etienne et al. reported an automated approach procedure for combined shear-force SECM imaging of large samples displaying complex topography features such as millimeter curvature/tilt [150]. The same group also proposed a setup for optimizing the shape of disk-in glass tips, enabling the glass sheath to be polished into a conical shape, while ensuring a perfect alignment of the tip versus

the substrate surface [151]. This notably resulted in enhancing the resolution of the topography images acquired in SF-SECM. In a subsequent related work, the authors addressed the key question of identifying resonance frequencies of the vibrating tip effectively enabling tip-surface control [152]. They noticed that using large excitation amplitudes enabled to enter a so-called hydrodynamic regime, where peaks recorded in the SF spectrum far from the substrate were associated with concomitant increase in tip current (i.e. with current peaks visible in a current vs. piezo excitation spectrum). They showed that the corresponding peak frequencies could subsequently be safely used, at low excitation amplitude, to approach the tip close to the substrate and record unperturbed SECM approach curves for kinetic measurements. It was also shown that the excitation amplitude and frequency, and also the tip size, modulated the spatial range of tip-surface SF-interactions, in the 1 -10 µm range.

It is worth mentioning that SF-SECM has shown to be particularly suitable for corrosion studies, since it enables millimeter to micrometer scale high aspect ratio features, typically covering corroded samples, to be readily imaged [153–155]. This capacity of SF-SECM to image large samples has also been exploited to characterize the electrochemical activity of a 350 µm x 350 µm sample bearing reduced graphene oxide, with a 5 µm resolution [156].

SF-controlled tip positioning has recently enabled a new SECM technique to be developed [157]. This technique, labeled Scanning Gel Electrochemical Microscopy (SGECM), employs a drop of ionically conducting gel electrodeposited onto a micro-sized UME as a local probe. The position of the gel-probe versus a sample of interest is controlled using shear force feedback, **Figure 24**.

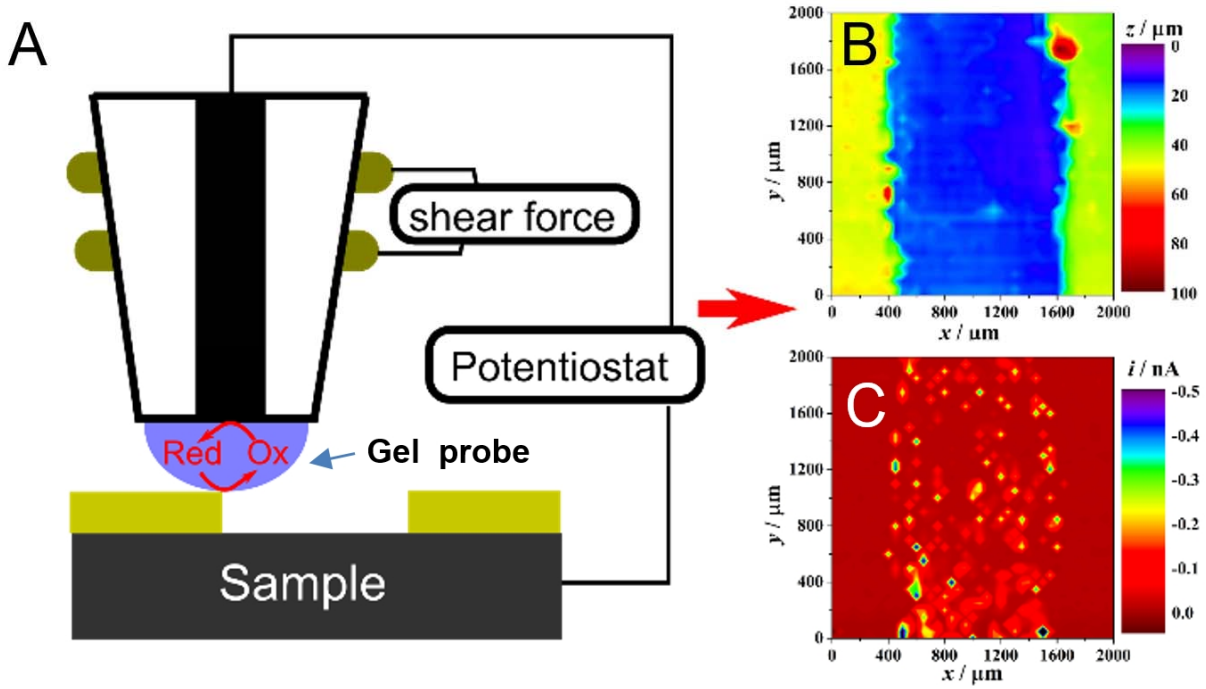

Figure 24. Scanning Gel ElectroChemical Microscopy (SGECM) (A) Principle of the method: a drop of an ionically conducting gel electrodeposited onto a micro-sized UME is used as a local probe. The position of the gel-probe versus a sample of interest is controlled using shear-force (SF). (B) Sample topography acquired using SF feedback (C) Simultaneous current image showing the local electrochemical reactivity of the sample. The sample is a steel plate covered by an insulating film, except for the region seen in the center of the topography image, where the film was vertically scratched to expose the metal. Reproduced with permission from L. Liu et al., *Anal. Chem.* 90, 8889–8895 (2018). Copyright 2018 American Chemical Society.

Upon contact of the gel with a conducting substrate, a local two-electrodes electrochemical cell forms, in a way similar to SECCM (see Chapter 15). SGECM can be used in amperometric mode, where a current characterizing the local reactivity of the sample is recorded, or in potentiometric mode, where the local corrosion potential of the substrate is measured [158]. In both cases SF control enables a topography image to be acquired simultaneously with the electrochemical image (see **Figure 24**). Electrochemical resolution is controlled by the area of the contact between the gel and the sample, which can be modulated through pulling or pressing the gel probe away/against the sample. Resolution in the 10 µm range was demonstrated [159].

3.1.1.2 Shear Force SECM at the sub-micron scale

All of above works have focused on needle type SECM tips having a diameter of the order of a few to tens of microns, positioned very close to a surface. Bringing such relatively "large" electrodes very close to a surface may be advantageous in the case where the tip is used

as a collector. However, for SECM imaging the "electrochemical" resolution is not only governed by the tip-substrate distance, which can be made very small using shear force, but also by the size of the disk-shaped UME. Moreover, the lateral resolution of the topography image, acquired simultaneously with the current image, is, in theory, limited by the overall size of the imaging tip, which includes the glass sheath surrounding the disk-shaped electrode. Note, in practice, the actual resolution is often higher than expected because the edge of the glass sheath (in the case of a non-perfect tip-sample alignment), or any small-sized protruding corrugation of the glass, can serve as an effective imaging tip.

However, reduction in tip-size is necessary for a better control of the imaging conditions and to improve both the topographical and electrochemical resolution of constant-distance mode SECM imaging. To this end, needle-type nanoelectrodes were fabricated by pulling Pt wires in glass capillaries. This method, described in detail in the chapter "Instrumentation and tip preparation" [**Chapter 2**], results in submicron-sized disk shaped Pt electrodes encased in long, thin glass capillaries [160].

It was found that, upon mechanical excitation, these nanoneedles displayed several resonance frequencies in the 150 – 300 kHz range; although only some were sensitive to the presence of the substrate and were thus suitable for use to control the tip-substrate approach and distance. By holding the submicron sized probes some ~100-200 nm away from a surface using shear force feedback, very high resolution topographic and constant-distance current images could be acquired [148].

In order to further improve the topographical resolution of constant-distance mode SECM a new generation of platinum nanoelectrodes were produced. Instead of the classical inlaid disk format these pulled-glass Pt electrodes were conically polished so that the Pt disk electrode was located hundreds of nanometers above the conical extremity of the tip. Due to the geometric shape the probe did not exhibit SECM feedback while approaching a sample. Thus, these probes are best suited for concentration gradient profiling at active submicron-sized

sites on a surface without interference from SECM feedback. As a proof-of-concept these electrodes were successfully used for imaging the diffusion layer of a redox mediator $[Ru(NH_3)_6]^{2+}$ generated at a complex test structure consisting of microcavities incorporating disk (cavity bottom) and ring (cavity walls) electrodes [161].

Even though shear force feedback has been successfully used for constant distance mode SECM imaging in many instances, it nevertheless has several shortcomings. One of the problems is that the imaging scan rate has to be low in order for the electronic feedback loop to reestablish the set-point value (hence distance) every time the tip is moved to a new position, otherwise tip-crash occurs. Additionally, the range of the shear force interaction can be very small (a few 100 nm's) and shear force-based feedback can thus only position tips at this distance or closer to the substrate. For very small tip-substrate separations the presence of the tip will block diffusion of species toward/away from the surface thus potentially interfering with the phenomenon to be probed, for example this is problematic when probing the activity of surface-attached enzymes.

Schuhmann and colleagues proposed a new imaging mode to address many of the above issues [162]; 4D shear force based constant distance SECM. Here, the tip is first approached under shear force control very close to the substrate. The tip current and vertical tip position are then recorded, allowing current and topography images to be reconstituted as usual. The tip is then retracted from the surface by small user-defined increments and the tip current at each distance is recorded. When the tip is retracted to its final position it is laterally moved to a new *x,y* position above the sample and approached again at this new location. This procedure minimizes both the risk of crashing the tip and tip-substrate interactions occurring during lateral tip motion. Ultimately a 4D data set (*x,y,z* tip current) is acquired from which topography and SECM images at different but constant tip-sample distances can be built. The feasibility of 4D imaging was demonstrated using amperometric feedback mode imaging of a Pt band electrode

array and mapping of the diffusion profile of a redox active species above a microelectrode in the generator/collector arrangement.

The work described above has demonstrated that monitoring shear force interactions between a vibrating needle SECM tip and a substrate is a robust approach for implementing constant distance SECM. As an important improvement of this combined technique, Mauzeroll and colleagues demonstrated that monitoring the phase change of the tip vibration associated with the onset of shear forces, instead of the amplitude change, could further improve the sensitivity of distance regulation [163]. Accordingly, Heinze et al. demonstrated that phase-operated shear force SECM enabled high resolution imaging of the electrochemical activity of single, 320 nm diameter, boron doped nanoelectrodes forming an array [164].

The 2010-2020 decade saw the publication of interesting contributions addressing many of the practical limitations of nanoscale shear force SECM, such as identifying tip resonance frequencies sensitive to the presence of the substrate (i.e., shear-force sensitive frequencies), or even describing new tip fabrication and insulation methods. Mauzeroll and co-workers reported a detailed fabrication protocol for pulled nanoelectrodes, characterized by an electrochemical radius in the 3 – 190 nm, and displaying long flexible tappers particularly suitable for SF control [165]. Several factors influencing the shear-force sensitivity of these electrodes were experimentally identified. The respective orientation of the dithering and receiving piezo was shown to have a strong influence on the shear force spectrum, 0° and 90 ° alignment yielding the highest sensitivity. At the opposite, no clear trend was noted regarding the effect of the distance separating the two piezos. Moreover, a new experimental approach was suggested for rapidly identifying shear-force sensitive frequencies from the global excitation spectrum of the tip, recorded in air and far from the surface: only those peaks associated with a drastic shift of phase ultimately enabled safe control of the tip-surface distance.

Interestingly shear force feedback was also used to ease the fabrication of SECM nanoelectrodes, by solving the major issue of insulating the whole body of nanoelectrodes while

leaving their very end exposed. [166] For this, conically etched carbon fibers were brought under shear force control into gentle contact with a soft substrate (silicon rubber). Electrodeposition of a thin polymer layer onto the carbon fiber was then triggered by applying a suitable potential. This resulted in deposition of an insulating polymer film on the whole body of the fiber beside the very end, where deposition was hampered by the presence of the substrate. Carbon nanoelectrodes characterized by an effective radius as small as 46 nm could thus be fabricated. In a similar approach shear force positioning was employed to position the extremity of a bundle of conically etched and gold coated optical fibers within a ~1µm thick PDMS layer deposited onto a glass slide [167]. Ensuing deposition of an electrophoretic paint resulted in insulating the body of the bundle, while leaving only exposed the conical extremity of the fibers, ultimately forming an arrays of conical nanoelectrodes.

3.1.2 Using quartz crystal resonators as shear force transducers for SECM

In 1995, a paper from the NSOM community introduced the use of a small oscillating piezoelectric component, a crystal oscillator in the shape of a mm sized tuning fork, as a transducer for detecting shear force damping of an oscillating optical fiber approaching a surface. [168] Typically, the fiber was glued onto one of the arms of the tuning fork which was mechanically excited by a dithering piezo. The tuning fork was oriented toward the substrate and hence the fiber was vibrated parallel to the sample surface. Here the excitation frequency was perfectly defined: it had to exactly match the resonance frequency of the tuning fork (*e.g.,* 32 kHz). The oscillation of the fork/fiber assembly was electrically monitored by measuring the voltage between electrical contacts on the prongs of the fork and analyzed using lock-in detection.

This shear force monitoring technique was later adapted to SECM by Smyrl et al. who replaced the optical fiber by an etched tungsten wire (~ 2 µm apex), insulated by dip coating, and acting as an SECM tip [169]. The conical tungsten tip was glued onto one of the prongs of

the tuning fork so that a few millimeters of the probe extremity was protruding from the fork. In order to avoid complete damping of the tuning fork (and tip) motion, only the very end of the probe was immersed into the solution *i.e.,* the tuning fork was in air. Thus, measurements were made in a thin film of solution (a few millimeters deep) bathing the substrate.

The tuning fork/tip assembly was mounted on the head of a commercial NSOM microscope, and the tuning fork oscillation amplitude used as a feedback signal to regulate the tip-substrate separation. With this set-up an extremely small tip-substrate separation of the order of 10-30 nm was maintained by the feedback loop. Constant distance SECM imaging in SG-TC mode of a 50 μm platinum disk UME was carried out. Topography and SECM images were simultaneously acquired validating the use of the tuning fork for shear force based constant distance SECM imaging. Later, feedback mode constant distance imaging of 5 μm gold wires aligned onto a substrate, using a gold coated pulled optical fiber as an SECM tip, was successfully carried out with the same tuning-fork based setup [170]. This approach has also been used to observe defects in hexadecanthiol monolayers at submicron resolution [171].

A similar configuration was later used by Bard and co-workers to develop a combined scanning electrochemical-optical microscope (see **section 4.1** also) [172,173]. Here the SECM tip, a conically etched platinum wire insulated with electrophoretic paint, was used to generate light *in-situ* via an electrogenerated (ECL) reaction. Due to the small effective size of the conical microelectrode tip (down to 155 nm), shear force monitoring had to be used to control the tip to substrate approach and distance. The tip was thus attached to one of the prongs of a tuning fork. Here again, and this is pertinent to all tuning fork-based systems used in solution, immersion of the tuning fork itself had to be avoided. Hence, only the last ~ 0.5 mm of the probe, protruding form the end of the tuning fork, was in contact with solution.

The tip was first brought into very close proximity to the surface by shear force feedback: the approach was stopped when a 3-5% damping of the fork oscillation was recorded. The tip was then withdrawn by 24 nm, before the ECL light intensity transmitted to the substrate

was monitored. This “tapping mode-like” procedure was repeated for every imaging position of the substrate. The tip was thus not scanned above the surface, but rather approached and then withdrawn, and only then translated laterally between measurements. This process minimized the chances of crashing the tip. Due to the small size of the tip, and the very close tip-substrate separation enabled by shear force distance control, sub-micrometer resolution ECL near-field images were acquired.

The same shear force based SECM setup was later employed using, this time as the tip, a pulled optical fiber bearing a ring-shape electrode at its apex. Shear force detection using the tuning fork signal set a constant tip-substrate distance while simultaneous topography, current and optical images of test substrates were acquired. Interdigitated band electrodes, consisting of 30 μm wide gold bands spaced by 25 μm glass were imaged. Even though the “tapping mode-like” scanning procedure was utilized it was observed that some samples were destroyed by the tip, for example, diatoms immobilized on glass [173]. This was a result of potentially destructive tip-substrate interactions which occur when a tuning fork is used as a shear force sensing element.

The recurring problem of imaging fragile biological material using a tuning-fork based shear force distance control was addressed by Matsue and Yamada by judicious choice of the imaging conditions in combination with the standard approach (STA) imaging mode [174–176], which is similar to the “tapping mode-like” mode introduced by Bard’s group [173]. Yamada et al. imaged a glass surface bearing co-immobilized diaphorase and albumin with an SECM equipped with a tuning fork [174]. Disk shaped platinum UMEs (2-10 μm) were used as the imaging tip that were cut to 4 mm length and glued onto the tuning fork. Only the last 0.5-1.5 mm of the tip was immersed in solution. Experimental conditions minimizing tip-substrate interactions were chosen, in particular a low setpoint which was 2% damping of the tip oscillation, and the amplitude of the shear fork excitation signal was kept at a minimum. Under these conditions, STA mode imaging allowed the enzyme layer to be preserved.

Later Yamada and Matsue showed that the STA mode could also safely be used for constant-distance SECM imaging of living cells provided the shear force excitation signal was kept low enough [175]. Here, a combined optical fiber / UME having an effective electrode radius ~ 35 nm, was used for imaging oxygen consumption by single PC12 cells in a culture medium. The local oxygen level was monitored amperometrically by the tip. Electrochemical images, reflecting the localized oxygen consumption by cell respiration, and topographic images of the single cell were acquired simultaneously with micron level resolution, **Figure 25**.

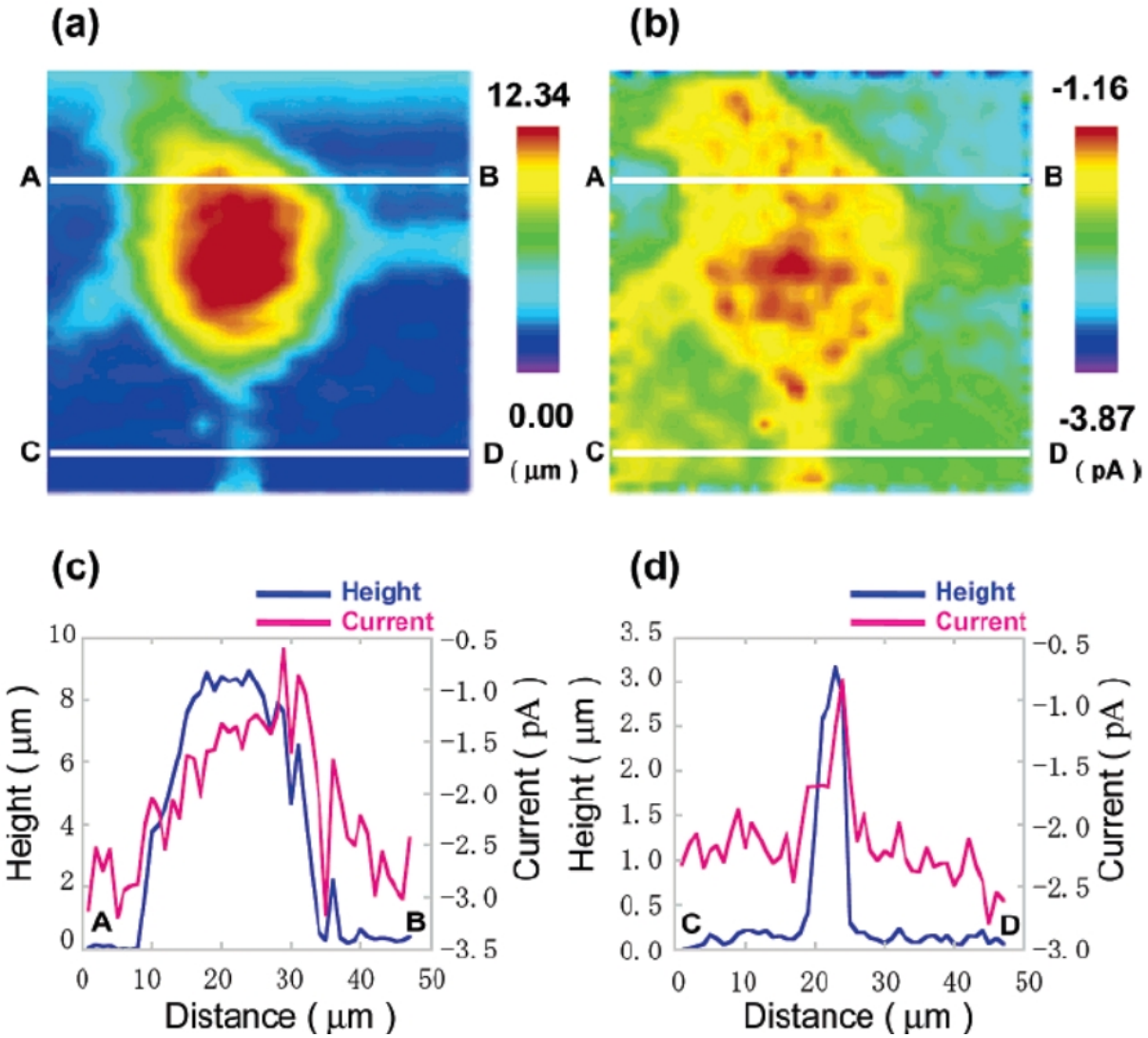

Figure 25. Constant distance SECM imaging using shear force feedback in the STA mode of model neurons (PC 12 cells). Topography (a) and electrochemical (b) images of PC12 in a PBS solution using a capillary electrode probe. The tip was biased at -0.50 V (vs Ag/AgCl) to reduce oxygen. Hence the contrast of the electrochemical image (b) reflects the local oxygen level. Oxygen depletion due to cell respiration is visualized as orange-red regions. The cross sections of the cell body (c) and axons (d) are shown for the topographic and electrochemical signals. The scan range was 47 μm x 47 μm, and the step size was 1.0 μm. The white lines in a and b indicate the position of the cross section. Adapted with

permission from Y. Takahashi et al., *Langmuir 22*, 10299-10306 (2016). Copyright 2006 American Chemical Society.

In related work, Matsue and co-workers investigated systematically the influence of the amplitude of the vibration of the tuning fork on cell imaging [176]. They showed that if too large amplitudes are used the cells were damaged whereas if too low amplitudes were employed the hydrodynamic forces caused by solution viscosity interfered with shear force detection and increased the noise level. Hence, an optimal amplitude has to be found. It was emphasized that this value actually depends on the shape of the probe and the depth of immersion of the probe into solution. Under optimal condition well resolved topography images of living cells could be obtained, **Figure 26**.

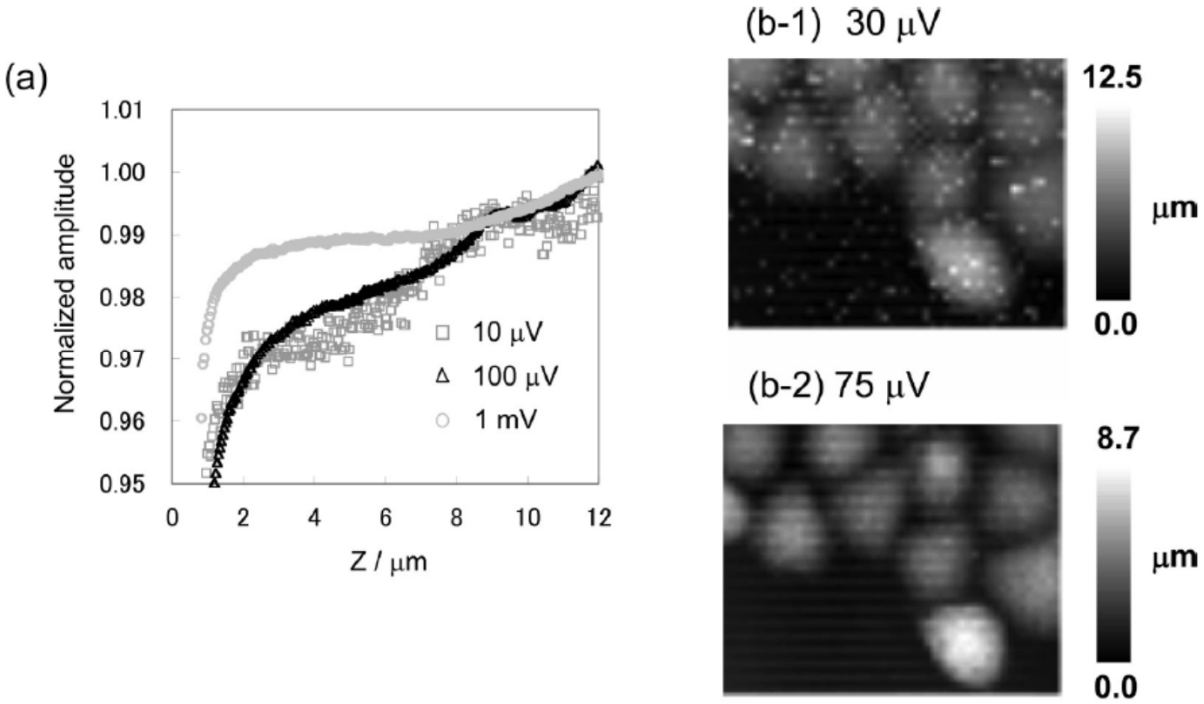

Figure 26. Imaging live HeLa cells using shear force feedback with a tuning fork transducer. Optimization of tuning-fork amplitude for living cell topography imaging. (a) Tuning for amplitude-distance profiles of a living cell. The cells are not detected in the approach curve (the tip probably impales the cells) if the tuning fork amplitude is too high (> 100 mV).(b) Topography images of HeLa cells at tuning fork amplitudes of 30 μV and 75 μV. Noise (white dots in image b-1) appears if a too low tuning fork amplitude is used. The scan range was 100 μm × 80 μm, and the step size was 2.0 μm. Adapted with permission from Y. Takahashi et al., *Anal. Chem*. 81, 9674-9681 (2009). Copyright 2009 American Chemical Society.

These images were acquired in STA mode using fast electronic circuitry to shorten the scanning time acquisition. Moreover, in this particular work, with the probe acting both as a UME and an optical fiber, topography, fluorescent and current images of single cells could be obtained in constant distance mode SECM-optical microcopy. Finally, Yamada et al. showed that using STA in a differential mode (d-STA), i.e. considering the differential output voltage of a tuning fork rather than its absolute value for distance control, enabled even softer imaging of living cells than regular STA mode [177,178].

Other improvements to shear force based SECM systems using tuning fork transducers have been reported [179,180]. Heinze et al. showed that by using high frequency (1 MHz) crystal oscillators, instead of the commonly used tuning fork (32 kHz) quartz, the dependence of the quartz resonance on the tip immersion depth could be minimized [179]. Moreover, by using the phase shift of the quartz oscillation, as a feedback signal rather than the amplitude, the system achieved a greater stability. Matsue and colleagues reported the use of beveled disk-in glass Pt UMEs glued to a tuning fork as a local probe for constant distance SECM shear force feedback imaging of enzyme activity [180], adopting a similar approach to Etienne et al. [161] discussed above in **section 3.1.2**.

Using quartz crystal resonators as shear force transducers for distance control in SECM is seemingly universal since it simply requires the gluing of a low mass probe to a crystal resonator to obtain a shear force sensing device. Sensing is straightforward as it can be performed simply by measuring the voltage at the electrical pins of the tuning fork. However, many parameters, including the immersion depth of the probe and even the amount of glue used to attach the tip can modify the crystal response, hence care is advised. Moreover, as the shear force signal is only obtained for extremely short tip-substrate distances, of the order of a few tens of nm, this translates to very intense tip-substrate interactions. However, researchers, as reviewed above, have proposed many alternative strategies to alleviate, if not to solve, these problems.

As a final word for this section, it seems important to stress out that within the last decade SF-coupled SECM has sufficiently gained in maturity for commercial instruments to be developed, they are now widely available [181,182].

3.2 Intermittent Contact-Scanning Electrochemical Microscopy (IC-SECM)

One of the most common modes of AFM imaging is tapping mode. Here the probe is oscillated close to resonance, A_o, and then brought into intermittent contact with the sample resulting in damping of the oscillation amplitude to a value, A [183]. The level of damping (A/A_o) is kept constant and used as the feedback signal to monitor the topography of the surface. The value of A/A_o denotes the hardness of the tap on the surface, with a light tap close to 1 and a hard tap much less than 1. By monitoring the phase, it is also possible to extract information on the material properties of the sample such as elasticity, adhesion *etc*.

This general concept has been applied to SECM by Unwin and co-workers to control the tip-substrate separation during imaging [184]. Here, a small AC positional perturbation is made to the piezoelectric positioner controlling the tip position normal to the surface of interest (z-axis). This is especially attractive as it requires minimal additional hardware and is easily implemented. Typically much lower oscillation frequencies (< 100 Hz with the system documented in reference [184]) are employed than in conventional tapping mode AFM (typically > two orders of magnitude higher). The amplitude of the oscillation is damped as the tip touches the surface. This damping is detected and used to provide information on the point of tip-substrate contact and hence can be used to quantify tip-surface separation (e.g., for approach curve measurements). The damping can also be used as a set point to determine the tip-substrate contact point at all *x,y* positions during a scan. Intermittent contact (IC-SECM) differs from the early tip position modulation (TPM) studies of Wipf and Bard [185], and their more recent development [186], in that here a non-electrochemical signal is used to provide the feedback and positioning sensitivity.

Key advantages over shear force are (i) the experimental set-up is much simpler, existing traditional glass coated SECM probes can be utilized, (ii) the level of immersion into the fluid of interest does not need to be controlled and (iii) the tip can be operated for imaging at any user defined tip-substrate separation. During imaging the tip typically scans across the surface in "tapping mode" recording the topography of the surface. At the same time it is possible to record the tip current (both mean current and AC current information). Here it is advantageous if the tip is polished at a slight angle or fortuitously the tip-substrate alignment is not exactly parallel so that direct contact is avoided between the substrate and electrode. This is especially problematic for conducting substrates. The tip can then retrace the topographical line scan for electrochemical imaging at any distance the user so chooses.

Figure 27(a) shows typical approach curves recorded with a 2 μm diameter Pt disk UME towards an insulating and conducting surface. Also simultaneously recorded is the oscillation amplitude (typically ~ 40 nm as used in this study).

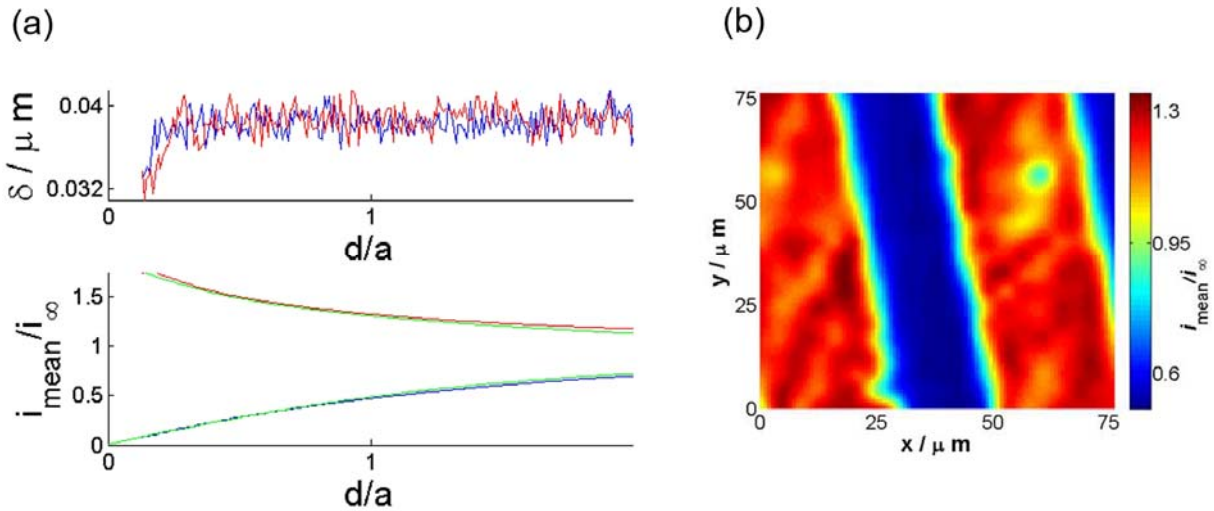

Figure 27. (a) Feedback approach curves to conducting, gold (red), and nonconducting, glass (blue), substrates. 1 μm radius Pt disk electrode oscillated at 70 Hz, oscillation amplitude 39 nm in 2 mM $FcTMA^+$. Top: SECM tip oscillation amplitude as a function of the tip-substrate separation. Bottom: Mean SECM tip current, i_{mean}, as a function of the tip-substrate separation. The mean SECM current for the analytical approximation for the feedback response is shown in green. Excellent agreement is seen between theory and experiment for both positive and negative feedback. i_{mean} was normalized by the bulk steady-state SECM tip current. The distance from the substrate, *d*, was normalized by the SECM tip radius, *a*. (b) IC-SECM imaging of gold bands on glass obtained using a 1 μm radius Pt disk electrode (70 Hz, oscillation amplitude is 39 nm in 2 mM $FcTMA^+$. Average tip current in IC forward scan. Adapted with permission from K. McKelvey et al., *Anal. Chem*. 82, 6334-6337 (2010). Copyright 2010 American Chemical Society.

For the studies herein, contact was assumed when there was a greater than 15% sustained decrease in the z piezoelectric positioner strain gauge sensor oscillation amplitude, as compared to that in the bulk solution. **Figure 27(b)** shows a constant distance feedback SECM image (1 μm tip-substrate separation) recorded with a 1 μm radius Pt UME of Au bands 25 μm wide on glass, separated by 20 μm. Beyond the above mentioned initial works, significant developments and new applications of IC-SECM have been reported in the last decade.

It was first demonstrated that IC-SECM could be used to visualize and quantify molecular transport thought a porous membrane [187]. Pressure induced ruthenium hexaammine transport through dentine was employed as a model system. IC-controlled feedback enabled a 1 μm radius UME (RG ~ 10) to be brought within a constant distance of ~1 μm from the surface. Four independent signals were acquired while scanning the surface, enabling four corresponding images to be constructed, showing: (i) The sample topography, (ii) the DC (time averaged) tip current, (ii) the amplitude and (iv) the phase of the AC component of the tip current, which is modulated by the periodic UME motion. Due to the large RG value no useful information could be obtained from the topography image. However, The DC and AC amplitude current images revealed the heterogeneity of mass transport across the dentin surface. The DC images, especially the phase image, displayed a better resolution than AC images, enabling the identification of individual pores and measurement of individual fluxes (pore velocities).

Later, IC-SECM proved to be particularly suitable for mapping the heterogeneous electrochemical activity of diamond electrode surfaces [188,189]. At first, Unwin et al. quantitatively mapped the distribution of the local rate of electron transfer (ET) at a polycrystalline boron-doped diamond (pBDD) electrode surface [188]. A perfect overlap was observed between the ET rate constant map and dopant level density map, visualized through subsequent Raman imaging. A direct link between electron transfer kinetics and local doping

levels was thus evidenced. Later on, the same authors showed that defects in single crystal BDD electrodes could be straightforwardly evidenced and mapped by IC-SECM, since they displayed enhanced electron transfer due to higher doping levels [189].

Further work reported the expansion of IC-SECM to the nanoscale [190]. This required using sub-micron sized laser-pulled Pt nanoelectrodes, whose RG had to be decreased by ion beam etching to enable closer tip-substrate separation. In order to avoid breaking such fragile nanotips, the tip to substrate interaction forces, inherent to IC-operation, had to be decreased. This was achieved by introducing a piezo bender actuator which had a much smaller spring constant than the strain gauge sensor used previously, allowing better sensing of the tip-surface interactions. As a result, tip-surface forces were reduced from 3000 to 100 μN. Nanoscale IC-SECM was finally demonstrated by imaging a gold nanoband in positive feedback mode, a resolution better than 200 nm was achieved.

An improved version of IC-SECM, labelled Hopping Intermittent Contact-Scanning microscopy (HIC-SECM) was introduced by Unwin et al. [191]. A key feature of HIC is that the tip is not scanned over the surface once a set point amplitude damping is established, but rather sequentially brought in an out of feedback contact at every point of the surface. This type of hopping mode approach and imaging was previously implemented for shear force SECM [162,173,174]. Beyond minimizing tip-surface interaction, it provides the unique opportunity of acquiring information at any x, y, z position above the surface in the form of 3D data sets. For HIC-SECM information such as the DC tip current, amplitude and phase of AC tip current, and sample topography are acquired. The wealth of data collected enables hundreds of possible plots (images, 1D and 2D cross-sections, approach curves) to be constructed. The performances of HIC-SECM were first demonstrated by imaging test samples, such as band or disk electrodes [191]. This technique was later used to study the local dissolution of salicylic acid in saturated aqueous solution [192]. More recently IC- distance control was implemented for recording impedance data locally, in a so called IC-AC-SECM imaging mode [193,194].

As a final word, we note that the tip-surface forces involved in IC-SECM operation remain relatively strong, making this technique more indicated to characterize robust solid surfaces than fragile samples. It is also worth mentioning that at least one commercial SECM system featuring IC mode is available [17].

3.3 Alternating current–Scanning Electrochemical Microscopy (AC-SECM)

3.3.1 AC-SECM as a tip-positioning technique

AC-SECM is a specific mode of SECM which can also be used as an alternative to hybrid SECM techniques to set a constant tip-substrate distance during SECM imaging. The use of AC-SECM as a tip-positioning technique was initially introduced by Horrocks et al. [195]. The various applications of this technique were reviewed, and are therefore only briefly presented here [196]. In AC-SECM a low amplitude (~10 mV) alternating potential is superimposed on the tip bias while the ensuing modulation of the tip current is recorded. The current signal is then analyzed in terms of the AC-current magnitude and phase offset with respect to the tip potential excitation signal. Interestingly no redox mediator is required in solution since it is the local impedance of the tip-sample system which is probed.

In low supporting electrolyte solution (1-10 mM ionic strength) the impedance is dominated by the solution resistance. Both the current and phase have been shown to display a smooth tip-sample distance dependence. For insulating substrates this dependence originates from hindered ion movement in the tip substrate gap, which results in a decrease of the AC-tip current amplitude as the tip-substrate distance is made smaller, closely following negative feedback behavior. Importantly it was shown that, if a redox mediator is introduced in solution, the contribution of the faradaic process appears as a DC amperometric signal which can be electronically separated from the high frequency component of the full impedance signal. Hence for insulating substrates, the AC impedance signal can be used to hold the tip at a constant tip-substrate separation whilst the DC current, relates to local faradaic processes which can be independently and simultaneously measured [197].

The simplicity of AC-SECM is that it can be implemented using regular disk in glass SECM tips, *i.e.* no specific sophisticated tips have to be fabricated. However, a limitation of using AC-SECM as a vertical positioning technique is that it can only be confidently used if the substrate is *homogeneously* insulating. The reason is that the AC-signal is also modulated by the local conductivity of the sample surface: a higher AC-current is recorded over a conducting surface than over an insulating surface. Hence over conductive surfaces information regarding the topography and the local conductivity of the substrate cannot be separated from simply recording the AC-current signal.

However, a notable exception is when the conductive substrate is unbiased: it has been reported that, in such cases, provided a low AC-frequency and low supporting electrolyte concentration are used, an AC-SECM feedback signal, similar to the one recorded at insulating surfaces *i.e.* negative feedback, is obtained [198]. In this particular case, AC-current based constant distance amperometric SECM imaging can be implemented.

AC-SECM has notably been used for single cell studies. The specific advantage of AC-SECM for imaging cells is that, as mentioned above, no potentially toxic redox mediator has to be added to the solution. Hence AC-SECM imaging can be carried out directly in the cell growth media. Baur and Wipf et al. have shown that AC-based feedback can be used for constant impedance (*i.e.* distance) topographic imaging of model neurons PC12 cells, **Figure 28** [199]. The resolution obtained was slightly lower in this AC-mode than in amperometric constant-current DC-mode imaging.

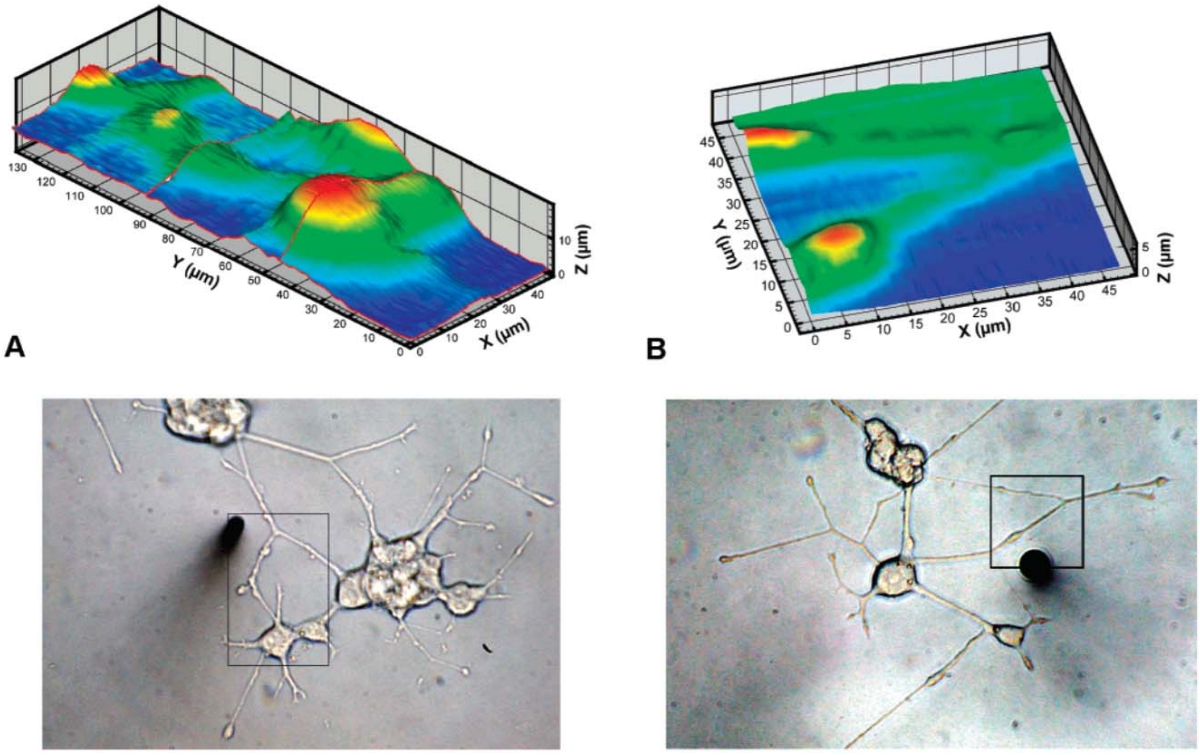

Figure 28. Topographic images of differentiated PC12 cells (model neurons) acquired using constant-impedance imaging (AC-SECM). (A) Mosaic image of several cells joined by neurites recorded in supplemented RPMI 1640 growth media; (B) closeup image of a neurite bifurcation recorded in HBSS (buffer). Conditions: 5- µm -diameter carbon fiber electrode, no mediator, and scan rate 7 µm/s. AC-signal: 90 kHz and 10 mVpp superimposed onto a 0.75 V (vs. 3 M NaCl Ag/AgCl) DC bias applied to the tip. Adapted with permission from R.T. Kurulugama et al., *Anal. Chem.* 77, 1111-1117 (2005). Copyright 2005 American Chemical Society.

The ability to amperometrically record vesicular release at the tip while using AC-current based distance feedback was also demonstrated [199]. It was observed that vesicular release did not significantly alter the local impedance (albeit ions were released) meaning constant distance imaging/positioning was unaffected. However, it was observed that the injection of a K^+ containing solution, used to depolarize the cell and trigger vesicular release, did cause a large decrease of the background impedance, thus prohibiting the use of AC-current based distance regulation *during* application of this stimulus.

It was therefore determined that provided the tip is initially positioned next to a cell, and at such a distance so that it cannot collide with the cell, the distance feedback loop can be disabled, the stimulus applied and the tip rastered at fixed height above the cell. In such a case the AC-current probes the tip position with respect to the cell, while the amperometric current

reveals individual release events, **Figure 29**. Impedance feedback control of the sample-probe separation was also used to position an SECM tip above single cells and monitor amperometrically metabolic cellular consumption [200].

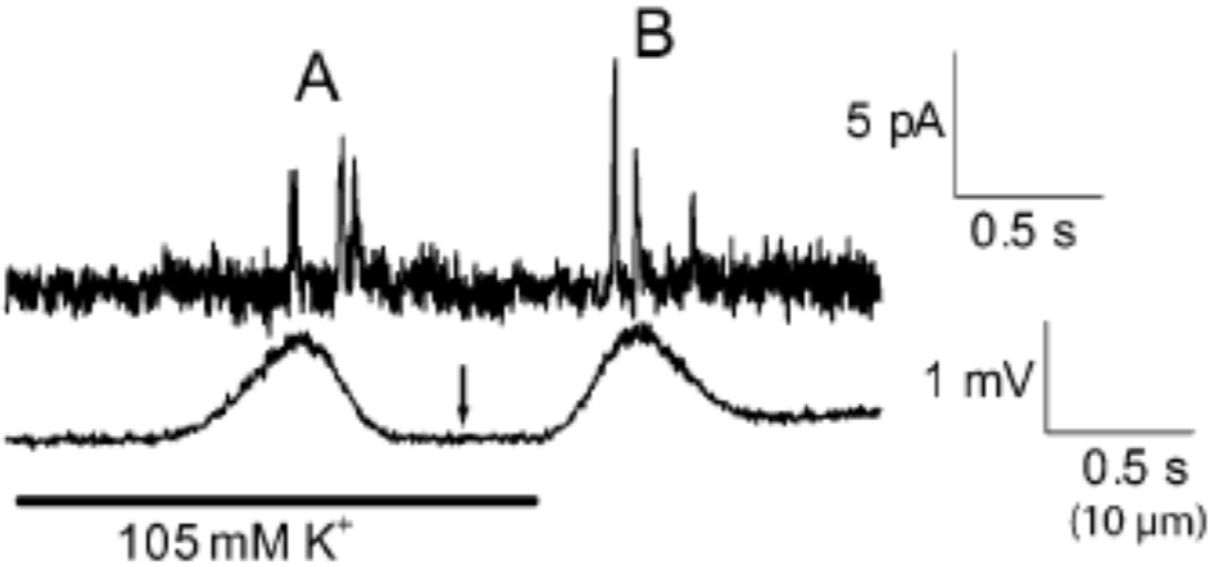

Figure 29. AC-SECM study of isolated cells. Simultaneous recordings of release by amperometry (upper trace) and cell morphology by tip impedance (lower trace) during a 6-s K^+ stimulus at an undifferentiated PC12 cell. The data were recorded during repeated line scans in the *x* direction at a constant *y* location. Arrows denote changes in direction (i.e., forward/reverse) of the x line scan. Conditions: HBSS buffer (no mediator), 5-µm-diameter carbon fiber electrode, and scan rate 20 µm/s. AC-signal: 90 kHz and 10 mVpp superimposed onto a 0.75 V (vs. 3 M NaCl Ag/AgCl) DC bias applied to the tip. Adapted with permission from R. T. Kurulugama et al., *Anal. Chem.* 77,1111-1117 (2005). Copyright 2005 American Chemical Society.

Improvements in the resolution of AC-SECM imaging is possible either by increasing the frequency of the AC voltage applied to the tip [201], or by implementing constant distance mode AC-SECM. This requires coupling AC-SECM with an external distance regulation mechanism such as shear force detection [106,149], intermittent-contact SECM (IC-SECM) [193,194], or AFM, the latter is illustrated in **Figure 30** [106,107].

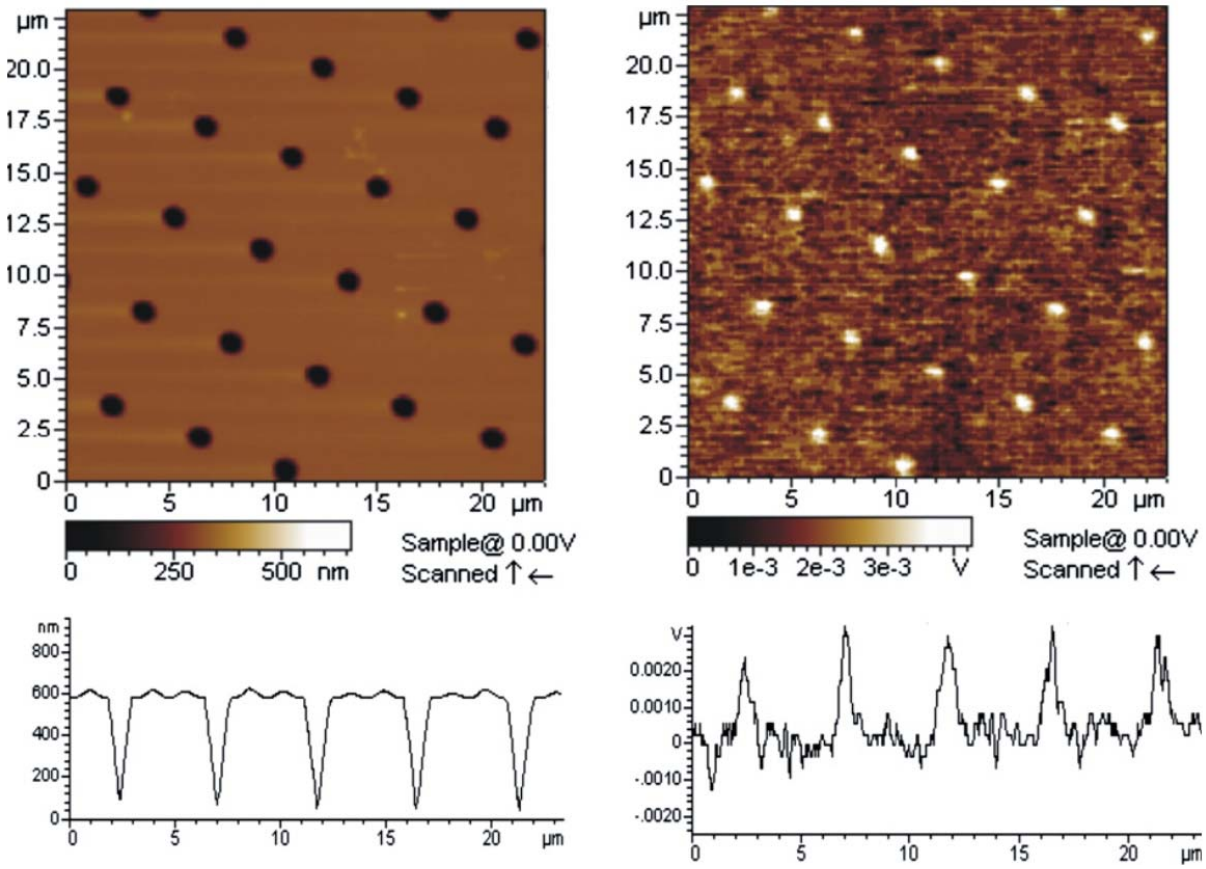

Figure 30. AC-SECM coupled with AFM. Images of periodically microstructured silicon nitride/gold structure with recessed 1 µm gold spots: (left) topography recorded in contact mode; scanned area: 25 · 25 µm; scan speed: 0.1 lines/s, (right) simultaneously recorded AC–SECM image at 14.92 kHz and 110 mVpp superimposed onto a 100 mV DC bias applied to the tip-integrated WE in 1 mM KCl. Adapted with permission from K. Eckhard et al., *Electrochem. Commun.* 9, 1311–1315 (2007). Copyright 2007 Elsevier B.V.

3.3.2 AC-SECM for local impedance measurement and scanning impedance microscopy, SEIM

So far only the use of AC-current measurements as a distance regulation mechanism have been considered, however, AC-SECM can also be used in the fixed height mode to carry out local impedance measurements, or to image the conductivity or reactivity of a sample. For example, it was shown that fixed height AC-SECM imaging reveals not only cell topography but also local variations in impedance linked to cell activity *e.g.* cell wall oscillation or release of metabolites [204]. Fixed height AC-SECM imaging was also used to image the reactivity of composite substrates such as model Pt-microband electrode arrays (25 µm width) [205] and recessed Pt UMEs (cavity electrodes, 60 µm in diameter) [197]. In this later case, amperometric

feedback and AC-impedance (electrolyte resistance) images were acquired simultaneously and displayed similar resolution of a few microns.

AC-SECM can equally be used to characterize the local impedance property of complex materials, for example to evidence localized hydrogen charging of aluminum alloys [194]. Studying the frequency dependence of the AC-SECM signals further extends the possibility of this technique by enabling local impedance *spectra* to be recorded [206–209]. Such a combination of AC-SECM with local impedance spectroscopy has been termed scanning electrochemical impedance spectroscopy (SEIM), and proposed as a new tool to study corrosion processes [210]. It has been employed to study electrochemical heterogeneities of iron oxide (hematite) surfaces at the µm scale [211], but also shown to be suitable for characterizing ultrathin (molecular) films on conducting surfaces. [212] Yet, SEIM is not limited to corrosion or material studies, indeed Ramanavicius et al. showed that it could be also successfully used to characterize the activity of glucose oxidase immobilized on a non-conducting surface [213]. Enzymatic activity was then sensed via changes in the impedance spectra resulting from the accumulation of the enzymatic reaction products. This study exemplified the possibilities opened by SEIM for the investigation of biosensor and biofuel surfaces.

A major limitation of SEIM is that varying (scanning) the frequency of the sinusoidal perturbation superimposed to the tip or substrate potential for recording an impedance spectrum at every tip position is very time-consuming. To address this issue, Ramanavicius et al. implemented fast Fourier transform electrochemical impedance spectroscopy (FFT-EIS) for SEIM [214–216]. In FFT-EIS 30-50 perturbation frequencies are simultaneously applied and the impedance data collected, so that FFT-EIS/SECM combination enables full impedance spectra to be rapidly collected at every tip position. This hybrid technique was used to investigate the electrochemical activity of yeast cells, in the presence of lipophilic vitamin K3 and hydrophilic vitamin K1 as redox mediators [217].

3.4 Optical feedback for distance controlled SECM

In an original approach, Willets, Zhang et al. reported the use of 3D Super-resolution optical imaging for visualizing and calculating the tip-substrate separation in SECM. [218] Their strategy relies on introducing two fluorescence emission sources, one at the substrate surface and the other at the SECM tip. In the latter case the source can be a fluorogenic reaction occurring at the tip, or a fluorescent nanoparticle (nanodiamond) attached to the glass sheath, in the former case a fluorescent bead is simply attached to the substrate. The substrate has to be transparent and placed onto an inverted microscope. The fluorescent sources are simultaneous visualized on the optical image acquired. By passing the emitted light through a special phase mask, the fluorescent sources were made to appear as two lobes forming an angle that depended on the distance separating them from the focal plane of the objective. The tip-to-substrate distance can thus ultimately be determined, with an accuracy of 25 nm over a dynamic range of 2 μm.

4. COMBINATION OF SECM WITH OPTICAL and SPECTROSCOPIC TECHIQUES

4.1 Scanning Electrochemical Microscopy-PhotoElectrochemical Microscopy (SPECM)

Coupling of SECM with photoelectrochemical microscopy (PEM) was originally described by Smyrl et al. and given the abbreviation SPECM [219,220]. Scanning PEM is a surface characterization technique which involves rastering a small spot of light across a surface while recording the total electrochemical current from the entire sample. The light spot, which is the effective local probe, is either focused laser light or light passed down an optical fiber. PEM is typically used to characterize semiconducting surfaces; the light spot produces a photocurrent by driving locally an electroassisted reaction at the surface. The photocurrent is plotted as a function of spot position to create a map of the electronic properties of the semiconducting surface.

To combine PEM with SECM a combined probe needs to be fabricated which can serve both as a SECM tip electrode and a light source. This is typically achieved by coating an optical fiber with a gold layer which is subsequently insulated. Exposing the end of the modified fiber yields a gold ring-electrode surrounding the fiber core. By recording the tip current (SECM) additional information regarding the local light-triggered photoelectrochemical reactions at the substrate can be obtained. For example the tip can be used as a collector to detect and identify products from the local surface reaction.

In the original paper from Smyrl's group a combined SECM/PEM tip probe was fabricated from a standard 50 μm diameter quartz optical fiber (125 μm cladding) which was coated with 15 μm gold and insulated by a 10 μm thick polyimide layer [219,220]. The fiber was cleaved and polished. The outer diameter of the overall cylindrical combined probe was thus quite large (175 μm), the external and internal diameters of the ring microelectrode were respectively, 155 μm and 140 μm. The probe was positioned approx. 40 μm above a Ti/TiO_2 substrate surface and rastered in constant height mode in a Br^- containing solution. Illumination of the TiO_2/Ti substrate by a 351 nm laser light guided through the fiber microelectrode initiated the local photooxidation of Br- at the surface. The produced Br_2 was collected at the gold ring electrode and reduced back to Br^-. Simultaneously acquired tip current (SECM) and substrate current (PEM) images allowed pitting precursor sites, a few tens of microns in size, to be identified on the Ti/TiO_2 surface.

In order to increase the resolution of SPECM the Smyrl group reported a technique to prepare micron-sized SPECM probes [221]. This involved chemically etching the optical fiber in dilute HF solutions to form a cone-shaped apex ~1 μm in size. The etched fiber was sputter-coated with a ~1 μm thick layer of gold and insulated with varnish. The disk-shaped gold ring electrode surrounding the fiber core was exposed by polishing. The final tip diameter of the gold probe, 3 – 5 μm, was very substantially reduced compared to previous work. Even though electrochemical characterization of the probes revealed imperfect insulation, these probes were

successfully employed for PEM and SECM imaging of a titanium surface. Since these initial reports SPECM has been used by several groups to gain insights into the mechanism of corrosion of metals and alloys [132,222].

Bard's group also reported the use of SPECM for rapid screening of photocatalysts [223,224]. Here, photocatalysts with different compositions were deposited as ~300 μm spots on a conducting glass substrate. Typically, these spots consisted of iron oxide doped with various metals (Ag, Pd, Eu, Rb). Under illumination the anodically biased spots catalyzed the oxidation of water (1M OH^-). In PEM mode, a fiber optic was scanned over the substrate and the performance of the spots could be evaluated by measuring the photocurrent at the substrate. In a SPECM configuration the product of water photooxidation (O_2) was also detected at the combined optical fiber/ ring electrode probe. For both configurations, fixed height mode was used (~50 μm) and the combined probes were unsharpened optical fibers. Due to the large number of spots which could be deposited and analyzed, this methodology constitutes an effective way to quickly identify metallic combinations which yield high photocatalytic effects.

In the last decade application of SECM to screen the activity of photocatalysts has been blooming [225–232]. this topic is reviewed in chapter 13 of the present book.

SPECM has also recently been extensively employed to study biophotocathodes, comprising natural photosystems I and II. Photosystem I (PSI) is a photosynthetic membrane protein complex that, in nature, utilizes light to generate electrons needed for producing the energy carrier NADPH, while simultaneously oxidizing plastocyanine. These reduction and oxidation reactions occur at distinct sites of PSI, labeled FB^- and P700, respectively. Schuhmann et al. integrated PSI into a redox hydrogel deposited on an electrode surface in such a way that the oxidizing P700 site was efficiently wired to the electrode via electron hoping between the gel-bound redox sites (**Figure 31**) [233].

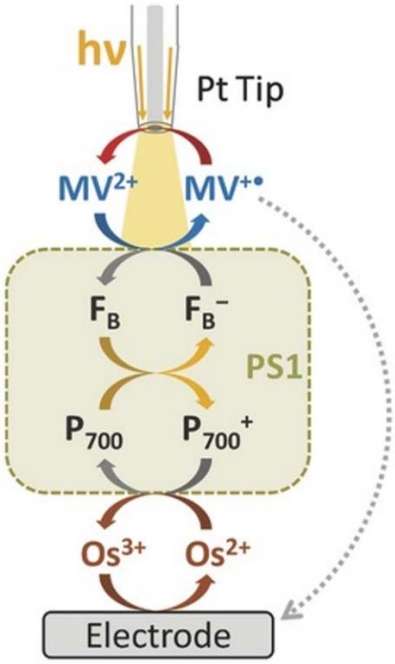

Figure 31. SPECM interrogation of Photosystem 1 (PS1) embedded in an osmium(Os)-based redox polymer deposited on an electrode surface. The sheath of the disk-in-glass SECM tip is used to convey light to locally trigger the photoactivity of PS1. A high energy electron is generated at the FB^- site of PS1 and a hole at its P700 site. Electrons propagate from the supporting electrode to the P700 site, by hopping between the osmium sites of the redox polymer. Concomitantly, an artificial electron acceptor species introduced in solution, methyl viologen (MV^{2+}), is reduced at the FB^- site to $MV^{+\cdot}$. The tip UME is biased to detect this later species. Reproduced with permission from F. Zhao et al., *Small* 13, 1604093 (2017). Copyright 2017 Wiley VCH.

A disk-in glass SECM UME was used as a light source (the glass sheath playing the role of a wave guide), to locally trigger the photoactivity of PSI, and also to collect the species formed at the FB^- site. Precious insights into the electron transfer processes associated with the activity of PSI could then be acquired by relating the UME current to the photocurrent recorded

at the substrate electrode. For example, when methyl viologen was added as a terminal electron acceptor for FB^- a charge recombination process (oxidation of reduced viologen at the substrate) could be evidenced [233]. In the absence of added electron acceptor, oxygen consumption and associated H_2O_2 production by PSI could be simultaneously evidenced using a dual UME. [234] In another set of experiments, platinum nanoparticles were attached near the FB^- site [235]. In this configuration H_2 was detected at the UME, evidencing via-PSI photocatalyzed reduction of H^+ at the Pt particles. For a more sensitive detection of H_2 the UME was later functionalized with a hydrogenase wired by a viologen-modified redox polymer [236]. Finally, the same SPECM configuration was also used to evaluate the performance of a photobioanode consisting of photo system II embedded into an osmium complex-modified redox polymer [237]. In nature PSII photocatalyses the 4 electrons oxidation of water into oxygen. Here an UME both locally illuminated the sample and collected oxygen. The use of a dual UME, capable of detecting O_2 and H_2O_2, evidenced the existence of a competing charge transfer pathway in the PS2 complex, resulting in incomplete oxygen reduction.

As a final word to the subject matter, it is worth mentioning that probe design for SPECM has been very recently reviewed in great length [238].

4.2 Scanning Electrochemical Microscopy - Scanning Optical Microscopy (SECM-OM)

The idea behind combining SECM with scanning optical microscopy is to be able to simultaneously probe the local electrochemical and the optical properties of interfaces at high spatial resolution. To accomplish SECM-OM a combined probe which can serve as a light source and as a microelectrode is required. To build an optical image, light transmitted through the substrate has to be detected, using, for example, a photomultiplier (PMT) placed under the substrate, **Figure 32** (left). Optical fiber / ring microelectrode combined probes, initially designed for SPECM (section 4.1) [219], are also suitable for SECM-OM, as shown in **Figure 32** (right).

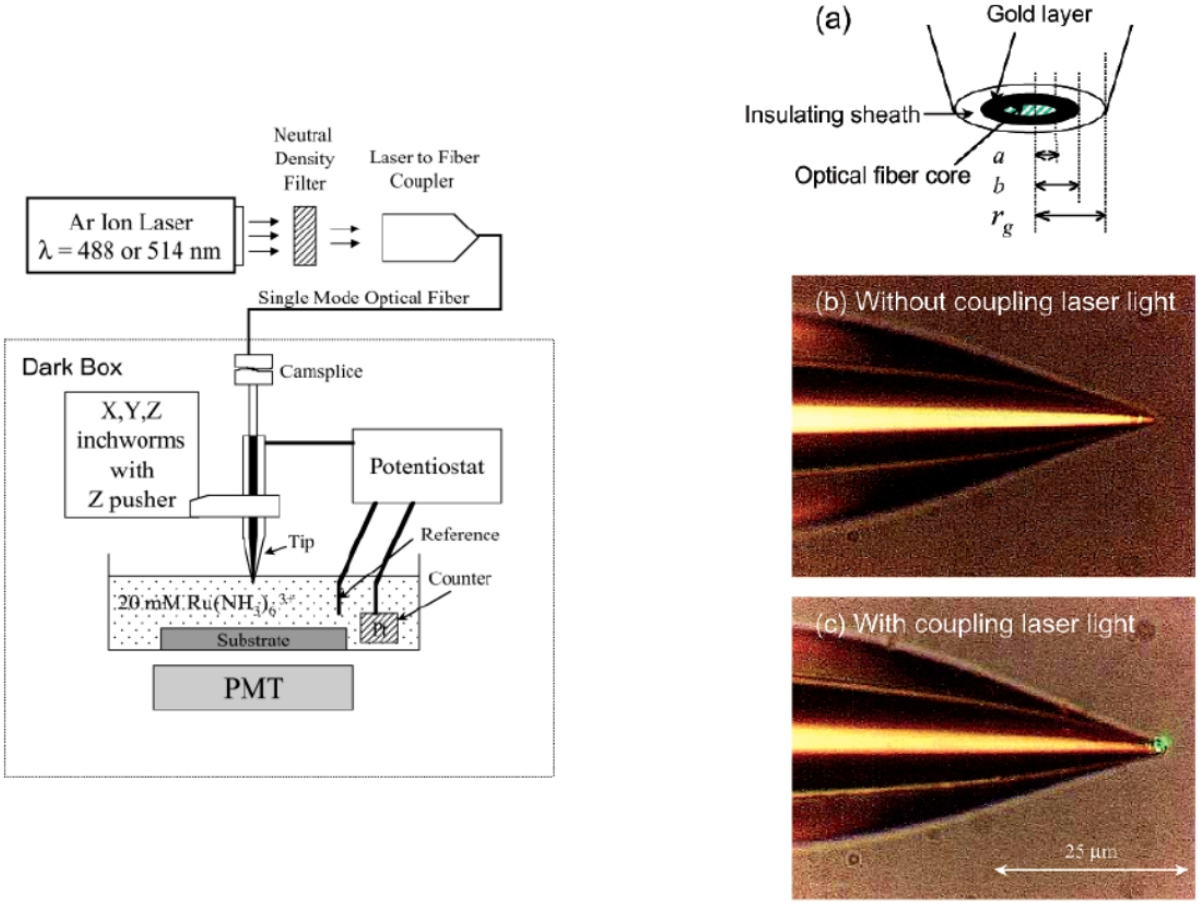

Figure 32. (Left) Block diagram of an experimental setup for combined scanning electrochemical and optical microscopy (SECM/OM). A photo multiplier tube (PMT) is positioned below the (partly transparent) substrate. (Right) (a) Schematic diagram of an ideal optical fiber/microelectrode tip for SECM/OM: A sharpened optical fiber bearing a ring-shaped microelectrode at its apex. Optical microscopy images of an anodic paint insulated combined SECM/OM tip (b) without and (c) with coupling of Ar ion laser light at 514 nm. Reproduced with permission from Y. Lee et al., *Anal. Chem.* 74, 3626-3633 (2002). Copyright 2002 American Chemical Society.

In developing SECM-OM the aim is to achieve < 100 nm resolution (as with NSOM) and thus ultra-small SECM-OM probes are required. Bard's group reported the fabrication of a combined probe with ring electrodes less than 1 µm in diameter (**Figure 32 b,**c) [239]. The procedure included (i) heating and pulling optical fibers using a laser puller, so that pulled fibers with a sharp conical apex were produced. (ii) Vacuum evaporating a thin gold film on the pulled fiber (~50-100 nm gold). (iii) Insulating the whole coated fiber body by electrophoretic deposition of an anodic paint, followed by heat curing at 150 °C. The insulating layer shrinks during this last heating step so that the sharp gold coated extremity of the tip is selectively exposed, while the rest of the tip surface remains insulated. These combined probes were

thoroughly characterized by CV and by recording SECM approach curves at both conducting and insulating surfaces. The voltammetric response of these probes was shown to be ideal, while SECM approach curves confirmed the ring shape of the gold microelectrode and allowed the outer and inner radii of the ring to be measured.

The imaging capability of the SECM-OM probes was tested using an interdigitated array (IDA) electrode which contained 30 μm gold bands spaced by 25 μm glass gaps. The solution contained 20 mM $Ru(NH_3)_6^{3+}$ as redox mediator in 0.1 M aqueous KCl. The SECM-OM fiber probe was approached toward the IDA substrate until an SECM feedback current was recorded corresponding to a tip-substrate separation of ~1 μm. Imaging was carried out in the fixed height mode.

An SECM electrochemical image and an optical image, obtained by plotting the intensity of the light transmitted thought the IDA as a function of the probe position, were simultaneously recorded, **Figure 33**.

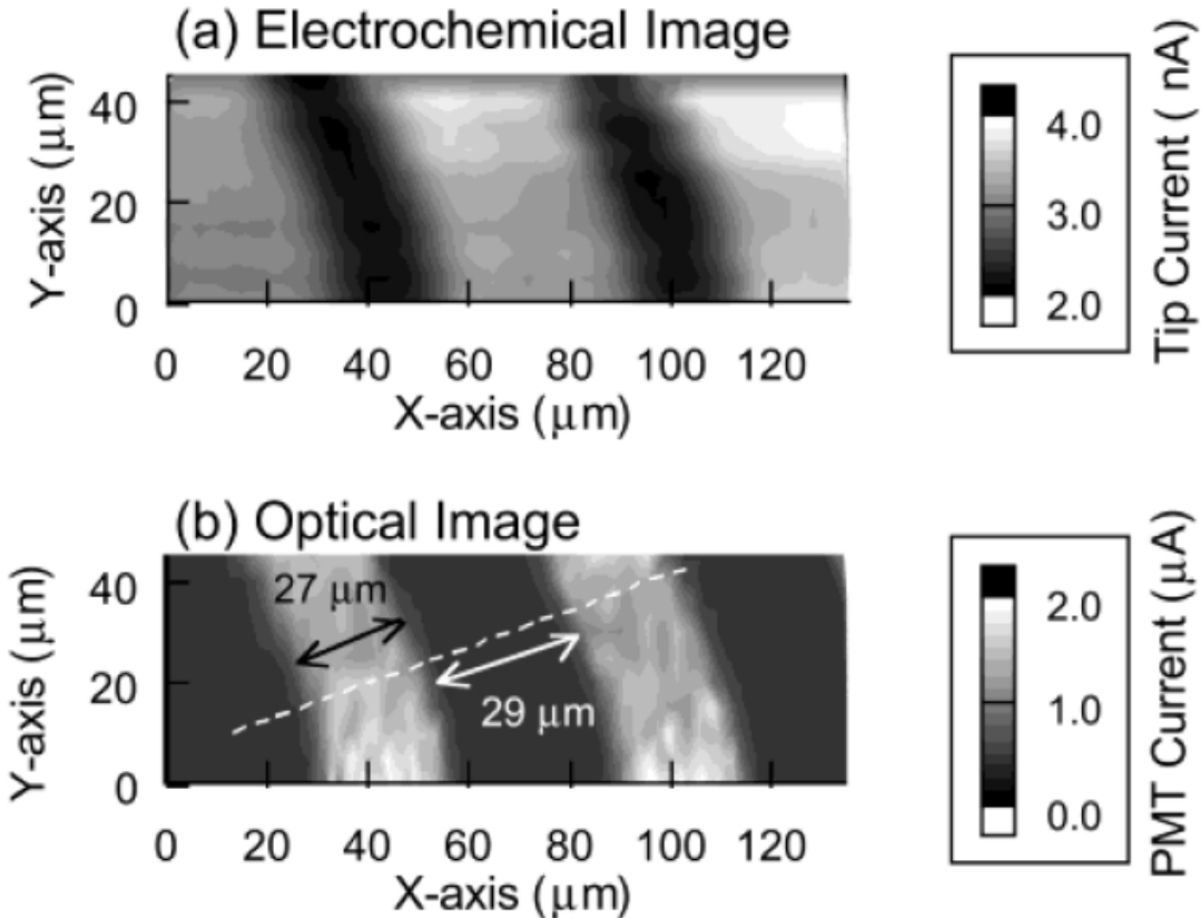

Figure 33. SECM/optical microscopy images of band microelectrodes (IDA electrode) acquired using

an optical fiber / microelectrode tip in the fixed-height mode. Simultaneously obtained (a) electrochemical and (b) optical images (d = 1 μm over the bands). Scan speed was 1 μm/s. Fiber apex (r_g) = 1. 75 μm. Reproduced with permission from Y. Lee et al., *Anal. Chem.* 74, 3626-3633 (2002). Copyright 2002 American Chemical Society.

As expected, positive and negative SECM feedback responses were recorded respectively when the tip was above a gold band or the glass interband spacing. The optical image correlated well with the SECM feedback image, showing dark and white areas respectively for the gold (opaque) and glass (transparent) bands. Hence the principle of acquiring SECM-OM images of microstructures was validated. Even though the width of the gold bands and glass spacing measured from the optical image matched relatively well with the actual IDA dimensions, the achieved spatial resolution was limited by the use of fixed height imaging.

In order to increase the imaging resolution, Bard and co-workers later modified their SECM-OM set-up to add a shear force based distance regulating mechanism, enabling constant distance imaging [173], as discussed in **section 3.1.2**. Three images were simultaneously obtained by plotting the following recorded data as a function of tip position, as shown in **Figure 34**.

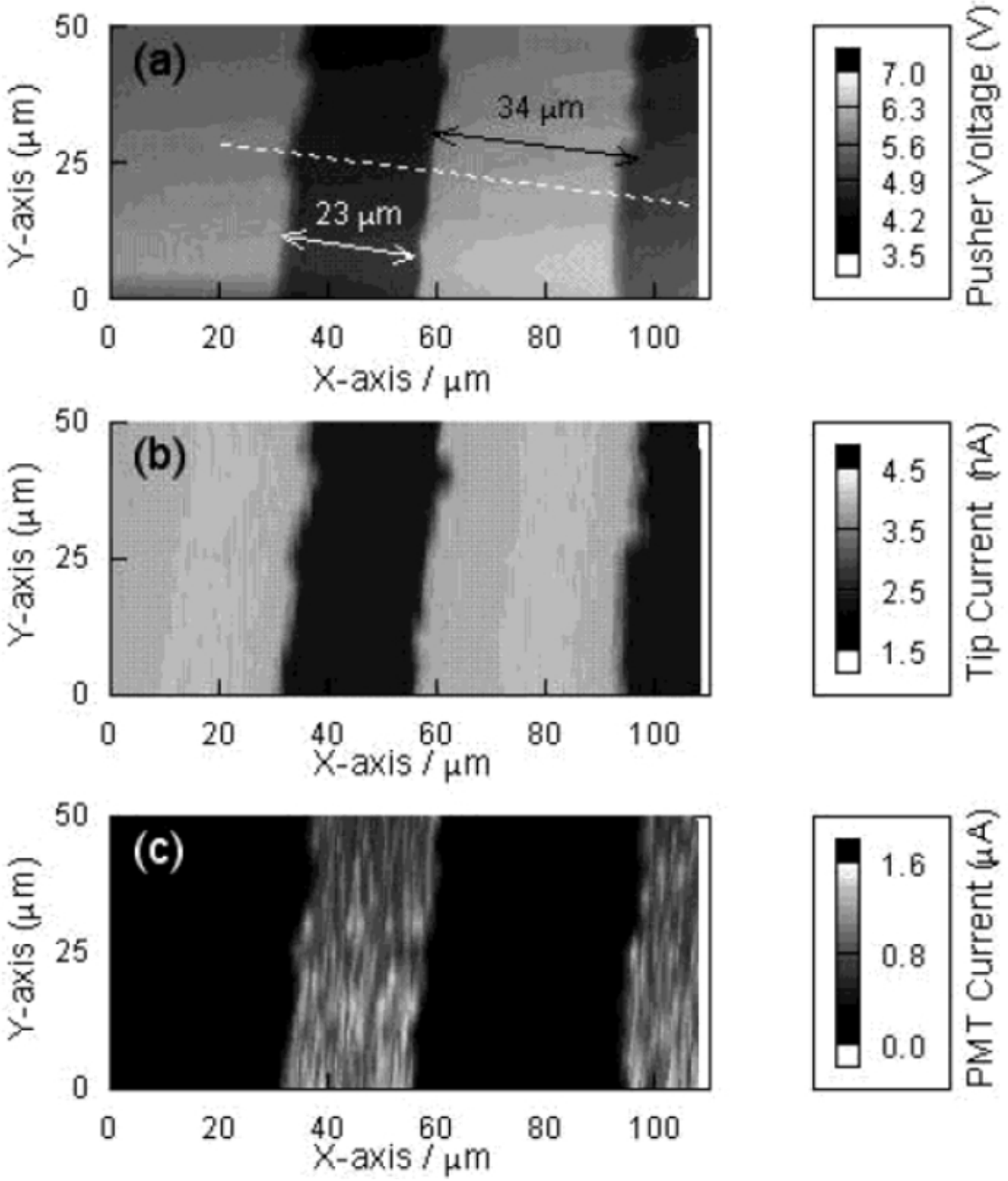

Figure 34. SECM/optical microscopy images of band microelectrodes (IDA electrode) acquired using an optical fiber / microelectrode tip in the constant-distance mode. Constant distance was maintained using shear force feedback. Simultaneously obtained (a) topographic, (b) electrochemical, and (c) optical images over an IDA electrode: 30-µm gold bands spaced by 25-µm glass. Fiber apex (r_g) = 1. 75 µm. Scan speed was 1 µm s^{-1}; 5-mV pusher voltage corresponds to 8 nm of distance change. Reproduced with permission from Y. Lee et al., *Anal. Chem.* 74, 3634-3643 (2002). Copyright 2002 American Chemical Society.

(1) The voltage applied to the piezoelectric pusher to bring the tip in "contact" with the surface *i.e.,* enabling a topographic image to be constructed. (2) The tip SECM current image,

providing a map of the electrochemical reactivity of the substrate, free from any topographic artifacts. (3) Light intensity data providing a map of the optical properties of the substrate.

This SECM-OM imaging technique was validated by acquiring simultaneously high resolution topographic, electrochemical and optical images of an IDA structure (30 μm wide gold bands separated by 25 μm wide glass gaps). It was observed that softer samples, such as diatoms immobilized on glass, could not be imaged using the reported tapping mode-like scanning mode, attributed to the strong interaction forces occurring between the vibrating tip and the diatoms. As an alternative to the tuning fork signal the SECM feedback current was used to regulate the tip sample separation, *i.e.,* imaging was carried out in constant-current-mode. Since SECM is a non-contact mode of imaging, deformation of the cell by the tip was fully avoided and simultaneous topography and optical images of live diatoms could be obtained.

An SECM-OM set up specifically designed to allow imaging of biological material was later developed in Matsue's group [175]. The combined optical fiber-microelectrode probes were based on laser-pulled fibers, coated with Ti/Pt by sputtering and subsequently insulated with a 900 nm thick layer of vapor deposited Parylene C. The electroactive area of the probe was created by blowing hot air (450°C) vertically toward the probe apex using a heat gun. The radius of curvature of the probe including the insulator was ca. 250 nm. The precise shape of the electroactive area of the probe could not be determined, but an electrochemical apparent radius of ~35 nm was determined form recording CVs at the probe. Combined SECM-OM constant distance images were acquired using shear force distance feedback.

Similar to Bard and co-workers approach, [172] the probe was initially brought in close "contact" with the substrate, using damping of the shear force oscillation to sense the surface, and retracted before electrochemical or optical data were acquired. This mode was labeled STA for standing approach mode [172], as discussed in **section 3.1.2**. The possibility of acquiring topographic images of live cells in STA mode using a glass fiber was also demonstrated,

indicating that with the reported shear force-based step up destructive tip-cell surface interactions were minimal. Finally, in a fully integrated configuration, simultaneous topographic, electrochemical and optical images of an IDA structure composed of alternating gold bands and glass gaps each 5µ µm wide were acquired, **Figure 35**.

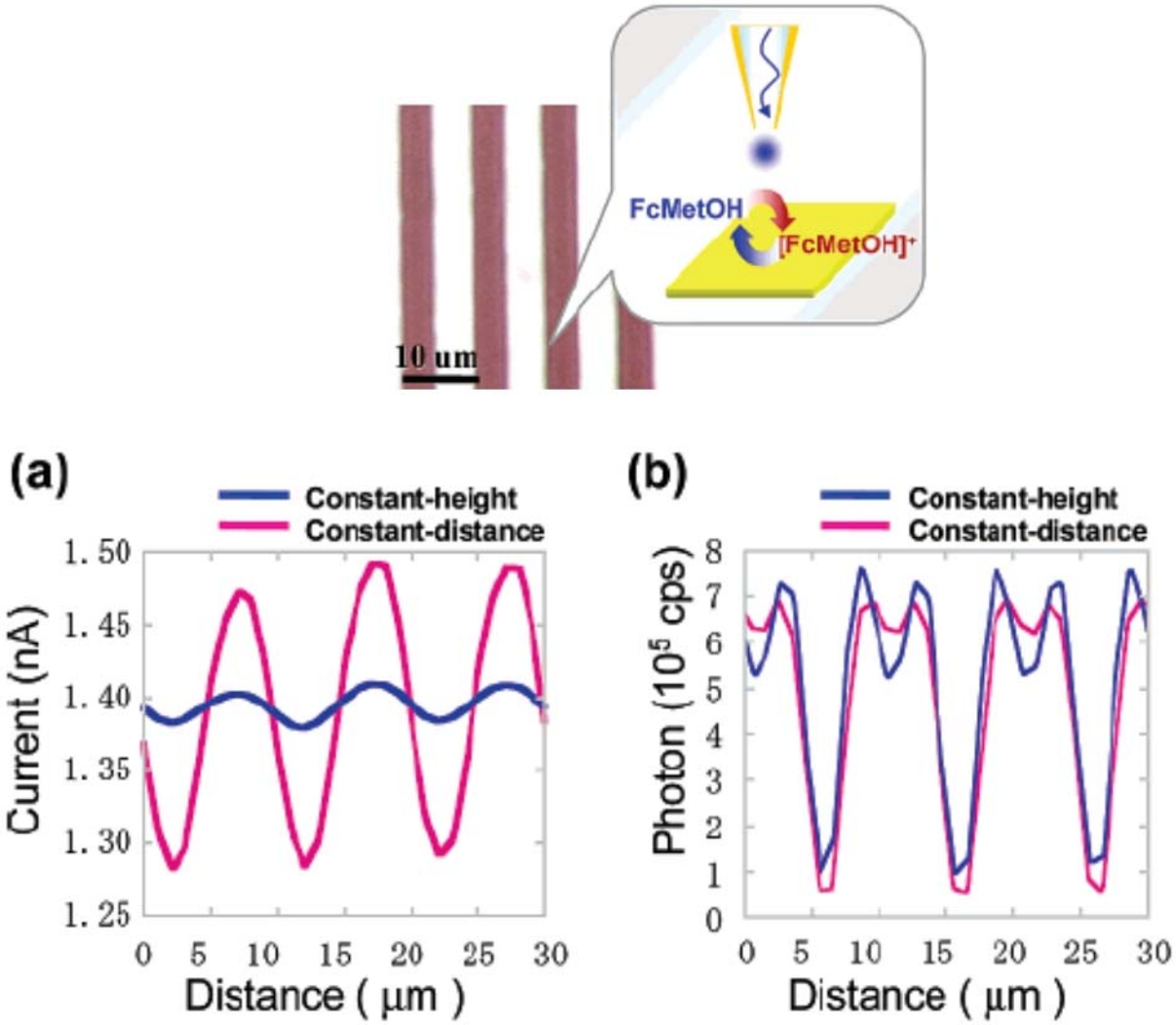

Figure 35. Comparison of the resolution achieved in constant height versus constant distance SECM/OM imaging of a Au band array. Current (a) and Optical (b) line scans recorded in constant height (blue traces) or constant distance (STA) mode (pink traces). The approximate size of the optical fiber microelectrode probe was 6.5 µm. Probe potential of +0.50 V (vs Ag/AgCl) in 0.5 mM FcMeOH, 0.1 M KCl. Adapted with permission from Y. Takahashi et al., *Langmuir* 22, 10299-10306 (2006). Copyright 2006 American Chemical Society.

Subsequently, Matsue's group described an improved SECM/OM setup allowing the simultaneous capture of electrochemical, fluorescent and topographic images of immobilized cells [176]. The authors improved their probe fabrication technique by using an ion beam to mill the apex of the probe to expose a better-defined sub-micron sized electroactive ring-shaped

area. This also had the effect of giving the tip apex a flat disk-like shape thus increasing the SECM feedback sensitivity of the probe. The shear force distance regulation was also optimized. In particular, the effect of the tuning fork free excitation amplitude on the tip-cell wall interaction was studied. It was shown that, provided a low enough tuning fork amplitude was used, shear force regulation could be safely employed to image living cells, **Figure 26**. Constant distance imaging was carried out in STA mode [174].

Simultaneous topography and fluorescent images of cells expressing the green fluorescent protein (GFP) was demonstrated. Simultaneous detection of topography, fluorescence and electrochemical activity was also demonstrated by imaging cells expressing both GFP but also secreting alkaline phosphatase, **Figure 36**.

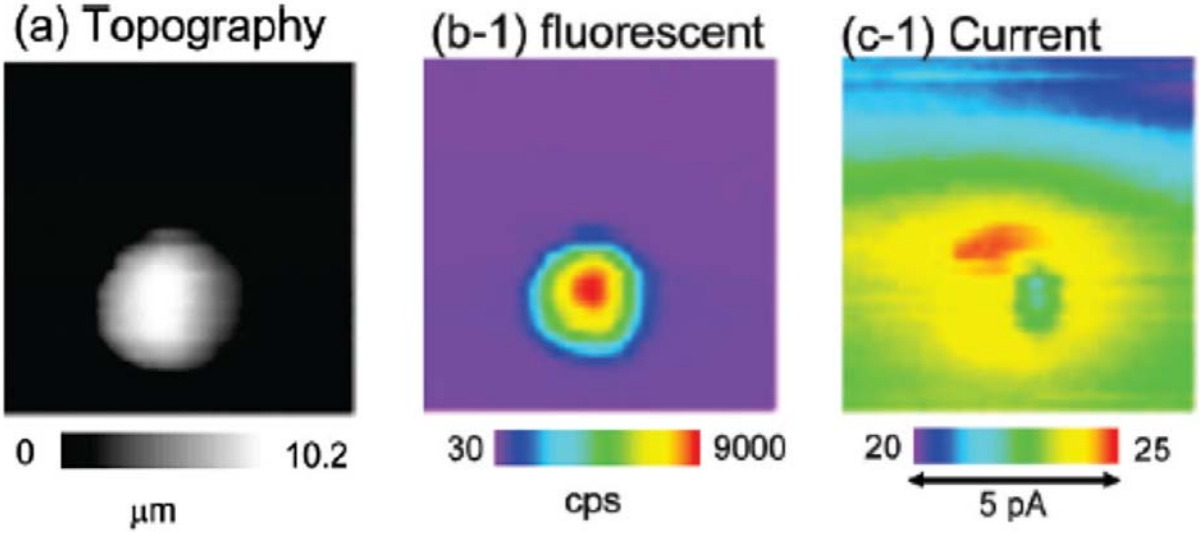

Figure 36. Simultaneous topographic (a), fluorescent (b-1), and electrochemical (c-1) images of a GFP (green fluorescent protein) - and SEAP (secreted alkaline phosphatase)- transfected single HeLa cell obtained in the constant-distance mode. The cell both expresses GFP and excretes the enzyme alkaline phosphatase. The combined SECM/OM tip, an optical fiber bearing a ring-shaped microelectrode at its apex, excites the fluorescence of GFP and collects the electroactive enzymatic product (*p*-aminophenyl). A tuning fork is used as a shear force transducer. The scan rate was 3 μm/s. The scan range was 40 μm × 40 μm, and the step size was 1.0 μm. Adapted with permission from Y. Takahashi et al., *Anal. Chem.* 81, 9674-9681 (2009). Copyright 2009 American Chemical Society.

The enzyme substrate PAPP (P-aminophenol phosphate) was added into the medium. Phosphatase liberated by the cell catalyzed the conversion of PAPP into p-aminophenol which was detected amperometrically (oxidized) at the tip. Hence in this work two proteins reporting gene cellular expression were simultaneously detected at the single cell level using SECM-OM.

Further improvement in SECM-OM includes optimizing the combined probe fabrication technique to yield probes of nanometer dimensions. This would improve the spatial resolution of SECM-OM and ultimately lead to NSOM-SECM. In this respect it is noted that the fabrication of nanometer-sized optical fiber electrode based on selective etching of fibers has already been reported [240].

4.3 Scanning Electrochemical Microscopy - Electrogenerated Chemiluminescence (SECM-ECL)

4.3.1 Using the SECM tip as a light source for Scanning Optical Microscopy

One motivation for coupling SECM with ECL is to be able to use the SECM tip as a controllable light source which locally illuminates the sample surface. To achieve this, the tip is biased so as to trigger an electrochemical reaction which produces light by chemiluminescence. The sample surface has to be at least partly transparent, and the emitted light is collected by a PMT tube located below the substrate. The ECL intensity measured by the PMT can then be plotted as a function of the tip position to form an image which reflects the local optical properties of the substrate *e.g.,* its absorbance. The setup is similar to the one used for SECM/Optical Microscopy described above in section 4.2.

One of the interests of using an SECM tip instead of a metal-coated fiber-optic probe as a light source is that preparation of the SECM tip is comparatively easier. Additionally, no laser is needed to illuminate the tip apex which avoids heating of the sample or tip. Moreover, the SECM tip current can provide feedback for positioning the light source in close proximity to the substrate surface. The first description of SECM-ECL in a scanning optical microscopy configuration was reported by Bard and co-workers [241]. In this pioneering work the choice of the tip-triggered ECL reaction was discussed together with the effect of tip-substrate distance on light emission.

Two kinds of ECL generating reactions were considered. The first one involved the annihilation of $Ru(bpy)_3^{3+}$ and $Ru(bpy)_3^{+}$ sequentially generated at the tip from the solution species $Ru(bpy)_3^{2+}$, by applying potential pulses (between +1.6 and -1.4 V versus SCE). The tip generated $Ru(bpy)_3^{3+}$ and $Ru(bpy)_3^{+}$ species encounter in a reaction zone located close to the surface of the tip electrode. A high energy electron transfer process takes place between these species, generating the excited species $Ru(bpy)_3^{2+*}$, which emits light upon deactivation. Due to the large tip potentials applied a non-aqueous solvent, such as acetonitrile, is required.

When the tip was approached towards an insulator the ECL intensity was observed to be steady until the tip was within a few tenths of the tip radius away. A sharp drop of the ECL intensity was recorded upon closer approach due to hindered diffusion of the ruthenium species in the tip-substrate gap. When the tip was approached toward a conducting substrate the ECL intensity was shown to again remain nearly steady until the tip-substrate separation distance was ~0.3 times the tip radius. For such a close tip-substrate separation, electron transfer at the conducting substrate competes with the annihilation reaction and limits the ECL intensity. However, the tip could be brought close enough to a test IDA substrate for a scanning optical image to be acquired. The resolution was limited to the micron range due to the relatively large tip size and tip-substrate spacing; ~ 5 μm disk-in-glass tip held at a constant height of 25 μm over the substrate.

The possibility of generating ECL from the co-oxidation of $Ru(bpy)_3^{2+}$ and tri-n-propylamine (TPrA) for combined SECM-ECL was also investigated. In this co-reactant ECL scheme the tip potential is set at a sufficiently anodic potential to oxidize both $Ru(bpy)_3^{2+}$ and TPrA. The ensuing reduction of the $Ru(bpy)_3^{2+/3+}$ species by the highly reductive radical species produced by TPrA oxidation ultimately results in the formation of the light emitting $Ru(bpy)_2^{2+*}$ species [242]. Compared to the annihilation reaction [241], this ECL reaction has the advantage of not requiring pulsing of the tip potential. Moreover, the ECL reaction takes place in a very thin reaction layer around the tip surface and is not broadened by diffusion of the reactants away

from the tip. This also allows for very close tip sample separations without interference from SECM feedback *i.e.,* the presence of the substrate.

The use of the TPrA - $Ru(bpy)_3^{2+}$ co-reactant scheme for generating ECL in acetonitrile was shown to result in rapid tip fouling which is problematic. However, in a following paper Bard and co-workers demonstrated that very stable ECL signals, enabling SECM-ECL imaging, could be obtained using the $Ru(bpy)_3^{2+}$ / TrPA system in an aqueous medium [172]. Using conically etched sub-micron sized Pt UMEs as tips the authors also considerably improved the resolution of SECM-ECL, reaching a resolution close to that achieved with NSOM, *i.e.,* of the order of ~ 100 nm, **Figure 37**.

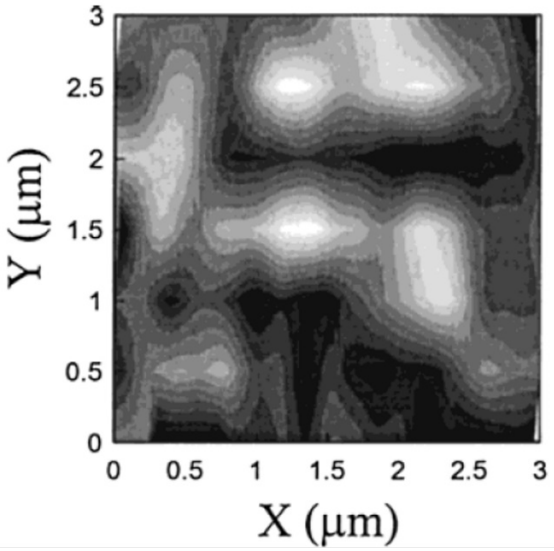

Figure 37 SECM/ECL near-field image of a test sample containing sub-micrometer holes. The tip was a conically etched Pt wire, insulated by an electrophoretic paint, and displaying a 172-nm effective diameter. ECL emission at the tip was triggered by biasing the tip at 1.2 V in a $Ru(bpy)_3^{2+}$/TPrA containing aqueous phosphate buffer solution (pH 7.5). A tuning fork-based shear force detection scheme is used to hold a constant tip-substrate distance during imaging. Data acquisition time, 8 min. Adapted with permission from Y. Zu et al., *Anal. Chem.* 73, 2153-2156 (2001). Copyright 2001 American Chemical Society.

As it was necessary to place the tip very close to the substrate, a shear force-based feedback had to be used to control the tip-substrate distance with sub-micrometer resolution. The cone shape of the Pt tip limited the effect of hindered diffusion of the ECL reagents to the tip surface which, in the case of disk-in-glass electrodes, decreased ECL intensity for insulating substrates at close tip-substrate separation.

At about the same time, Wightman and colleague described an alternative ECL system for scanning optical microscopy [243]. In this work 9,10-dihenylanthracene (DPA) and benzonitrile (BN) were respectively oxidized and reduced at a microelectrode which was alternatively biased at anodic and cathodic potentials. Electron transfer between the tip generated $BN^{\cdot-}$ and $DPA^{+\cdot}$ radicals generated an emissive excited state of DPA which gave out light. BN was not only a reactant but was also used as the solvent.

A conically shaped carbon fiber, with a high aspect ratio, functioned as the microelectrode for these studies. Interestingly, the electrode was not insulated to its very apex as it was demonstrated that ECL emission could be forced to occur selectively at the tip apex by using high frequency (20 kHz) tip potential modulation. With this ECL scheme as one of the reactants was the solvent, the reaction layer, where light is emitted, is located very close to the tip electrode surface. Thus, the presence of the substrate interferes much less with light generation, *i.e.* there is no SECM feedback effect on the ECL intensity. The tip was placed at fixed height above the sample and the substrate was raster scanned in the *x* and *y* dimensions. The absence of a feedback mechanism enabled fast scan rates. The resolution attained was of the order of 600 nm.

Finally it is worth noting that SECM-ECL has been used to investigate the mechanism of ECL emission for the $Ru(bpy)_3^{2+}$ / TrPA and $Ru(bpy)_3^{2+}$ /oxalate systems [242,244].

4.3.2 Detection of enzyme activity by SECM-ECL

The SECM-ECL configuration was also used to image the activity of enzymes immobilized on a surface [245,246]. In particular, the chemiluminescence and topography of a glass surface bearing immobilized enzyme horseradish peroxidase (HRP) were simultaneously imaged. [245] The SECM tip was scanned over the enzyme-bearing surface in a luminol containing solution. The tip was biased so as to generate the enzyme substrate (H_2O_2) by reduction of dissolved oxygen. When the tip passed over an enzyme-containing region the tip–generated H_2O_2 diffused to the immobilized HRP-catalyzed and reacted with luminol to emit

light. The distribution of active enzyme "spots" on the surface was thus mapped by plotting the collected light intensity as a function of the tip position. Since the tip current was not affected by the presence or the absence of the enzyme, but solely controlled by oxygen diffusion, the variation of the current during the (fixed height) scan could be translated into surface topography. Hence dual chemiluminescent and tip current SECM images could be acquired simultaneously without interference.

In a more recent work a similar experimental configuration was used to image the biocatalytic activity of localized GOx-containing surface structures [246]. In this paper the oxidized form of luminol was generated at the SECM tip. When the tip was scanned over active GOx spots light was emitted due to the reaction of oxidized luminol with H_2O_2 produced by the glucose oxidase-catalyzed oxidation of glucose, **Figure 38**.

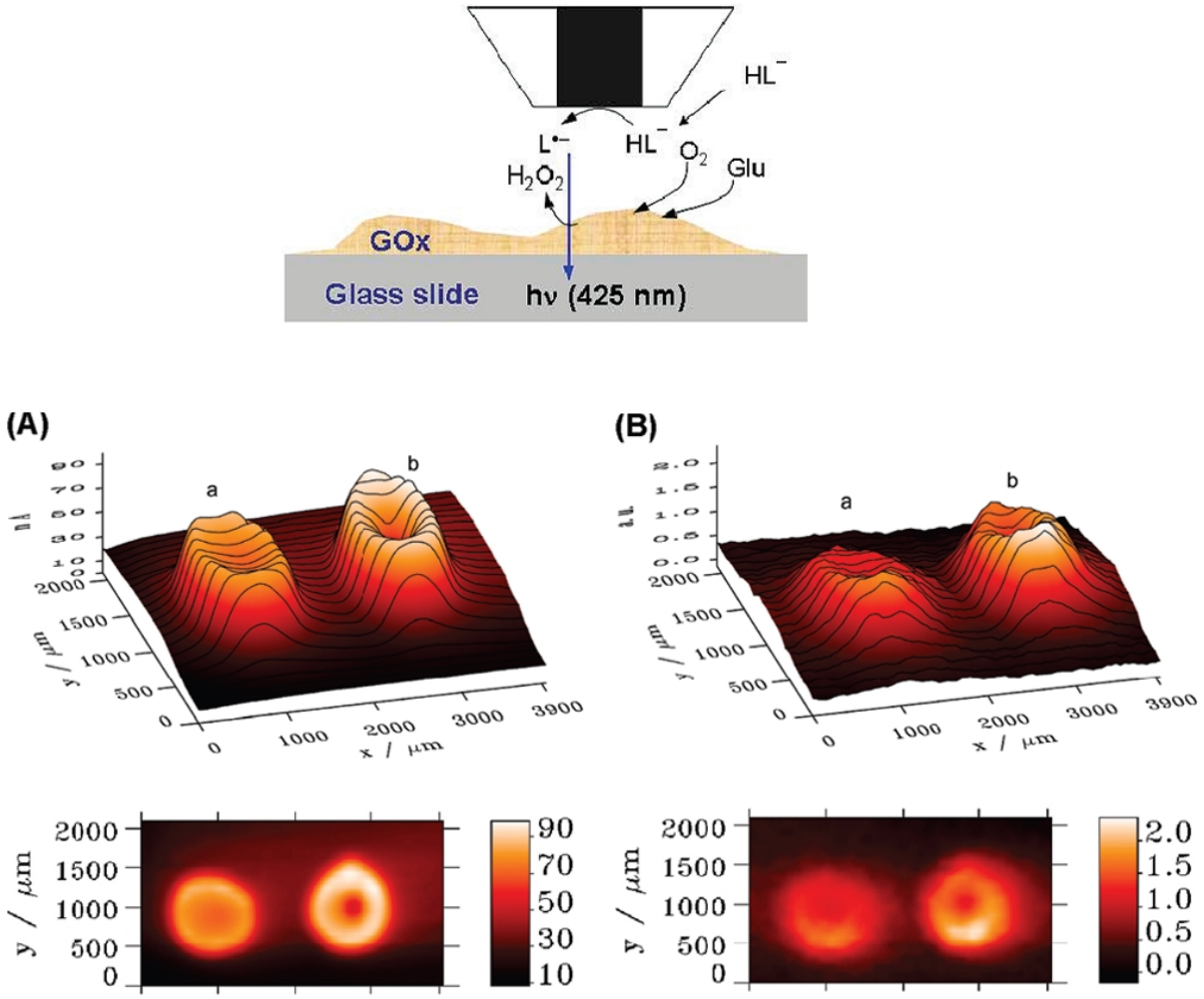

Figure 38. SECM/ECL for studying local biocatalytic activity of enzyme-polymer spots. *Top*: Working principle. The oxidized form of luminol (L^-) is generated at the SECM tip. When the tip is scanned over active glucose oxidase (Gox) spots light is emitted due to the reaction of oxidized luminol with H_2O_2

produced by the GOx-catalyzed oxidation of glucose. *Bottom*: (A) GC-SECM image of GOx-polymer spots in 100 mM glucose and 0.20 M phosphate buffer (pH 6.8); (B) ECL image of the same spots as SECM in 100 mM glucose, 1 mM luminol, and 0.20 M Tris-HCl buffer (pH 8.5) using a 250 μm Pt disk as tip electrode (RG 2.2). Adapted with permission from R. Lei et al., *Anal. Chem.* 81, 5070–5074 (2009). Copyright 2009 American Chemical Society.

Large Pt disk electrodes, 250 μm in diameter, had to be employed due to the limited amount of H_2O_2 generated by the enzyme-catalyzed reaction. To increase sensitivity, the ECL emission was modulated by oscillating the tip potential and using a phase-sensitive lock-in amplifier for light detection.

4.4 Scanning Electrochemical Microscopy – Fluorescence Microscopy

In sections 4.1 – 4.3, the tip was primarily used as the light source, providing the same probe with both spatial optical and electrochemical information. However, there is still much to be gained by mounting an SECM on an optical microscope. At the simplest level an optical microscope can be used to aid positioning of an SECM tip over a feature of interest, for example a single cell, provided it is within the resolution limit of the microscope. By using a fluorescent microscope, it is possible to spatially locate fluorescently active zones on the surface. Hence fluorescent labeling is often employed to aid identification of areas of interest on a substrate.

Taking this approach one step further by using a confocal laser scanning microscope (CLSM) it is possible to obtain higher resolution than any other conventional microscope, especially in the depth (z) direction, due to the reduction of out-of-focus blur [247]. This enables direct, non-invasive serial optical sectioning of objects or profiling of multilayer structures. The ultimate sensitivity is provided by *single molecule* fluorescence spectroscopy which requires both the optical detection volume to be confined to femtolitres and concentration of the analyte of interest to be at the nanomolar and lower level. This can be achieved in two ways: (1) for surfaces, the use of total internal reflection fluorescent microscopy enables single molecules immobilized on a surface to be detected and (2) in solution, a laser beam is focused

to a diffraction limited spot size. When the fluorescent molecules traverse the detection volume a burst of photons is generated. To date there have been many interesting applications of SECM combined with fluorescent microscopy.

4.4.1 Solution studies

Unwin and co-workers used CLSM to quantify three dimensional pH diffusion gradients generated at UMEs in solution [248,249]. Two reactions were studies: (i) the reduction of 1,4-benzoquinone (BQ) in an unbuffered solution of fluorescein; fluorescein exhibits a pH sensitive fluorescence signal. As this process involves the addition of two protons and two electrons, the local consumption of protons, causes the pH to increase locally at the surface of the electrode which in turn causes the fluorescein to fluoresce with greater intensity. (ii) The reduction of oxygen at Pt UMEs and the reduction of water at both Pt and Au UMEs, in unbuffered electrolyte solutions containing fluorescein. Both processes result in the production of hydroxide ions which again causes fluorescein to fluoresce with greater intensity.

Figure 39 shows CLSM profiles for the reduction of BQ as a function of driving potential [249].

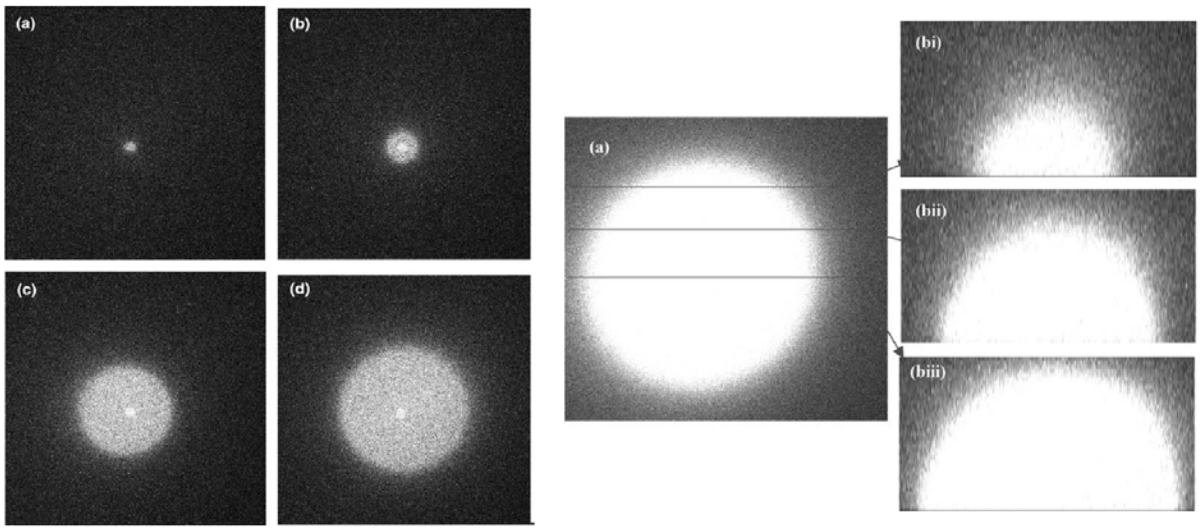

Figure 39: (Left) CLSM images of fluorescence profiles for the reduction of 1 mM benzoquinone in disodium fluorescein solution, at the surface of a 25 μm Pt disc electrode (clearly seen in the center of the image). Potential held at (a) -0.10 V, (b) -0.15 V, (c) -0.20 V, (d) -0.25 V. Image size, 650 μm × 650 μm. (Right) Fluorescence images of an electrode surface at -0.25 V. (a) Two-dimensional x–y image at a distance 2 μm above the electrode. (b i–iii) Cross sections through the x-axis in the z-direction (normal to the electrode surface) of the image (a) at marked distances. This series of x–z-axis scans was taken

over a distance of 200 μm in the z-direction, which is the height scale on these images. Reproduced with permission from S. Cannan et al., *Electrochem. Commun.* 4, 886-892 (2002). Copyright 2002 Elsevier B.V.

As the reaction is driven to more negative potentials the size of the pH dependent diffusion field can be seen, by CLSM, to increase in size, as expected. Taking advantage of the CLSM's ability to cross section in the z direction, it was also possible to map the diffusion profile in 3D. **Figure 39** displays *x, z* profiles recorded in different zones of the 3D pH diffusion profile. Using FEM modeling the experimental observations were found to be in very good agreement with the theoretical predictions [249].

Using CLSM it was also possible to map the pH diffusion profile of an electrode only 80 nm in diameter given that the size of the diffusion field is significantly larger than the size of the active site, thus illustrating the power of the technique for identifying sub-microscopic sites on a surface [248]. For the reduction of oxygen at a Pt UME, FEM modeling showed that the size of the resulting pH dependent diffusion field correlated with the number of electrons, *n*, transferred in the process. In this way it was possible to determine *n* for oxygen reduction at a Pt UME [248].

Finally by coupling SECM with CLSM it was possible to quantitatively measure the permeation of a weak acid through a bilayer lipid membrane (BLM) [250]. Here an UME placed close to a BLM was used to deliver weak acids in a well-defined manner by the electrogeneration of protons in the presence of weak acid anions and fluorescein, **Figure 40**.

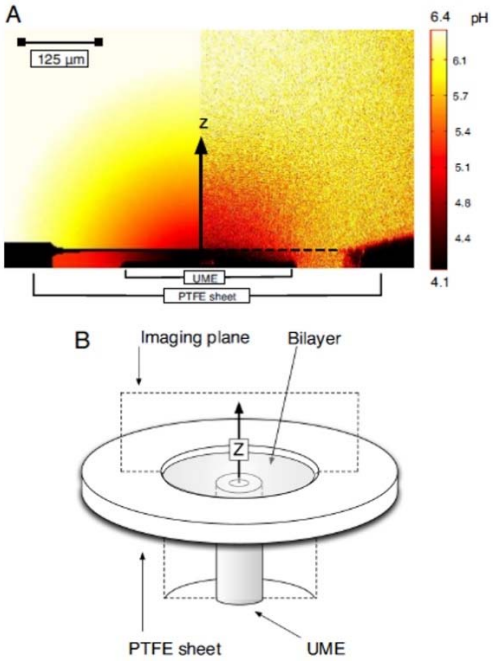

Figure 40: Image and imaging plane for the visualization of electrochemically induced passive transport. (A) Simulated pH profile (Left) and experimental pH profile (Right) for the permeation of hexanoic acid. Bilayer position is marked by a solid line in the simulated profile and a dashed line in the experimental profile. (B) Illustration of the LCSM scan plane with respect to the experimental bilayer. Reproduced with permission from J. M. A. Grime et al., *Proc. Natl. Acad. Sci.* 105,14277-14282 (2008). Copyright 2008 National Academy of Sciences, U.S.A.

The resulting steady-state pH distribution in the vicinity of the UME and on either side of the BLM, visualized using CLSM, was found to be, from FEM simulation, highly dependent on the distribution of the weak acid and the BLM permeation coefficient. Hence by matching experiment to theory it was possible to determine permeation coefficients for a series of aliphatic weak acids. Significantly, the data obtained cast doubt on the applicability of a well-known existing model which had been previously employed to extract permeation values.

In an exciting development Heinze and Börsch combined SECM with single molecule fluorescence spectroscopy (SMFS) to generate space and time-controlled pH gradients in solution, in a similar way to that discussed above. However, here fluorescence detection was

possible at the single molecule level and information was also provided on the real-time behavior of systems in response to pH gradients [251]. The pH dependent fluorophore used in these studies was SNARF-1-dextran. For solution work the optical detection volume was positioned inside the proton or hydroxide generated diffusion field, whilst for pH profiling of fluorophores immobilized on a surface, total internal reflection excitation was employed.

Initial studies focused on generating pH gradients at UMEs of sizes over the wide range 2 nm – 5 μm and mapping the resulting fluorescent intensity either in solution or at a fluorescently labeled surface; for the latter a UME positioned in close proximity provides a local pH gradient. Both the oxidation of nitrite to nitrate (generates protons) and the reduction of BQ (consumes protons) where employed to generate pH diffusion profiles. To demonstrate a biological application, the researchers studied the enzyme ATP synthase embedded in a liposome. In response to a proton gradient the ATP synthase is stimulated to produce ATP. When ATP is synthesized the head unit of the enzyme rotates in one direction, conversely when ATP is hydrolyzed the head unit rotates in the opposite direction. Fluorophores were added to two of the ATP synthase sub-units so that rotation of the two units relative to one another during ATP synthesis and hydrolysis could be studied using single molecule fluorescence resonance energy transfer (FRET). The SECM tip was used to create a pH gradient. When the liposome carrying the enzyme diffused into this gradient, the enzyme responded to the changing pH. Although there was no direct evidence for ATP synthesis, the resulting FRET patterns observed indicated that the system was likely to be rotating in the correct direction for ATP production [252].

4.4.2 Surface measurements

Combined SECM – CLSM was employed by Matsue and colleagues to both identify fluorescently active spots of the enzyme diaphorase supported on a substrate surface (CLSM) and provide information on the activity of the enzyme towards turnover of NADH (SECM) [253]. It was also shown that by using both CLSM and SECM it was possible to locally pattern

the enzyme. This was achieved by using an enzyme covered substrate and then selectively de-activating the enzyme in defined zones. With CLSM this was undertaken by irradiating the sample with very strong light from a focused laser beam (to photodegrade the enzyme). By scanning the beam over the surface, the enzyme could be deactivated in selected regions. Using electrochemistry, the tip UME was used to electrogenerate Br_2 from Br^- which when coupled with water formed HOBr a strong oxidant. Diffusion of HOBR to the substrate surface resulted in degradation of the enzyme in the zones where the SECM tip scanned. The regions of deactivated enzyme could then be visualized using CLSM, as photodegradation caused the fluorescently intensity of the enzyme to greatly reduce [253].

Bard and co-workers used an SECM tip to selectively pattern redox inactive fluorescent labeled molecules onto an azido functionalized glass substrate using "click" chemistry [254]. The tip UME was utilized to produce Cu^+ from Cu^{2+} salen oxidation in DMF (to stabilize the Cu^+) in the small gap between the Au UME and the underlying substrate. The Cu^+ served as a catalyst to "click" the fluorescently labeled alkyne on to the glass supported azide molecules. The size of the patterned zones could then be visualized using fluorescence microscopy. They were found to be bigger than the size of the UME employed, which was thought to result from the reaction rate of the click process and the thick insulating layer around the Au UME.

Fluorescence microscopy was also coupled with SECM for single cells studies, by Lai and co-authors, with the aim of detecting reactive oxygen species (ROS) in prostate cancer cells [255]. An inverted epifluorescence microscope was used to locate individual cells on the bottom of a petri-dish, and also to position a 10 µm UME in their vicinity. Negative feedback current of added ruthenium hexaammine was used to place the UME at a fix height of about 8 µm from the bottom of the dish. Thanks to optical monitoring, the tip could then be linearly scanned precisely across individual cells. The resulting current profile showed pure negative feedback above the cells. When the ruthenium hexaammine was then removed from the dish, and the tip biased at a negative enough potential to detect O_2 and H_2O_2, the current profile showed distinct

positive feedback features. This was attributed to the released of oxygenated species by the cell, as dismutation products of the reactive oxygen species it likely contained. Epifluorescence microscopy was used to confirm such a proper (yet indirect) SECM detection of ROS, by making use of a fluorophore (carboxy-H2DCFA) which specifically revealed the presence of ROS inside the cell.

4.4.3 SECM-Fluorescence microscopy using electrofluorochromic dyes as redox mediators

In the SECM-fluorescence coupling schemes reviewed above, the fluorescence and electrochemical signals originated from different molecular species. Conversely, Miomandre et al. reported the use of molecules being both electroactive *and* luminescent as SECM mediators. [256] They first selected electrofluorochromic tetrazine (Tz) molecules, whose fluorescence can be turned from "on" to "off" upon reduction at an electrode. Using a classical SECM setup placed on top of an inverted epifluorescence microscope, they approached a 20 µm diameter UME from a conducting and an insulating transparent substrate, while recording the current due to Tz reduction and its fluorescence emission. They were thus able to construct correlated current and fluorescence approach curves. The fluorescence signal was plotted as a normalized amplitude signal (IM), which actually reflected the relative magnitude of fluorescence *extinction* due to Tz reduction. The current approach curves displayed the behavior expected for negative or positive feedback, depending on the surface conductivity. However, the IM approach curves displayed a similar shape for both types of substrates, IM increasing as the tip-substrate distance was decreased. Far from the surface IM was low because the tip was not in the field of view of the microscope, whereas at closer tip-substrate separation "darkening" of the area surrounding the tip, due to Tz reduction, was better sensed, so IM was higher. This effect was sensed at much longer distances than either positive or negative feedback were. These results suggest that monitoring fluorescence in such a way could be used for controlling the tip-to-surface distance in SECM independently from the surface reactivity.

In a subsequent paper the same group reproduced similar experiments but using this time the water soluble electrofluorochromic species resorufin as a SECM mediator [257]. Finally, they showed that fluorescence approach curves could also be constructed by plotting not only IM but also the fluorescence lifetime of the tetrazine mediator chloromethoxy-1,2,4,5-tetrazine. Both IM and fluorescence approach curves displayed similar shapes, increasing upon approaching the tip to the substrate [258].

4.5 Scanning Electrochemical Microscopy – Surface Plasmon Resonance (SECM-SPR)

A surface plasmon is an electromagnetic wave that propagates along the surface of a metal in contact with a dielectric. Surface plasmons can thus be generated at the surface of metal electrodes in contact with an electrolyte. A configuration coupling SPR with electrochemistry typically uses a thin layer of gold (~ 50 nm) deposited on a glass prism, as the working electrode, **Figure 41**. A polarized laser beam is directed through the prism in order to illuminate the back side of the gold/solution interface, under total reflection conditions. The intensity of the reflected light is monitored as a function of the incident angle of the laser with respect to the gold surface. At a defined angle there is coupling of the incident light with the surface plasmon modes and consequently the intensity of the reflected light decreases. Hence the reflected intensity vs. illumination angle curve presents a very distinct minimum, whose

position on the incident angle axis is extremely dependent on the local optical properties of the electrode/ solution interface, **Figure 41**.

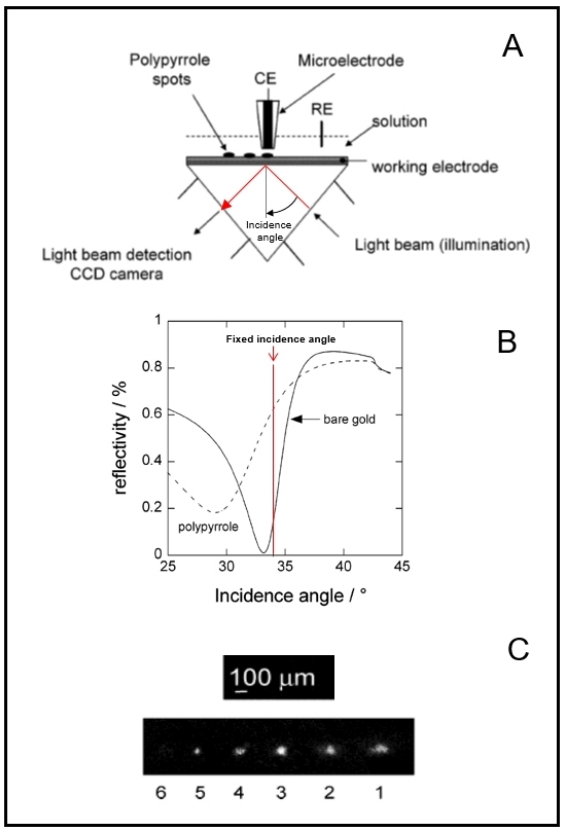

Figure 41. Combining SECM with Surface Plasmon Resonance imaging (SPRi). (A) Principle for simultaneously writing and imaging micropatterns on a surface in SECM/SPRi. (B) Reflectivity versus incident angle curves recorded at a gold substrate, either bare (solid line), or coated with a polypyrrole ultrathin film (dashed line). The vertical red line shows the fixed incidence angle used for SPR imaging. One can see that for the angle chosen the presence of the polypyrrole film translates into a higher substrate reflectivity. (C) SPR-i images of polypyrrole dots locally deposited onto the substrate using the SECM tip as the counter electrode. Tip-substrate distance during deposition ~ 10 µm. Spots of varying sizes and thicknesses were deposited by decreasing the deposition time from 600 ms (spot 1) down to 1 ms (spot 6). The last visible spot (spot 5) was only ~ 3 nm thick. Adapted with permission from S. Szunerits et al., *Langmuir* 20, 9236-9241(2004). Copyright 2004 American Chemical Society.

Deposition of minute amounts of material onto the gold electrode surface, e.g., polymer or macromolecular ultrathin-films, modifies these optical properties (optical index) resulting in detectable shifts of the angular position of the SPR minimum. The magnitude of this shift allows the thickness of even nanometer thick films to be quantified. SPR can thus be used to probe interfacial phenomena at a fixed location, corresponding to the position of a focused laser spot on the surface (~ tens of µm), but can also be used to map film deposition over a larger illuminated surface area (few mm's) in SPR- imaging mode (SPR-i). Here the incidence angle

of the laser is kept constant, and an image of the illuminated area is acquired using a CCD camera. The presence of the deposited layer results in a shift of the reflectivity curve so that more light is reflected from areas where the film is deposited, as shown in **Figure 41 b**. Hence areas covered with film appear as bright zones in SPR-i images.

Coupling of SECM with SPR-i was originally described in the seminal work by Szunerits et al. [259,260]. In the proposed configuration, SECM was used to locally deposit polypyrrole and polypyrrole-oligonucleotides microspots onto the gold surface of a SPR gold sensor. A 10 μm diameter SECM disk-in-glass tip was initially positioned ~5 –10 μm from the gold SPR substrate using the positive feedback response of a redox mediator. The SECM cell was then flushed, rinsed and filled with a pyrrole containing solution. For polypyrrole deposition short duration pulses were applied to the gold substrate while the SECM tip was used as a counter electrode. As a result, polypyrrole spots were specifically deposited below the tip, Figure **41c**.

In this configuration the thickness and lateral dimensions of the deposited polypyrrole spots could be monitored (read) from the SPR-i image during in situ-deposition by SECM (writing). Using only SECM to deposit and subsequently image the spots would have been possible in principle but would have required significantly more time. Moreover, the exquisite sensitivity of SPR-i allowed very thin (~ 3 nm thick) polypyrrole spots to be clearly visualized. The respective influence of the pyrrole monomer concentration and of the potential pulse time on the dimensions of the polypyrrole and polypyrrole-oligonucleotides were quantified.

Combination of SPR with SECM was also reported by Zhou et al. [261]. In these studies, the back-side of the gold SPR surface was illuminated using a ~100 μm diameter focused laser and the angular position of the SPR minimum was monitored using a photodetector. In the first set of experiments, molecular layers of 6-ferrocenyl–1-hexanethiol were assembled onto the gold surface and a redox mediator (Ce^{3+}) was introduced in solution. A 10 μm diameter SECM tip was then positioned 10 μm above the illuminated portion of the gold substrate. The SECM

tip was biased so as to generate the oxidizing Ce^{4+} species which, upon reaching the gold surface locally oxidized the surface containing ferrocene moieties.

It was observed that this oxidation was accompanied by a marked shift of the SPR minimum which was attributed to a local change of the thickness of the film due to the repulsion between adjacent ferrocenium ions. Based on this model system it was thus demonstrated that SECM-SPR was viable for determining local variations in thin film thickness induced by redox reactions. Here, redox conversion of surface bound species was achieved using SECM tip generated species and not by biasing the substrate. Hence the interfering effect of an applied substrate potential on the SPR signal was eliminated.

This approach was further extended to the determination of redox-induced conformational changes of cytochrome *c* molecules electrostatically attached to the gold surface. Conversion of cytochrome c from its oxidized to its reduced state by tip generated methyl viologen monocations was found to result in a ~ 0.27 Å increase in protein size. The same SECM-SPR approach was used for real time detection of Cu^{2+} sequestration and release by an immobilized metalloprotein, metallothionein-2 (MT) [262]. Copper ions were stripped from a Cu-coated SECM tip positioned close to a gold SPR surface bearing MT molecules. Stepwise changes in the time-resolved SPR minimum shifts were observed and ascribed to conversion of MT between three stable structures sequestrating 5, 9 and 12 copper ions. Conversely metal release by MT was triggered by locally acidifying the solution with protons generated from hydroquinone oxidation at the SECM tip. The simultaneously recorded time resolved SPR shifts showed that metal release also proceeded through the three conformations identified. More recently, the same group employed SECM-SPR to trigger and study oxidation of MT by $OH^{\cdot}$ radicals [263]. The SECM tip was used to generate H_2O_2 in the vicinity of a gold surface bearing MT complexed with copper ions which catalyzed $OH^{\cdot}$ production from H_2O_2. An irreversible variation in the SPR signal, attributed to oxidative damages to MT was then observed.

The advantage of using an SECM based configuration is that the fast mass transfer achieved at the local scale avoids the mass transfer limitation on kinetic measurements commonly encountered in flow injection SPR systems. This work evidenced that SECM-SPR is amenable for studies of rapid functional and dynamic conformational changes of protein at the solid/liquid interface.

4.6 SECM and nanoparticle plasmonics

In a series of seminal works, Willets et al. have described an SECM approach for probing the plasmon-mediated photoelectrochemical activity of nanoparticles [264,265]. The configuration used is typical of many SECM-coupled optical techniques : a transparent sample is mounted on an inverted optical microscope, and locally illuminated from below using a laser beam. Yet here the sample, glass or ITO, is covered with gold nanoparticles deposited by thermal evaporation. Surface plasmons of the nanoparticles, excited by the laser, decay via heat generation. The authors have shown that a SECM tip, positioned a few microns above the substrate, could locally probe such a photothermal heating, via enhanced mass transfer of a SECM redox mediator introduced in solution. In their most recent contribution these authors demonstrated that the same configuration can also be used to evidence the generation of hot carriers at the nanoparticles, and determine their energy distribution [266]. There, hot carriers reacted with the SECM mediators, decreasing their local concentration and hence modulating the tip current in a quantifiable way.

4.7 Scanning Electrochemical Microscopy–Attenuated Total Reflection Spectroscopy (SECM-ATR)

A novel combination of SECM with mid-infrared (IR) (3 –25 μm wavelength region) spectroscopy was reported by Kranz and colleagues [267,268]. Here the SECM substrate is the flat top of a hemispherical ZnSe attenuated total reflection (ATR) single bounce crystal. IR radiation is directed through the crystal and focused onto a small spot at the ATR crystal/solution interface. The locally created evanescent field penetrates a few microns into

solution and the radiation reflected at the interface (internally reflected) is directed toward a photodetector. Hence IR adsorbing molecules present in the close vicinity of the interface can be spectroscopically probed, *i.e.,* an evanescent field adsorption spectrum is acquired.

One of the interests of combining IR-ATR spectroscopy with SECM is that this configuration affords a current independent way of determining tip-substrate distance [267]. Indeed, when the SECM tip is approached toward the IR-irradiated spot of the ATR crystal, so that it enters the evanescent field, IR spectra corresponding to the IR-adsorption of the borosilicate glass sheath of SECM tips can be detected. Since the IR-evanescent field decays exponentially away from the surface, the closer the tip is approached the more intense the absorbance of the IR radiation by the tip. Hence the absolute tip-substrate distance can be quantitatively determined from the magnitude of the IR adsorption bands of the glass spectrum (Si-O stretching and bending mode). Alternatively, provided an aqueous solvent is used, the O-H bending mode of water can also be recorded and used for distance calibration. A narrowing tip-substrate gap translates into a decreasing OH band due to water being expelled from the gap upon the approach.

A major interest of ATR-SECM is that this combined technique allows for the specific spectroscopic probing of species either located in the narrow tip-substrate gap or locally adsorbed at the ATR surface. Moreover, since the "finger print" regime of the IR spectrum is used (10 –25 μm wavelength) almost any organic molecule can be unambiguously identified from the distinct adsorption pattern acquired. In that respect it should be noted that using IR-ATR spectroscopy provides a high surface sensitivity and alleviates the usual problem of the strong IR adsorption of water which otherwise limits the use of in-situ IR spectroscopy.

The possibility of using ATR-SECM for in-situ studies of an electrochemically induced process has been demonstrated by spectroscopically monitoring the deposition of polymer micro-spots induced by SECM in feedback mode [268]. In this work Wang et al. coated the surface of an ATR crystal with a ~ 300 nm thick water-insoluble layer of 2,5-di-(2-thienyl)-

pyrrole (SNS) monomer. Local polymerization of SNS was then triggered by approaching a 25 μm Pt tip, generating the oxidizing species $Ru(bpy)_3^{3+}$, toward the surface. Polymerization of SNS was simultaneously monitored by recording evanescent field absorption intensity changes of SNS specific bands, providing information on the polymerization mechanism.

So far only insulating ATR-SECM substrates (ATR-crystals) have been used. However, ATR-SECM conducting substrates could, in principle, be fabricated by coating ATR crystals with mid-infrared transparent conducting thin films (such as diamond-like films). Combining ATR-SECM with AFM for simultaneous in situ studies on topography, infrared spectroscopy and electrochemical processes is also contemplated [268].

4.8 Scanning Electrochemical Microscopy–Raman Spectroscopy (SECM-Raman)

Combination of SECM with Raman spectroscopy was originally described by Etienne et al. in the framework of corrosion studies [153]. These authors combined shear force regulated SECM with Raman microscopy using an original setup comprising a 25 μm Pt in glass microelectrode positioned at a 30° angle from the opaque sample surface, which is attached to a confocal microscope stage. With this arrangement, optical images of the surface showing the exact position of the tip can be acquired. The laser spot, which is the excitation source for Raman spectroscopy, can then be aligned with the tip extremity, ensuring that the exact same surface location interrogated by the tip is also probed by Raman spectroscopy. Exploration of the sample can be carried out by lateral motion of the microscope stage, without compromising the tip/laser alignment. It is worth noting that this original setup is, by design, suitable for analyzing opaque samples. Etienne et al. used it to characterize a corroding sample, consisting of a steel sample covered with metallic and organic coatings. A millimeter-wide strip of the organic coating was removed, and corrosion of the so-exposed metal was analyzed by constant distance (shear force) SECM coupled to Raman, at first in the presence of a redox mediator (ruthenium hexaammine). Sample topography, electrochemical current and Raman spectra were acquired

at several locations across the metal strip. A very good correlation was observed between the topography, the tip current, and the intensity of a Raman band at 450 cm^{-1} evidencing depletion of the TiO_2-containing coating across the strip. This was the first demonstration of the ability of SECM-Raman to correlate in-situ the local chemical composition of a sample with electrochemical activity. The corrosion behavior of the sample was further studied by replacing the amperometric UME by a pH sensitive probe. The Raman spectra, acquired simultaneously with the pH profile, revealed the formation of zinc chloride hydroxide monohydrate (simonkolleite) at the corroding metal surface.

Still in the field of material characterization, coupling between Raman spectroscopy and SECM was later reported by Bron et al. [269], who made use of an inverted confocal microscope to study the electrochemical activity of Ni/Fe thin films deposited on a transparent ITO-coated quartz slide. Such a configuration enables optical alignment of a SECM tip with the laser spot of the Raman spectrometer illuminating the ITO surface from below. It is of course restricted to transparent samples. The activity of the Ni/Fe thin films toward oxygen evolution (OER) was studied by using a 25 μm Pt tip to detect O_2 produced at the surface, while simultaneously recording Raman spectra of the sample. Upon biasing the electrode at the anodic potentials required for OER, specific Raman peaks appeared, revealing the formation of NiOOH in the thin film. Formation of this species was shown to be necessary, albeit not sufficient, for good OER activity.

Schuhmann and colleagues also reported the coupling of constant height SECM with Raman with the aim of probing local modifications of molecular films on surfaces [270]. In their setup, designed for opaque samples, the Raman excitation laser was oriented with an angle of 30° with respect to the vertical tip, enabling alignment and simultaneous electrochemical and spectroscopic investigations of the same sample area. The sample could be moved laterally to acquire line scans. Self-assembled monolayers of p-nitrophenol (p-NTP) on gold were investigated by with this setup. For such molecular system, surface enhancement of Raman

scattering is expected to potentially enable the interrogation of a few molecules at a time. Here galvanostatic pulses were first applied between a SECM tip and the surface, in order to locally reduce p-NTP into p-aminothiophenol (p-ATP), forming p-ATP spots in a p-NTP matrix. Raman-SECM line scans were subsequently acquired across these spots in a constant height, positive feedback mode, with $Fe(CN)_6^{3-}$ as a redox mediator. Enhanced tip current was recorded at the level of some locations, that specific Raman bands enabled to confirm as being p-ATP spots. This was a proof-of-concept demonstration of simultaneous chemical identification of a surface adsorbed molecular species associated with locally enhanced electron transfer activity, afforded by (SERS) Raman-SECM coupling.

A third group, Rodriguez-Lopez group at Urbana-Champaign, also recently combined Raman spectroscopy with SECM [271]. Their setup was based on an inverted microscope, and as such suited to characterize transparent substrates. As discussed above, this configuration enables straightforward alignment of the Raman excitation laser with the SECM tip position, so that the same substrate location is probed simultaneously by both techniques. In an initial report these authors interrogated thin films of redox active colloidal (RAC) particles, consisting in cross-linked polymeric material incorporating a high concentration of redox active methylviologen. [271] 80 nm and 135 nm RAC particles were deposited as a monolayer on a glass slide, from which a Pt UME was approached using negative feedback of ferrocenemethanol (FcMeOH) mediator added in solution. The ferricinium ion generated at the UME was then used to locally oxidize (i.e., to titrate) the RAC-contained viologen moieties located in the immediate vicinity of the tip. This titration was monitored in real time by following the intensity of a Raman peak specific of the locally generated viologen radical anion over time. Similar titration kinetics were found for both sizes of RAC, showing that they displayed a similar concentration in viologen and oxidation mechanism.

In their most recent study the same authors used their Raman-SECM setup for characterizing, and even *imaging*, electron transfer properties of graphene electrodes [272]. Multilayered

graphene electrode surfaces, consisting of ~ 10 stacked graphed layers, were grown by CVD. Reactive ion etching (RIE) was then used to define 50 µm diameter disk-shaped regions where the number of graphene layer was etched down to three. Raman-SECM was then used to investigate the constant height feedback response and Raman scattering of these regions. By rastering the substrate stage, simultaneous electrochemical and Raman scattering images could be produced for the first time, with a high spatial resolution of 5 µm and a time resolution of 5 s per pixel (**Figure 42**).

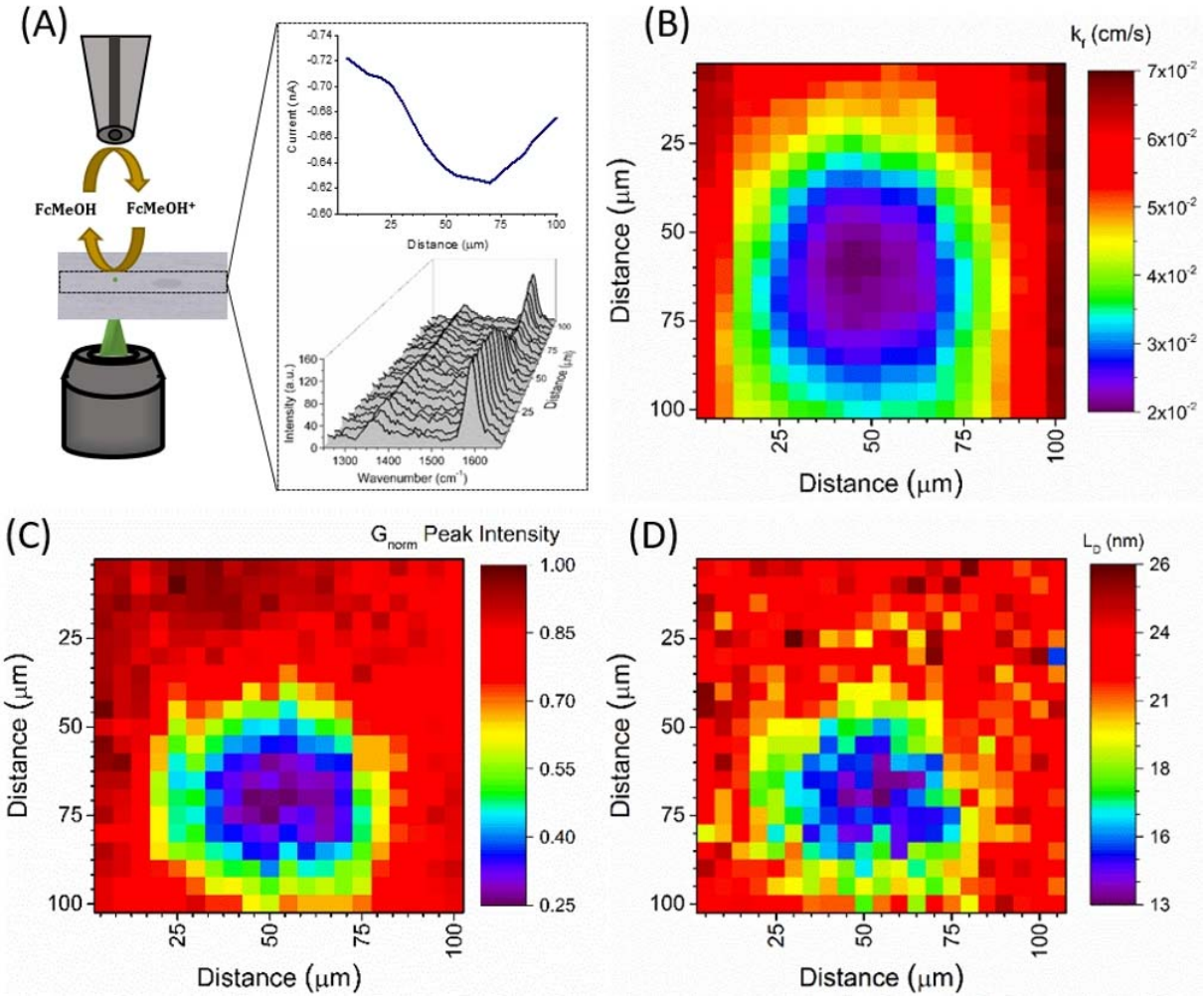

Figure 42. Combined SECM and Raman imaging of a patterned graphene surface. The surface consists of 10 stacked layers of graphene expect in disk-shaped patterned regions where the number of layers is reduced to 3. One of such regions is imaged. (A) Depiction of the set up and of the alignment between the SECM tip and Raman laser. (B) Calculated local electron transfer rate at the graphene surface from the current feedback at the UME. (C) Image of the normalized G peak intensity of the local Raman spectrum of the surface (D). Distance between defects determined from the intensity ratio of the D and G Raman bands. 1mM Ferrocene methanol in 100 mM KNO_3 was used as the SECM mediator. Reproduced with permission from N. B. Schorr et al., *Anal. Chem.* 90, 7848–7854 (2018). Copyright 2018 American Chemical Society.

Raman images showing the intensity of the G peak of graphene (**Figure 42C**), enabled the circular regions consisting of only three stacked graphene layers to be identified. The simultaneously acquired tip current image (**Figure 42B**), converted into an electron transfer rate image, evidenced that such regions were associated with much reduced electron transfer kinetics.

5. Scanning Electrochemical Microscopy – Quartz Crystal Microbalance (SECM-QCM).

The quartz crystal microbalance consists of a quartz crystal which is electrically driven into oscillation. The resonance frequency of the crystal is monitored. This frequency is highly dependent on any mass added to the crystal surface. Hence the mass-dependence of the QCM resonance frequency can be, in air, used to "weigh" minute amounts of material with a sensitivity of the order of 1 ng cm^{-2}. QCM can also be coupled with electrochemistry; here the quartz crystal surface is coated with an appropriate electrode material e.g., thin film gold. This electrochemical-QCM (EQCM) configuration can be used to monitor electrochemically triggered surface processes associated with the deposition (or loss) of material at the working electrode surface. However, in liquid medium the frequency shift of the QCM crystal is not solely sensitive to added mass but is also influenced by changes in the local property of the medium associated with the surface electrochemical process of interest. For example, density or viscosity variation of the medium in the electrode vicinity, in addition to variation in the viscoelastic properties of the deposited layer, can cause shifts in the resonant frequency of QCM.

The main interest in coupling QCM with SECM is that the SECM tip can *specifically* monitor the flux of electroactive species associated with the surface electrochemical process. This additional information can help to quantify the actual contribution of electroactive flux to the apparent total mass change derived from the QCM frequency shift. The combination of SECM with EQCM was initially described by Ward and Hillier [273]. The authors used a

SECM tip to trigger the electrodeposition of a small amount of copper on pre-defined locations of the QCM surface. By monitoring the ensuing frequency shift of the QCM, the radial sensitivity of the QCM crystal was mapped.

The first use of SECM-QCM in a SG-TC configuration was later reported by Bard et al. [274,275] The tip was used to detect C_{60}^- ions released during the potential cycling of the quartz substrate surface bearing either an insoluble C_{60} film or C_{60} caged in ter-butylcalix[8]arene, cast as a particle film. In the first of these studies the effect of the lateral and vertical motion of the SECM tip on the QCM response was investigated [274]. It was shown that both motions resulted in a frequency shift of the QCM, which led to the conclusion that SECM-QCM measurements should be performed with a stationary tip in order to avoid tip-motion induced frequency shifts. Further studies by Bartlett et al. [276] and Heinze et al. [277] confirmed these effects, and showed they could be minimized by using small tips (with small RG) or tips with high aspect ratio cone-shaped glass sheath. However the tip-substrate distance dependence of the QCM frequency shift can also be used to set the tip-substrate distance in SECM-QCM in a current independent way [278].

SECM-QCM has been employed to monitor localized corrosion processes [279], the electrochemical growth of poly(o-phenylenediamine) thin films, [280] and ion exchange at the poly(butyl viologen)-electrolyte interface [281].

6. Fast-Scan Cyclic Voltammetry – Scanning Electrochemical Microscopy (FSCV-SECM)

The coupling of fast scan CV with SECM to resolve the distribution of chemical species generated at a substrate surface was first introduced by Wipf's group [282,283]. In FSCV-SECM, CV is carried out at an SECM tip using rapid scan rates, typically between 10 and 1000 Vs^{-1}. The vertical and lateral positions of the SECM tip over the substrate have to be recorded concomitantly with the transient tip CV. Unlike "classical " amperometric SECM, where the tip potential is typically held constant, in FSCV-SECM the tip potential is scanned so that

several species of interest giving rise to differing CV peaks can be simultaneously detected i.e., images of multiple analytes can be recorded in a single surface scan.

The species are probed over a distance corresponding to the transient diffusion layer created at the tip which, at high enough scan rates, can be made much smaller than the tip-substrate distance. Hence no diffusional feedback interaction occurs, and the recorded signal (and hence images) are free from perturbations due to substrate topography. Interestingly images of the concentration profile of non-electroactive species can also be acquired in FSCV-SECM since the only requirement for detection is that the surface released species modifies in some way the fast scan CV. For example, the localized concentration of chloride ions was mapped by collecting the chloride at a mercury SECM tip [282]. The Hg tip was first scanned anodically to form a calomel layer (Hg_2Cl_2) on the tip surface. The cathodic (return) CV scan then showed a characteristic chloride dependent peak corresponding to the stripping of the Hg_2Cl_2 layer. FSCV-SECM has also been notably employed to map simultaneously oxygen and hydrogen peroxide released during the oxidative bursts of stimulated macrophage cells [284].

FSCV-SECM combines the spatial resolution of SECM with the specificity of CV. A theoretical description of the CV response of a disk UME facing an insulating substrate, *i.e.* in a negative feedback FSCV-SECM configuration, can be found in literature [285].

As an important improvement of FSCV-SECM, coupling with AC-SECM for constant distance imaging has been reported [286]. To this aim a small sinusoidal signal (10 mV rms) was added to the tip bias on top of the triangular potential ramp used for voltammetry. Instrumental conditions were identified where FSCV and AC currents did not interfere. This allowed the AC signal to be used as a feedback parameter to set the tip-substrate distance, while recording unperturbed CVs at any pixel of the image scan. Such FSCV-AC-SECM coupling enabled PC 12 cells to be located from topography images, while their oxygen consumption was simultaneously mapped by recording the reduction CV of oxygen at high scan rate (450 V/s), see **Figure 43**.

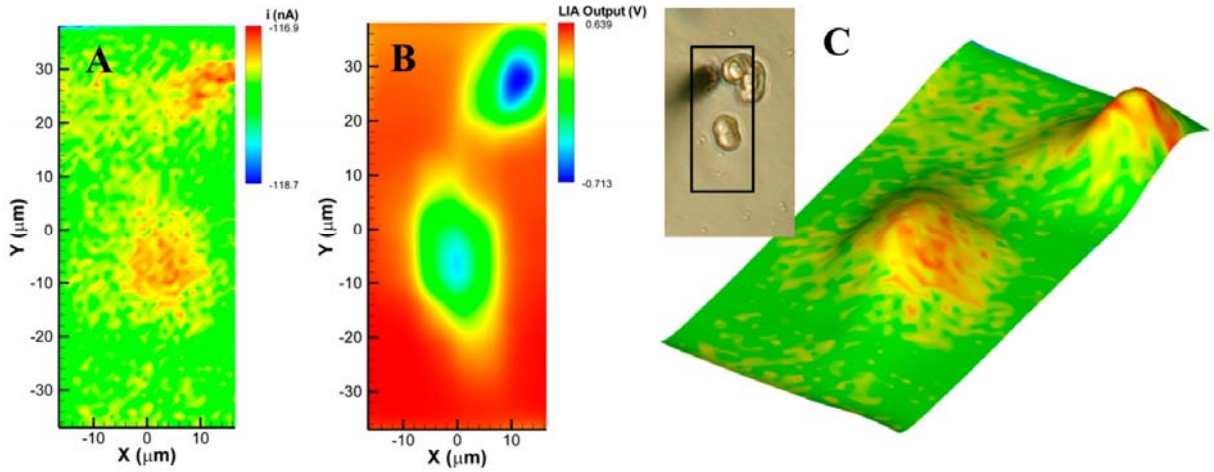

Figure 43. Combining alternating current SECM with fast-scan voltammetry. (A) Cathodic peak current of the fast-scan O_2 reduction CV, recorded as a function of probe position. (B) Simultaneously acquired local impedance data. (C) Overlay of the oxygen reduction current (from (A)) on the sample topography derived from (B). Displayed in inset is an optical image showing the two cells identified in (B) and the SECM tip. Reproduced with permission from J. A. Koch. et al., *Anal. Chem.* 84, 9537–9543 (2012). Copyright 2012 American Chemical Society.

Bibliography

[1] J. V Macpherson, P.R. Unwin, Combined Scanning Electrochemical - Atomic Force Microscopy, Anal. Chem. 72 (2000) 276–285.

[2] C. Kranz, G. Friedbacher, B. Mizaikoff, A. Lugstein, J. Smoliner, E. Bertagnolli, Integrating an Ultramicroelectrode in an AFM Cantilever: Combined Technology for Enhanced Information, Anal. Chem. 73 (2001) 2491–2500. doi:10.1021/ac001099v.

[3] C.J. Slevin, N.J. Gray, J. V Macpherson, M.A. Webb, P.R. Unwin, Fabrication and characterisation of nanometre-sized platinum electrodes for voltammetric analysis and imaging, Electrochem. Commun. 1 (1999) 282–288. doi:10.1016/S1388-2481(99)00059-4.

[4] C.E. Gardner, J. V. Macpherson, Atomic force microscopy probes go electrochemical, Anal. Chem. 74 (2002) 576–584.

[5] G. Wittstock, M. Burchardt, S.E. Pust, Y. Shen, C. Zhao, Scanning Electrochemical Microscopy for Direct Imaging of Reaction Rates, Angew. Chemie Int. Ed. 46 (2007) 1584–1617. doi:10.1002/anie.200602750.

[6] A. Eifert, C. Kranz, Hyphenating Atomic Force Microscopy, Anal. Chem. 86 (2014) 5190–5200. doi:10.1021/ac5008128.

[7] C. Kranz, Recent advancements in nanoelectrodes and nanopipettes used in combined scanning electrochemical microscopy techniques., Analyst. 139 (2014) 336–352. doi:10.1039/c3an01651j.

[8] A.N. Patel, C. Kranz, (Multi)functional Atomic Force Microscopy Imaging, Annu. Rev. Anal. Chem. 11 (2018) 329–350. doi:10.1146/annurev-anchem-061417-125716.

[9] X. Shi, W. Qing, T. Marhaba, W. Zhang, Atomic force microscopy - Scanning electrochemical microscopy (AFM-SECM) for nanoscale topographical and electrochemical characterization: Principles, applications and perspectives, Electrochim. Acta. 332 (2020) 135472. doi:10.1016/j.electacta.2019.135472.

[10] G. Binnig, C.F. Quate, C. Gerber, Atomic Force Microscope, Phys. Rev. Lett. 56 (1986) 930–933.

[11] R.M. Penner, M.J. Heben, T.L. Longin, N.S. Lewis, Fabrication and use of nanometer-sized electrodes in electrochemistry, Science 250 (1990) 1118–1121. doi:10.1126/science.250.4984.1118.

[12] L.A. Nagahara, T. Thundat, S.M. Lindsay, Preparation and characterization of STM tips for electrochemical studies., Rev. Sci. Instrum. 60 (1989) 3128–3130. doi:10.1063/1.1140590.

[13] J. V Macpherson, P.R. Unwin, Noncontact Electrochemical Imaging with Combined Scanning Electrochemical Atomic Force Microscopy, Anal. Chem. 73 (2001) 550–557. doi:10.1021/ac001072b.

[14] J. Abbou, C. Demaille, M. Druet, J. Moiroux, Fabrication of Submicrometer-Sized Gold Electrodes of Controlled Geometry for Scanning Electrochemical-Atomic Force Microscopy, Anal. Chem. 74 (2002) 6355–6363. doi:10.1021/ac020385z.

[15] R.D. Rodriguez, A. Anne, E. Cambril, C. Demaille, Optimized hand fabricated AFM probes for simultaneous topographical and electrochemical tapping mode imaging., Ultramicroscopy. 111 (2011) 973–981. doi:10.1016/j.ultramic.2011.02.001.

[16] A. Anne, E. Cambril, A. Chovin, C. Demaille, C. Goyer, Electrochemical Atomic Force Microscopy Using a Tip-Attached Redox Mediator for Topographic and Functional Imaging of Nanosystems, ACS Nano. 3 (2009) 2927–2940.

[17] BIOLOGIC IC-SECM, (n.d.). https://www.biologic.net/products/ic-secm-m470/.

[18] A. Davoodi, A. Farzadi, J. Pan, C. Leygraf, Y. Zhu, Developing an AFM-Based SECM System; Instrumental Setup, SECM Simulation, Characterization, and Calibration., J. Electrochem. Soc. 155 (2008) C474–C485. doi:10.1149/1.2943324.

[19] A. Davoodi, J. Pan, C. Leygraf, S. Norgren, Probing of local dissolution of Al alloys in chloride solutions by AFM and SECM., Appl. Surf. Sci. 252 (2006) 5499–5503. doi:10.1016/j.apsusc.2005.12.023.

[20] A. Davoodi, J. Pan, C. Leygraf, S. Norgren, Integrated AFM and SECM for in situ studies of localized corrosion of Al alloys., Electrochim. Acta. 52 (2007) 7697–7705. doi:10.1016/j.electacta.2006.12.073.

[21] A. Davoodi, J. Pan, C. Leygraf, S. Norgren, In Situ Investigation of Localized Corrosion of Aluminum Alloys in Chloride Solution Using Integrated EC-AFM/SECM Techniques., Electrochem. Solid-State Lett. 8 (2005) B21–B24. doi:10.1149/1.1911900.

[22] A. Davoodi, J. Pan, C. Leygraf, S. Norgren, The Role of Intermetallic Particles in Localized Corrosion of an Aluminum Alloy Studied by SKPFM and Integrated AFM/SECM, J. Electrochem. Soc. 155 (2008) C211. doi:10.1149/1.2883737.

[23] A. Davoodi, J. Pan, C. Leygraf, S. Norgren, Multianalytical and In Situ Studies of Localized Corrosion of EN AW-3003 Alloy—Influence of Intermetallic Particles, J. Electrochem. Soc. 155 (2008) C138. doi:10.1149/1.2834454.

[24] J. Velmurugan, A. Agrawal, S. An, E. Choudhary, V.A. Szalai, Fabrication of Scanning Electrochemical Microscopy-Atomic Force Microscopy Probes to Image Surface Topography and Reactivity at the Nanoscale, Anal. Chem. 89 (2017) 2687–2691. doi:10.1021/acs.analchem.7b00210.

[25] G. Schuermann, P.F. Indermuehle, U. Staufer, N.F. de Rooij, Micromachined SPM Probes with

Sub-100 nm Features at Tip Apex, Surf. Interface Anal. 27 (1999) 299–301.

[26] Y. Hirata, S. Yabuki, F. Mizutani, Application of integrated SECM ultra-micro-electrode and AFM force probe to biosensor surfaces., Bioelectrochemistry. 63 (2004) 217–224. doi:10.1016/j.bioelechem.2004.01.001.

[27] M.A. Derylo, K.C. Morton, L.A. Baker, Parylene Insulated Probes for Scanning Electrochemical-Atomic Force Microscopy, Langmuir. 27 (2011) 13925–13930. doi:10.1021/la203032u.

[28] D.J. Comstock, J.W. Elam, M.J. Pellin, M.C. Hersam, High aspect ratio nanoneedle probes with an integrated electrode at the tip apex, Rev. Sci. Instrum. 83 (2012) 113704. doi:10.1063/1.4767248.

[29] A.J. Wain, D. Cox, S. Zhou, A. Turnbull, High-aspect ratio needle probes for combined scanning electrochemical microscopy — Atomic force microscopy, Electrochem. Commun. 13 (2011) 78–81. doi:10.1016/j.elecom.2010.11.018.

[30] P. Knittel, O. Bibikova, C. Kranz, Challenges in nanoelectrochemical and nanomechanical studies of individual anisotropic gold nanoparticles, Faraday Discuss. 193 (2016) 353–369. doi:10.1039/C6FD00128A.

[31] P. Knittel, M.J. Higgins, C. Kranz, Nanoscopic polypyrrole AFM–SECM probes enabling force measurements under potential control, Nanoscale. 6 (2014) 2255. doi:10.1039/c3nr05086f.

[32] A. Eifert, B. Mizaikoff, C. Kranz, Advanced fabrication process for combined atomic force-scanning electrochemical microscopy (AFM-SECM) probes, Micron. 68 (2015) 27–35. doi:10.1016/j.micron.2014.08.008.

[33] D.P. Burt, N.R. Wilson, J.M.R. Weaver, P.S. Dobson, J. V. Macpherson, Nanowire Probes for High Resolution Combined Scanning Electrochemical Microscopy − Atomic Force Microscopy, Nano Lett. 5 (2005) 639–643. doi:10.1021/nl050018d.

[34] S. Sekine, H. Kaji, M. Nishizawa, Integration of an electrochemical-based biolithography technique into an AFM system, Anal. Bioanal. Chem. 391 (2008) 2711–2716.

doi:10.1007/s00216-008-1952-9.

[35] J. Wiedemair, B. Balu, J.-S. Moon, D.W. Hess, B. Mizaikoff, C. Kranz, Plasma-Deposited Fluorocarbon Films: Insulation Material for Microelectrodes and Combined Atomic Force Microscopy−Scanning Electrochemical Microscopy Probes, Anal. Chem. 80 (2008) 5260–5265. doi:10.1021/ac800246q.

[36] A. Avdic, A. Lugstein, M. Wu, B. Gollas, I. Pobelov, T. Wandlowski, K. Leonhardt, G. Denuault, E. Bertagnolli, Fabrication of cone-shaped boron doped diamond and gold nanoelectrodes for AFM-SECM., Nanotechnology. 22 (2011) 145306/1-145306/6. doi:10.1088/0957-4484/22/14/145306.

[37] W. Smirnov, A. Kriele, R. Hoffmann, E. Sillero, J. Hees, O.A. Williams, N. Yang, C. Kranz, C.E. Nebel, Diamond-Modified AFM Probes: From Diamond Nanowires to Atomic Force Microscopy-Integrated Boron-Doped Diamond Electrodes, Anal. Chem. 83 (2011) 4936–4941. doi:10.1021/ac200659e.

[38] A. Eifert, W. Smirnov, S. Frittmann, C. Nebel, B. Mizaikoff, C. Kranz, Atomic force microscopy probes with integrated boron doped diamond electrodes: Fabrication and application, Electrochem. Commun. 25 (2012) 30–34. doi:10.1016/j.elecom.2012.09.011.

[39] E. Lee, M. Kim, J. Seong, H. Shin, G. Lim, An L-shaped nanoprobe for scanning electrochemical microscopy-atomic force microscopy, Phys. Status Solidi - Rapid Res. Lett. 7 (2013) 406–409. doi:10.1002/pssr.201307120.

[40] I. V Pobelov, M. Mohos, K. Yoshida, V. Kolivoska, A. Avdic, A. Lugstein, E. Bertagnolli, K. Leonhardt, G. Denuault, B. Gollas, T. Wandlowski, Electrochemical current-sensing atomic force microscopy in conductive solutions, Nanotechnology. 24 (2013) 115501. doi:10.1088/0957-4484/24/11/115501.

[41] T. Akiyama, M.R. Gullo, N.F. De Rooij, A. Tonin, H.-R. Hidber, P.L.T.M. Frederix, A. Engel, U. Staufer, Development of Insulated Conductive Probes with Platinum Silicide Tips for Atomic Force Microscopy in Cell Biology, Jpn. J. Appl. Phys. 43 (2004) 3865–3867. doi:10.1143/JJAP.43.3865.

[42] H. Shin, P.J. Hesketh, B. Mizaikoff, C. Kranz, Development of wafer-level batch fabrication for combined atomic force – scanning electrochemical microscopy (AFM – SECM) probes, Sens. Actuators, B. 134 (2008) 488–495. doi:10.1016/j.snb.2008.05.039.

[43] A.J. Wain, A.J. Pollard, C. Richter, High-Resolution Electrochemical and Topographical Imaging Using Batch-Fabricated Cantilever Probes, Anal. Chem. 86 (2014) 5143–5149. doi:10.1021/ac500946v.

[44] R.J. Fasching, S.-J. Bai, T. Fabian, F.B. Prinz, Nanoscale electrochemical probes for single cell analysis., Microelectron. Eng. 83 (2006) 1638–1641. doi:10.1016/j.mee.2006.01.262.

[45] R.J. Fasching, Y. Tao, F.B. Prinz, Cantilever tip probe arrays for simultaneous SECM and AFM analysis., Sensors Actuators, B Chem. 108 (2005) 964–972. doi:10.1016/j.snb.2004.10.058.

[46] P.L.T.M. Frederix, P.D. Bosshart, T. Akiyama, M. Chami, M.R. Gullo, J.J. Blackstock, K. Dooleweerdt, N.F. de Rooij, U. Staufer, A. Engel, Conductive supports for combined AFM–SECM on biological membranes, Nanotechnology. 19 (2008) 384004. doi:10.1088/0957-4484/19/38/384004.

[47] P.S. Dobson, J.M.R. Weaver, M.N. Holder, P.R. Unwin, J. V Macpherson, Characterization of Batch-Microfabricated Scanning Electrochemical-Atomic Force Microscopy Probes, Anal. Chem. 77 (2005) 424–433.

[48] P.S. Dobson, J.M.R. Weaver, D.P. Burt, M.N. Holder, N.R. Wilson, P.R. Unwin, J. V Macpherson, Electron beam lithographically-defined scanning electrochemical-atomic force microscopy probes: fabrication method and application to high resolution imaging on heterogeneously active surfaces, Phys. Chem. Chem. Phys. 8 (2006) 3909. doi:10.1039/b605828k.

[49] M. Salomo, S.E. Pust, G. Wittstock, E. Oesterschulze, Integrated cantilever probes for SECM/AFM characterization of surfaces, Microelectron. Eng. 87 (2010) 1537–1539. doi:10.1016/j.mee.2009.11.032.

[50] S.E. Pust, M. Salomo, E. Oesterschulze, G. Wittstock, Influence of electrode size and geometry

on electrochemical experiments with combined SECM-SFM probes., Nanotechnology. 21 (2010) 105709/1-105709/12. doi:10.1088/0957-4484/21/10/105709.

[51] H. Shin, P.J. Hesketh, B. Mizaikoff, C. Kranz, Batch fabrication of atomic force microscopy probes with recessed integrated ring microelectrodes at a wafer level., Anal. Chem. 79 (2007) 4769–4777. doi:10.1021/ac070598u.

[52] P.L.T.M. Frederix, M.R. Gullo, T. Akiyama, A. Tonin, N.F. De Rooij, U. Staufer, A. Engel, Assessment of insulated conductive cantilevers for biology and electrochemistry, Nanotechnology. 16 (2005) 997–1005. doi:10.1088/0957-4484/16/8/001.

[53] M.R. Gullo, P.L.T.M. Frederix, T. Akiyama, A. Engel, N.F. DeRooij, U. Staufer, Characterization of microfabricated probes for combined atomic force and high-resolution scanning electrochemical microscopy, Anal. Chem. 78 (2006) 5436–5442. doi:10.1021/ac0521495.

[54] S.-J. Bai, T. Fabian, F. Prinz, R.J. Fasching, Nanoscale probe system for cell-organelle analysis, Sensors Actuators B Chem. 130 (2008) 249–257. doi:10.1016/j.snb.2007.07.143.

[55] Y. Wu, T. Akiyama, S. Gautsch, P.D. van der Wal, N.F. de Rooij, In-plane fabrication of insulated gold-tip probes for electrochemical and force spectroscopy molecular experiments, Sensors Actuators A Phys. 215 (2014) 184–188. doi:10.1016/j.sna.2013.08.043.

[56] Vollkopf, Rudow, Leinhos, Mihalcea, Oesterschulze, Modified fabrication process for aperture probe cantilevers, J. Microsc. 194 (1999) 344–348. doi:10.1046/j.1365-2818.1999.00535.x.

[57] Y. Birhane, J. Otero, F. Pérez-Murano, L. Fumagalli, G. Gomila, J. Bausells, Batch fabrication of insulated conductive scanning probe microscopy probes with reduced capacitive coupling, Microelectron. Eng. 119 (2014) 44–47. doi:10.1016/j.mee.2014.01.018.

[58] P. Knittel, B. Mizaikoff, C. Kranz, Simultaneous Nanomechanical and Electrochemical Mapping: Combining Peak Force Tapping Atomic Force Microscopy with Scanning Electrochemical Microscopy, Anal. Chem. 88 (2016) 6174–6178. doi:10.1021/acs.analchem.6b01086.

[59] E.L.H. Heintz, C. Kranz, B. Mizaikoff, H.-S. Noh, P. Hesketh, A. Lugsteirs, E. Bertagnolli,

Characterization of Parylene coated combined scanning probe tips for in-situ electrochemical and topographical imaging, in: Proc. IEEE Conf. Nanotechnol., 2001. doi:10.1109/NANO.2001.966446.

[60] A. Lugstein, E. Bertagnolli, C. Kranz, B. Mizaikoff, Fabrication of a ring nanoelectrode in an AFM tip: novel approach towards simultaneous electrochemical and topographical imaging, Surf. Interface Anal. 33 (2002) 146–150. doi:10.1002/sia.1178.

[61] A. Lugstein, E. Bertagnolli, C. Kranz, A. Kueng, B. Mizaikoff, Integrating micro- and nanoelectrodes into atomic force microscopy cantilevers using focused ion beam techniques, Appl. Phys. Lett. 81 (2002) 349–351. doi:10.1063/1.1492304.

[62] J.-S. Moon, H. Shin, B. Mizaikoff, C. Kranz, Bitmap-Assisted Focused Ion Beam Fabrication of Combined Atomic Force Scanning Electrochemical Microscopy Probes, J. Korean Phys. Soc. 51 (2007) 920. doi:10.3938/jkps.51.920.

[63] A. Kueng, C. Kranz, A. Lugstein, E. Bertagnolli, B. Mizaikoff, Integrated AFM–SECM in Tapping Mode: Simultaneous Topographical and Electrochemical Imaging of Enzyme Activity, Angew. Chemie Int. Ed. 42 (2003) 3238–3240. doi:10.1002/anie.200351111.

[64] S.K. Guin, P. Knittel, S. Daboss, A. Breusow, C. Kranz, Template- and Additive-free Electrosynthesis and Characterization of Spherical Gold Nanoparticles on Hydrophobic Conducting Polydimethylsiloxane, Chem. - An Asian J. 12 (2017) 1615–1624. doi:10.1002/asia.201700444.

[65] C. Kranz, A. Kueng, A. Lugstein, E. Bertagnolli, B. Mizaikoff, Mapping of enzyme activity by detection of enzymatic products during AFM imaging with integrated SECM–AFM probes, Ultramicroscopy. 100 (2004) 127–134. doi:10.1016/j.ultramic.2003.10.004.

[66] E. Lee, J. Sung, T. An, H. Shin, H. Gil Nam, G. Lim, Simultaneous imaging of the topography and electrochemical activity of a 2D carbon nanotube network using a dual functional L-shaped nanoprobe, Analyst. 140 (2015) 3150–3156. doi:10.1039/C4AN02139H.

[67] K.C. Morton, M.A. Derylo, L.A. Baker, Conductive Atomic Force Microscopy Probes from Pyrolyzed Parylene, J. Electrochem. Soc. 159 (2012) H662–H667. doi:10.1149/2.061207jes.

[68] N.R. Wilson, J. V Macpherson, Carbon nanotube tips for atomic force microscopy, Nat. Nanotechnol. 4 (2009) 483–491. doi:10.1038/nnano.2009.154.

[69] Nauganeedles, (n.d.). https://nauganeedles.com/product-category/scanning-electrochemical-microscopy/.

[70] W.A. Ducker, T.J. Senden, R.M. Pashley, Direct measurement of colloidal forces using an atomic force microscope, Nature. 353 (1991) 239–241. doi:10.1038/353239a0.

[71] H.-J. Butt, Measuring electrostatic, van der Waals, and hydration forces in electrolyte solutions with an atomic force microscope, Biophys. J. 60 (1991) 1438–1444. doi:10.1016/S0006-3495(91)82180-4.

[72] P. Knittel, H. Zhang, C. Kranz, G.G. Wallace, M.J. Higgins, Probing the PEDOT:PSS/cell interface with conductive colloidal probe AFM-SECM, Nanoscale. 8 (2016) 4475–4481. doi:10.1039/C5NR07155K.

[73] S. Daboss, J. Lin, M. Godejohann, C. Kranz, Redox Switchable Polydopamine-Modified AFM-SECM Probes: A Probe for Electrochemical Force Spectroscopy, Anal. Chem. 92 (2020) 8404–8413. doi:10.1021/acs.analchem.0c00995.

[74] J. V. Macpherson, J.-P. Gueneau de Mussy, J.-L. Delplancke, High-Resolution Electrochemical, Electrical, and Structural Characterization of a Dimensionally Stable Ti/TiO[sub 2]/Pt Electrode, J. Electrochem. Soc. 149 (2002) B306. doi:10.1149/1.1479158.

[75] S. Daboss, P. Knittel, C.E. Nebel, C. Kranz, Multifunctional Boron-Doped Diamond Colloidal AFM Probes, Small. 15 (2019) 1902099. doi:10.1002/smll.201902099.

[76] Nanonics Imaging Ltd. AFM-SECM probes, (n.d.).

[77] Scuba Probe Technology, (n.d.).

[78] Z. Huang, P. De Wolf, R. Poddar, C. Li, A. Mark, M.R. Nellist, Y. Chen, J. Jiang, G. Papastavrou, S.W. Boettcher, C. Xiang, B.S. Brunschwig, PeakForce Scanning Electrochemical Microscopy with Nanoelectrode Probes, Micros. Today. 24 (2016) 18–25. doi:10.1017/S1551929516000882.

[79] Bruker, (n.d.).

[80] O. Sklyar, A. Kueng, C. Kranz, B. Mizaikoff, A. Lugstein, E. Bertagnolli, G. Wittstock, Numerical Simulation of Scanning Electrochemical Microscopy Experiments with Frame-Shaped Integrated Atomic Force Microscopy-SECM Probes Using the Boundary Element Method, Anal. Chem. 77 (2005) 764–771.

[81] D.P. Burt, N.R. Wilson, U. Janus, J. V. Macpherson, P.R. Unwin, In-Situ Atomic Force Microscopy (AFM) Imaging: Influence of AFM Probe Geometry on Diffusion to Microscopic Surfaces, Langmuir. 24 (2008) 12867–12876. doi:10.1021/la8003323.

[82] K. Leonhardt, A. Avdic, A. Lugstein, I. Pobelov, T. Wandlowski, M. Wu, B. Gollas, G. Denuault, Atomic Force Microscopy-Scanning Electrochemical Microscopy: Influence of Tip Geometry and Insulation Defects on Diffusion Controlled Currents at Conical Electrodes, Anal. Chem. 83 (2011) 2971–2977. doi:10.1021/ac103083y.

[83] A. Mirabal, S. Calabrese Barton, Numerical Correction of In Situ AFM-SECM Measurements, Anal. Chem. 93 (2021) 12495–12503. doi:10.1021/acs.analchem.1c00770.

[84] J. Abbou, A. Anne, C. Demaille, Probing the Structure and Dynamics of End-Grafted Flexible Polymer Chain Layers by Combined Atomic Force−Electrochemical Microscopy. Cyclic Voltammetry within Nanometer-Thick Macromolecular Poly(ethylene glycol) Layers, J. Am. Chem. Soc. 126 (2004) 10095–10108. doi:10.1021/ja0493502.

[85] T.O. Paiva, K. Torbensen, A.N. Patel, A. Anne, A. Chovin, C. Demaille, L. Bataille, T. Michon, Probing the Enzymatic Activity of Individual Biocatalytic fd -Viral Particles by Electrochemical-Atomic Force Microscopy, ACS Catal. 10 (2020) 7843–7856. doi:10.1021/acscatal.0c01920.

[86] K. Torbensen, A.N. Patel, A. Anne, A. Chovin, C. Demaille, L. Bataille, T. Michon, E. Grelet, Immuno-Based Molecular Scaffolding of Glucose Dehydrogenase and Ferrocene Mediator on fd Viral Particles Yields Enhanced Bioelectrocatalysis, ACS Catal. 9 (2019) 5783–5796. doi:10.1021/acscatal.9b01263.

[87] K. Wang, C. Goyer, A. Anne, C. Demaille, Exploring the Motional Dynamics of End-Grafted DNA Oligonucleotides by in Situ Electrochemical Atomic Force Microscopy, J. Phys. Chem.

B. 111 (2007) 6051–6058. doi:10.1021/jp070432x.

[88] A. Anne, C. Bonnaudat, C. Demaille, K. Wang, Enzymatic Redox 3‘-End-Labeling of DNA Oligonucleotide Monolayers on Gold Surfaces Using Terminal Deoxynucleotidyl Transferase (TdT)-Mediated Single Base Extension, J. Am. Chem. Soc. 129 (2007) 2734–2735. doi:10.1021/ja067954v.

[89] A. Anne, E. Cambril, A. Chovin, C. Demaille, Touching Surface-Attached Molecules with a Microelectrode: Mapping the Distribution of Redox-Labeled Macromolecules by Electrochemical-Atomic Force Microscopy, Anal. Chem. 82 (2010) 6353–6362. doi:10.1021/ac1012464.

[90] A. Anne, A. Chovin, C. Demaille, M. Lafouresse, High-Resolution Mapping of Redox-Immunomarked Proteins Using Electrochemical–Atomic Force Microscopy in Molecule Touching Mode, Anal. Chem. 83 (2011) 7924–7932. doi:10.1021/ac201907v.

[91] K. Chennit, J. Trasobares, A. Anne, E. Cambril, A. Chovin, N. Clément, C. Demaille, Electrochemical Imaging of Dense Molecular Nanoarrays, Anal. Chem. 89 (2017) 11061–11069. doi:10.1021/acs.analchem.7b03111.

[92] A. Ghorbal, F. Grisotto, J. Charlier, S. Palacin, C. Goyer, C. Demaille, A. Brahim, Nano-Electrochemistry and Nano-Electrografting with an Original Combined AFM-SECM, Nanomaterials. 3 (2013) 303–316. doi:10.3390/nano3020303.

[93] A. Ghorbal, F. Grisotto, J. Charlier, S. Palacin, C. Goyer, C. Demaille, Localized Electrografting of Vinylic Monomers on a Conducting Substrate by Means of an Integrated Electrochemical AFM Probe, ChemPhysChem. 10 (2009) 1053–1057. doi:10.1002/cphc.200800803.

[94] K. Huang, A. Anne, M.A. Bahri, C. Demaille, Probing Individual Redox PEGylated Gold Nanoparticles by Electrochemical–Atomic Force Microscopy, ACS Nano. 7 (2013) 4151–4163. doi:10.1021/nn400527u.

[95] L. Nault, C. Taofifenua, A. Anne, A. Chovin, C. Demaille, J. Besong-Ndika, D. Cardinale, N. Carette, T. Michon, J. Walter, Electrochemical Atomic Force Microscopy Imaging of Redox-

Immunomarked Proteins on Native Potyviruses: From Subparticle to Single-Protein Resolution, ACS Nano. 9 (2015) 4911–4924. doi:10.1021/acsnano.5b00952.

[96] S. Hu, L. Mininni, Y. Hu, N. Erina, J. Kindt, C. Su, High-speed atomic force microscopy and peak force tapping control, in: A. Starikov (Ed.), SPIE Adv. Lithogr., 2012: p. 83241O. doi:10.1117/12.928545.

[97] B.. Derjaguin, V.. Muller, Y.. Toporov, Effect of contact deformations on the adhesion of particles, J. Colloid Interface Sci. 53 (1975) 314–326. doi:10.1016/0021-9797(75)90018-1.

[98] J. Jiang, Z. Huang, C. Xiang, R. Poddar, H. Lewerenz, K.M. Papadantonakis, N.S. Lewis, B.S. Brunschwig, Nanoelectrical and Nanoelectrochemical Imaging of Pt/p-Si and Pt/p + -Si Electrodes, ChemSusChem. 10 (2017) 4657–4663. doi:10.1002/cssc.201700893.

[99] K. Mahankali, N.K. Thangavel, L.M. Reddy Arava, In Situ Electrochemical Mapping of Lithium–Sulfur Battery Interfaces Using AFM–SECM, Nano Lett. 19 (2019) 5229–5236. doi:10.1021/acs.nanolett.9b01636.

[100] M.R. Nellist, Y. Chen, A. Mark, S. Gödrich, C. Stelling, J. Jiang, R. Poddar, C. Li, R. Kumar, G. Papastavrou, M. Retsch, B.S. Brunschwig, Z. Huang, C. Xiang, S.W. Boettcher, Atomic force microscopy with nanoelectrode tips for high resolution electrochemical, nanoadhesion and nanoelectrical imaging, Nanotechnology. 28 (2017) 095711. doi:10.1088/1361-6528/aa5839.

[101] F.J. Giessibl, High-speed force sensor for force microscopy and profilometry utilizing a quartz tuning fork, Appl. Phys. Lett. 73 (1998) 3956–3958. doi:10.1063/1.122948.

[102] S. Kolagatla, P. Subramanian, A. Schechter, Insights on the Electrochemical Atomic Force Microscopic Catalytic Oxygen Reduction on Tip Guided Platinum Particle Deposits, Electrochim. Acta. 217 (2016) 100–107. doi:10.1016/j.electacta.2016.09.042.

[103] S. Kolagatla, P. Subramanian, A. Schechter, Catalytic current mapping of oxygen reduction on isolated Pt particles by atomic force microscopy-scanning electrochemical microscopy, Appl. Catal. B Environ. 256 (2019) 117843. doi:10.1016/j.apcatb.2019.117843.

[104] S. Kolagatla, P. Subramanian, A. Schechter, Simultaneous Mapping of Oxygen Reduction

Activity and Hydrogen Peroxide Generation on Electrocatalytic Surfaces, ChemSusChem. 12 (2019) 2708–2714. doi:10.1002/cssc.201900656.

[105] S. Kolagatla, P. Subramanian, A. Schechter, Nanoscale mapping of catalytic hotspots on Fe, N-modified HOPG by scanning electrochemical microscopy-atomic force microscopy, Nanoscale. 10 (2018) 6962–6970. doi:10.1039/C8NR00849C.

[106] K. Eckhard, H. Shin, B. Mizaikoff, W. Schuhmann, C. Kranz, Alternating current (AC) impedance imaging with combined atomic force scanning electrochemical microscopy (AFM-SECM), Electrochem. Commun. 9 (2007) 1311–1315. doi:10.1016/j.elecom.2007.01.027.

[107] K. Eckhard, C. Kranz, H. Shin, B. Mizaikoff, W. Schuhmann, Frequency Dependence of the Electrochemical Activity Contrast in AC-Scanning Electrochemical Microscopy and Atomic Force Microscopy-AC-Scanning Electrochemical Microscopy Imaging, Anal. Chem. 79 (2007) 5435–5438. doi:10.1021/ac070605e.

[108] U.M. Tefashe, G. Wittstock, Quantitative characterization of shear force regulation for scanning electrochemical microscopy, Comptes Rendus Chim. 16 (2013) 7–14. doi:10.1016/j.crci.2012.03.011.

[109] J. V. Macpherson, J.-P.G. de Mussy, J.-L. Delplancke, Conducting-Atomic Force Microscopy Investigation of the Local Electrical Characteristics of a Ti/TiO[sub 2]/Pt Anode, Electrochem. Solid-State Lett. 4 (2001) E33. doi:10.1149/1.1388195.

[110] R. Ma, G. Lin, Y. Zhou, Q. Liu, T. Zhang, G. Shan, M. Yang, J. Wang, A review of oxygen reduction mechanisms for metal-free carbon-based electrocatalysts, Npj Comput. Mater. 5 (2019) 78. doi:10.1038/s41524-019-0210-3.

[111] A. Davoodi, J. Pan, C. Leygraf, S. Norgren, Probing of local dissolution of Al-alloys in chloride solutions by AFM and SECM, Appl. Surf. Sci. 252 (2006) 5499–5503. doi:10.1016/j.apsusc.2005.12.023.

[112] J. Izquierdo, A. Eifert, R.M. Souto, C. Kranz, Simultaneous pit generation and visualization of pit topography using combined atomic force–scanning electrochemical microscopy, Electrochem. Commun. 51 (2015) 15–18. doi:10.1016/j.elecom.2014.11.017.

[113] J. Izquierdo, A. Eifert, C. Kranz, R.M. Souto, In Situ Monitoring of Pit Nucleation and Growth at an Iron Passive Oxide Layer by using Combined Atomic Force and Scanning Electrochemical Microscopy, ChemElectroChem. 2 (2015) 1847–1856. doi:10.1002/celc.201500100.

[114] J. Izquierdo, B.M. Fernández-Pérez, A. Eifert, R.M. Souto, C. Kranz, Simultaneous Atomic Force—Scanning Electrochemical Microscopy (AFM-SECM) Imaging of Copper Dissolution, Electrochim. Acta. 201 (2016) 320–332. doi:10.1016/j.electacta.2015.12.160.

[115] J. Izquierdo, A. Eifert, C. Kranz, R.M. Souto, In situ investigation of copper corrosion in acidic chloride solution using atomic force—scanning electrochemical microscopy, Electrochim. Acta. 247 (2017). doi:10.1016/j.electacta.2017.07.042.

[116] J. Izquierdo, P. Knittel, C. Kranz, Scanning electrochemical microscopy: an analytical perspective, Anal. Bioanal. Chem. 410 (2018) 307–324. doi:10.1007/s00216-017-0742-7.

[117] S. Sekine, H. Kaji, M. Nishizawa, Spatiotemporal sub-cellular biopatterning using an AFM-assisted electrochemical system, Electrochem. Commun. 11 (2009) 1781–1784. doi:10.1016/j.elecom.2009.07.016.

[118] J. V. Macpherson, C.E. Jones, A.L. Barker, P.R. Unwin, Electrochemical Imaging of Diffusion through Single Nanoscale Pores, Anal. Chem. 74 (2002) 1841–1848. doi:10.1021/ac0157472.

[119] Y. Liu, A. Holzinger, P. Knittel, L. Poltorak, A. Gamero-Quijano, W.D.A. Rickard, A. Walcarius, G. Herzog, C. Kranz, D.W.M. Arrigan, Visualization of Diffusion within Nanoarrays, Anal. Chem. 88 (2016) 6689–6695. doi:10.1021/acs.analchem.6b00513.

[120] A. Kueng, C. Kranz, A. Lugstein, E. Bertagnolli, B. Mizaikoff, AFM-Tip-Integrated Amperometric Microbiosensors: High-Resolution Imaging of Membrane Transport, Angew. Chemie Int. Ed. 44 (2005) 3419–3422. doi:10.1002/anie.200461556.

[121] M.D. Scanlon, J. Strutwolf, A. Blake, D. Iacopino, A.J. Quinn, D.W.M. Arrigan, Ion-Transfer Electrochemistry at Arrays of Nanointerfaces between Immiscible Electrolyte Solutions Confined within Silicon Nitride Nanopore Membranes, Anal. Chem. 82 (2010) 6115–6123. doi:10.1021/ac1008282.

[122] M. Sairi, N. Chen-Tan, G. Neusser, C. Kranz, D.W.M. Arrigan, Electrochemical Characterisation of Nanoscale Liquid|Liquid Interfaces Located at Focused Ion Beam-Milled Silicon Nitride Membranes, ChemElectroChem. 2 (2015) 98–105. doi:10.1002/celc.201402252.

[123] A.N. Patel, A. Anne, A. Chovin, C. Demaille, E. Grelet, T. Michon, C. Taofifenua, Scaffolding of Enzymes on Virus Nanoarrays: Effects of Confinement and Virus Organization on Biocatalysis, Small. 13 (2017) 1603163. doi:10.1002/smll.201603163.

[124] Z. Zhao, J. Fu, S. Dhakal, A. Johnson-Buck, M. Liu, T. Zhang, N.W. Woodbury, Y. Liu, N.G. Walter, H. Yan, Nanocaged enzymes with enhanced catalytic activity and increased stability against protease digestion, Nat. Commun. 7 (2016) 10619. doi:10.1038/ncomms10619.

[125] Y.F. Dufrêne, A.E. Pelling, Force nanoscopy of cell mechanics and cell adhesion, Nanoscale. 5 (2013) 4094. doi:10.1039/c3nr00340j.

[126] H. Hertz, Ueber die Berührung fester elastischer Körper., J. Für Die Reine Und Angew. Math. 1882 (1882) 156–171. doi:10.1515/crll.1882.92.156.

[127] G. Zampardi, S. Klink, V. Kuznetsov, T. Erichsen, A. Maljusch, F. La Mantia, W. Schuhmann, E. Ventosa, Combined AFM/SECM Investigation of the Solid Electrolyte Interphase in Li-Ion Batteries, ChemElectroChem. 2 (2015) 1607–1611. doi:10.1002/celc.201500085.

[128] T.S. Watkins, D. Sarbapalli, M.J. Counihan, A.S. Danis, J. Zhang, L. Zhang, K.R. Zavadil, J. Rodríguez-López, A combined SECM and electrochemical AFM approach to probe interfacial processes affecting molecular reactivity at redox flow battery electrodes, J. Mater. Chem. A. 8 (2020) 15734–15745. doi:10.1039/D0TA00836B.

[129] F.-R.F. Fan, A.J. Bard;, R. Guckenberger, M. Heim, STM on Wet Insulators: Electrochemistry or Tunneling?, Science 270 (1995) 1849–1852. doi:10.1126/science.270.5243.1849.

[130] R. Guckenberger, M. Heim, G. Cevc, H. Knapp, W. Wiegrabe, A. Hillebrand, Scanning tunneling microscopy of insulators and biological specimens based on lateral conductivity of ultrathin water films, Science 266 (1994) 1538–1540. doi:10.1126/science.7985024.

[131] Y. Zhu, D.E. Williams, Scanning Electrochemical Microscopic Observation of a Precursor

State to Pitting Corrosion of Stainless Steel, J. Electrochem. Soc. 144 (1997) L43–L45. doi:10.1149/1.1837487.

[132] D.E. Williams, T.F. Mohiuddin, Y.Y. Zhu, Elucidation of a Trigger Mechanism for Pitting Corrosion of Stainless Steels Using Submicron Resolution Scanning Electrochemical and Photoelectrochemical Microscopy, J. Electrochem. Soc. 145 (1998) 2664–2672. doi:10.1149/1.1838697.

[133] J. Meier, K.A. Friedrich, U. Stimming, Novel method for the investigation of single nanoparticle reactivity., Faraday Discuss. (2002) 365–372; discussion 441-462. doi:10.1039/b200014h.

[134] T.H. Treutler, G. Wittstock, Combination of an electrochemical tunneling microscope (ECSTM) and a scanning electrochemical microscope (SECM): application for tip-induced modification of self-assembled monolayers, Electrochim. Acta. 48 (2003) 2923–2932. doi:10.1016/S0013-4686(03)00357-8.

[135] E. Ammann, C. Beuret, P.-F. Indermühle, R. Kötz, N.F. de Rooij, H. Siegenthaler, Local pH-controlled reactivity investigations by thin-layer scanning tunnelling microscopy, Electrochim. Acta. 47 (2001) 327–334. doi:10.1016/s0013-4686(01)00579-5.

[136] J.F. Edmondson, G.N. Meloni, G. Costantini, P.R. Unwin, Synchronous Electrical Conductance- and Electron Tunnelling-Scanning Electrochemical Microscopy Measurements, ChemElectroChem. 7 (2020) 697–706. doi:https://doi.org/10.1002/celc.201901721.

[137] T. Sun, D. Wang, M. V Mirkin, Tunneling Mode of Scanning Electrochemical Microscopy: Probing Electrochemical Processes at Single Nanoparticles, Angew. Chemie Int. Ed. 57 (2018) 7463–7467. doi:https://doi.org/10.1002/anie.201801115.

[138] E. Betzig, P.L. Finn, J.S. Weiner, Combined shear force and near-field scanning optical microscopy, Appl. Phys. Lett. 60 (1992) 2484–2486. doi:10.1063/1.106940.

[139] M. Ludwig, C. Kranz, W. Schuhmann, H.E. Gaub, Topography feedback mechanism for the scanning electrochemical microscope based on hydrodynamic forces between tip and sample, Rev. Sci. Instrum. 66 (1995) 2857–2860. doi:10.1063/1.1145568.

[140] A. Hengstenberg, C. Kranz, W. Schuhmann, Facilitated tip-positioning and applications of non-electrode tips in scanning electrochemical microscopy using a shear force based constant-distance mode, Chem. - A Eur. J. 6 (2000) 1547–1554. doi:10.1002/(SICI)1521-3765(20000502)6:9.

[141] M. Etienne, A. Schulte, S. Mann, G. Jordan, I.D. Dietzel, W. Schuhmann, Constant-Distance Mode Scanning Potentiometry. 1. Visualization of Calcium Carbonate Dissolution in Aqueous Solution, Anal. Chem. 76 (2004) 3682–3688. doi:10.1021/ac0349227.

[142] M. Etienne, P. Dierkes, T. Erichsen, W. Schuhmann, I. Fritsch, Constant-distance mode scanning potentiometry. High resolution pH measurements in three-dimensions, Electroanalysis. 19 (2007) 318–323.

[143] I. Turyan, M. Etienne, D. Mandler, W. Schuhmann, Improved Resolution of Local Metal Deposition by Means of Constant Distance Mode Scanning Electrochemical Microscopy, Electroanalysis. 17 (2005) 538–542. doi:10.1002/elan.200403179.

[144] A. Hengstenberg, A. Blöchl, I.D. Dietzel, W. Schuhmann, Spatially Resolved Detection of Neurotransmitter Secretion from Individual Cells by Means of Scanning Electrochemical Microscopy, Angew. Chemie Int. Ed. 40 (2001) 905–908. doi:10.1002/1521-3773(20010302)40:5.

[145] S. Isik, W. Schuhmann, Detection of nitric oxide release from single cells by using constant-distance-mode scanning electrochemical microscopy, Angew. Chem. Int. Ed. 45 (2006) 7451–7454.

[146] M. Nebel, S. Grützke, N. Diab, A. Schulte, W. Schuhmann, Visualization of Oxygen Consumption of Single Living Cells by Scanning Electrochemical Microscopy: The Influence of the Faradaic Tip Reaction, Angew. Chemie Int. Ed. 52 (2013) 6335–6338. doi:10.1002/anie.201301098.

[147] A. Schulte, M. Nebel, W. Schuhmann, Chapter twelve - Single Live Cell Topography and Activity Imaging with the Shear-Force-Based Constant-Distance Scanning Electrochemical Microscope, in: P.M.B.T.-M. in E. conn (Ed.), Imaging Spectrosc. Anal. Living Cells,

Academic Press, 2012: pp. 237–254. doi:https://doi.org/10.1016/B978-0-12-391857-4.00012-4.

[148] B. Ballesteros Katemann, A. Schulte, W. Schuhmann, Constant-Distance Mode Scanning Electrochemical Microscopy (SECM)—Part I: Adaptation of a Non-Optical Shear-Force-Based Positioning Mode for SECM Tips, Chem. - A Eur. J. 9 (2003) 2025–2033. doi:10.1002/chem.200204267.

[149] M. Etienne, A. Schulte, W. Schuhmann, High resolution constant-distance mode alternating current scanning electrochemical microscopy (AC-SECM), Electrochem. Commun. 6 (2004) 288–293. doi:10.1016/j.elecom.2004.01.006.

[150] K. Eckhard, M. Etienne, A. Schulte, W. Schuhmann, Constant-distance mode AC-SECM for the visualisation of corrosion pits, Electrochem. Commun. 9 (2007) 1793–1797. doi:10.1016/j.elecom.2007.03.035.

[151] M. Etienne, B. Layoussifi, T. Giornelli, D. Jacquet, SECM-based automate equipped with a shearforce detection for the characterization of large and complex samples, Electrochem. Commun. 15 (2012) 70–73. doi:https://doi.org/10.1016/j.elecom.2011.11.028.

[152] M. Etienne, J.-P. Moulin, S. Gourhand, Accurate control of the electrode shape for high resolution shearforce regulated SECM, Electrochim. Acta. in press (2013). doi:10.1016/j.electacta.2013.03.096.

[153] M. Etienne, S. Lhenry, R. Cornut, C. Lefrou, Optimization of the shearforce signal for scanning electrochemical microscopy and application for kinetic analysis, Electrochim. Acta. 88 (2013) 877–884. doi:10.1016/j.electacta.2012.09.063.

[154] M. Etienne, M. Dossot, J. Grausem, G. Herzog, Combined raman microspectrometer and shearforce regulated SECM for corrosion and self-healing analysis, Anal. Chem. 86 (2014) 11203–11210. doi:10.1021/ac502670t.

[155] P. Dauphin-Ducharme, W.J. Binns, M.E. Snowden, D.W. Shoesmith, J. Mauzeroll, Determination of the local corrosion rate of magnesium alloys using a shear force mounted scanning microcapillary method, Faraday Discuss. 180 (2015) 331–345. doi:10.1039/C4FD00276H.

[156] M. Etienne, E. Rocca, N. Chahboun, D. Veys-Renaux, Local Evolution of pH with Time Determined by Shear Force-based Scanning Electrochemical Microscopy: Surface Reactivity of Anodized Aluminium, Electroanalysis. 28 (2016) 2466–2471. doi:https://doi.org/10.1002/elan.201600294.

[157] C. Reiner-Rozman, J. Schodl, C. Nowak, C. Kleber, Scanning Electrochemical Microscopy as a Characterization Tool for Reduced Graphene Oxide Field Effect Transistors, E-Journal Surf. Sci. Nanotechnol. 13 (2015) 366–372. doi:10.1380/ejssnt.2015.366.

[158] L. Liu, M. Etienne, A. Walcarius, Scanning Gel Electrochemical Microscopy for Topography and Electrochemical Imaging, Anal. Chem. 90 (2018) 8889–8895. doi:10.1021/acs.analchem.8b01011.

[159] N. Dang, M. Etienne, A. Walcarius, L. Liu, Scanning gel electrochemical microscopy (SGECM): The potentiometric measurements, Electrochem. Commun. 97 (2018) 64–67. doi:https://doi.org/10.1016/j.elecom.2018.10.020.

[160] N. Dang, M. Etienne, A. Walcarius, L. Liu, Scanning Gel Electrochemical Microscopy (SGECM): Lateral Physical Resolution by Current and Shear Force Feedback, Anal. Chem. 92 (2020) 6415–6422. doi:10.1021/acs.analchem.9b05538.

[161] B. Ballesteros Katemann, A. Schulte, W. Schuhmann, Constant-Distance Mode Scanning Electrochemical Microscopy. Part II: High-Resolution SECM Imaging Employing Pt Nanoelectrodes as Miniaturized Scanning Probes, Electroanalysis. 16 (2004) 60–65. doi:10.1002/elan.200302918.

[162] M. Etienne, E.C. Anderson, S.R. Evans, W. Schuhmann, I. Fritsch, Feedback-Independent Pt Nanoelectrodes for Shear Force-Based Constant-Distance Mode Scanning Electrochemical Microscopy, Anal. Chem. 78 (2006) 7317–7324. doi:10.1021/ac061310o.

[163] M. Nebel, K. Eckhard, T. Erichsen, A. Schulte, W. Schuhmann, 4D shearforce-based constant-distance mode scanning electrochemical microscopy., Anal. Chem. 82 (2010) 7842–7848. doi:10.1021/ac1008805.

[164] C. Cougnon, K. Bauer-Espindola, D.S. Fabre, J. Mauzeroll, Development of a Phase-

Controlled Constant-Distance Scanning Electrochemical Microscope, Anal. Chem. 81 (2009) 3654–3659. doi:10.1021/ac802211u.

[165] C. Dincer, E. Laubender, J. Hees, C.E. Nebel, G. Urban, J. Heinze, SECM detection of single boron doped diamond nanodes and nanoelectrode arrays using phase-operated shear force technique, Electrochem. Commun. 24 (2012) 123–127. doi:10.1016/j.elecom.2012.08.005.

[166] L. Danis, M.E. Snowden, U.M. Tefashe, C.N. Heinemann, J. Mauzeroll, Development of Nano-Disc electrodes for Application as Shear Force Sensitive Electrochemical Probes, Electrochim. Acta. 136 (2014) 121–129. doi:https://doi.org/10.1016/j.electacta.2014.05.047.

[167] E.M. Hussien, W. Schuhmann, A. Schulte, Shearforce-Based Constant-Distance Scanning Electrochemical Microscopy as Fabrication Tool for Needle-Type Carbon-Fiber Nanoelectrodes, Anal. Chem. 82 (2010) 5900–5905. doi:10.1021/ac100738b.

[168] C. Adam, F. Kanoufi, N. Sojic, M. Etienne, Shearforce positioning of nanoprobe electrode arrays for scanning electrochemical microscopy experiments, Electrochim. Acta. 179 (2015) 45–56. doi:https://doi.org/10.1016/j.electacta.2015.04.140.

[169] K. Karrai, R.D. Grober, Piezoelectric tip-sample distance control for near field optical microscopes, Appl. Phys. Lett. 66 (1995) 1842–1844. doi:10.1063/1.113340.

[170] P.I. James, L.F. Garfias-Mesias, P.J. Moyer, W.H. Smyrl, Scanning Electrochemical Microscopy with Simultaneous Independent Topography, J. Electrochem. Soc. 145 (1998) L64–L66. doi:10.1149/1.1838417.

[171] M. Büchler, S.C. Kelley, W.H. Smyrl, Scanning electrochemical microscopy with shear force feedback. Investigation of the lateral resolution of different experimental configurations, Electrochem. Solid-State Lett. 3 (2000) 35–38. doi:10.1149/1.1390950.

[172] H. Yamada, M. Ogata, T. Koike, Scanning Electrochemical Microscope Observation of Defects in a Hexadecanethiol Monolayer on Gold with Shear Force-Based Tip−Substrate Positioning, Langmuir. 22 (2006) 7923–7927. doi:10.1021/la0613171.

[173] Y. Zu, Z. Ding, J. Zhou, Y. Lee, A.J. Bard, Z. Ding, A.J. Bard, Scanning Optical Microscopy with an Electrogenerated Chemiluminescent Light Source at a Nanometer Tip, Anal. Chem. 77

(2002) 1785–1790. doi:10.1021/ac015713u.

[174] Y. Lee, Z. Ding, A.J. Bard, Combined Scanning Electrochemical/Optical Microscopy with Shear Force and Current Feedback, Anal. Chem. 74 (2002) 3634–3643. doi:10.1021/ac015713u.

[175] H. Yamada, H. Fukumoto, T. Yokoyama, T. Koike, Immobilized Diaphorase Surfaces Observed by Scanning Electrochemical Microscope with Shear Force Based Tip−Substrate Positioning, Anal. Chem. 77 (2005) 1785–1790. doi:10.1021/ac048582g.

[176] Y. Takahashi, Y. Hirano, T. Yasukawa, H. Shiku, H. Yamada, T. Matsue, Topographic, electrochemical, and optical images captured using standing approach mode scanning electrochemical/optical microscopy., Langmuir. 22 (2006) 10299–10306. doi:10.1021/la0611763.

[177] Y. Takahashi, H. Shiku, T. Murata, T. Yasukawa, T. Matsue, Transfected Single-Cell Imaging by Scanning Electrochemical Optical Microscopy with Shear Force Feedback Regulation, Anal. Chem. 81 (2009) 9674–9681. doi:10.1021/ac901796r.

[178] H. Yamada, Imaging a Single Living Cell via Shear Force-based Scanning Ion Conductance Microscopy in Standing Approach Mode with Differential Control, Electrochim. Acta. 136 (2014) 233–239. doi:https://doi.org/10.1016/j.electacta.2014.05.109.

[179] H. Yamada, D. Haraguchi, K. Yasunaga, Fabrication and Characterization of a K+-Selective Nanoelectrode and Simultaneous Imaging of Topography and Local K+ Flux Using Scanning Electrochemical Microscopy, Anal. Chem. 86 (2014) 8547–8552. doi:10.1021/ac502444y.

[180] M. Florencia Garay, J. Ufheil, K. Borgwarth, J. Heinze, Retrospective chemical analysis of tree rings by means of the scanning electrochemical microscopy with shear force feedback, Phys. Chem. Chem. Phys. 6 (2004) 4028. doi:10.1039/b402458c.

[181] D. Oyamatsu, Y. Hirano, N. Kanaya, Y. Mase, M. Nishizawa, T. Matsue, Imaging of enzyme activity by scanning electrochemical microscope equipped with a feedback control for substrate–probe distance, Bioelectrochemistry. 60 (2003) 115–121. doi:10.1016/S1567-5394(03)00055-0.

[182] HEKA, (n.d.). https://www.elproscan.com/shear-force/.

[183] Sensolytics, (n.d.).

[184] P.K. Hansma, J.P. Cleveland, M. Radmacher, D.A. Walters, P.E. Hillner, M. Bezanilla, M. Fritz, D. Vie, H.G. Hansma, C.B. Prater, J. Massie, L. Fukunaga, J. Gurley, V. Elings, Tapping mode atomic force microscopy in liquids, Appl. Phys. Lett. 64 (1994) 1738–1740. doi:10.1063/1.111795.

[185] K. McKelvey, M.A. Edwards, P.R. Unwin, Intermittent contact-scanning electrochemical microscopy (IC-SECM): A new approach for tip positioning and simultaneous imaging of interfacial topography and activity, Anal. Chem. 82 (2010) 6334–6337. doi:10.1021/ac101099e.

[186] D.O. Wipf, A.J. Bard, Scanning electrochemical microscopy. 15. Improvements in imaging via tip-position modulation and lock-in detection, Anal. Chem. 64 (1992) 1362–1367. doi:10.1021/ac00037a011.

[187] M.A. Edwards, A.L. Whitworth, P.R. Unwin, Quantitative Analysis and Application of Tip Position Modulation-Scanning Electrochemical Microscopy, Anal. Chem. 83 (2011) 1977–1984. doi:10.1021/ac102680v.

[188] K. McKelvey, M.E. Snowden, M. Peruffo, P.R. Unwin, Quantitative Visualization of Molecular Transport through Porous Membranes: Enhanced Resolution and Contrast Using Intermittent Contact-Scanning Electrochemical Microscopy, Anal. Chem. 83 (2011) 6447–6454. doi:10.1021/ac201489c.

[189] H. V Patten, K.E. Meadows, L.A. Hutton, J.G. Iacobini, D. Battistel, K. McKelvey, A.W. Colburn, M.E. Newton, J. V Macpherson, P.R. Unwin, Electrochemical Mapping Reveals Direct Correlation between Heterogeneous Electron-Transfer Kinetics and Local Density of States in Diamond Electrodes, Angew. Chemie Int. Ed. 51 (2012) 7002–7006. doi:https://doi.org/10.1002/anie.201203057.

[190] L.I. Tomlinson, H. V. Patten, B.L. Green, J. Iacobini, K.E. Meadows, K. McKelvey, P.R. Unwin, M.E. Newton, J. V. Macpherson, Intermittent-contact Scanning Electrochemical

Microscopy (IC-SECM) as a Quantitative Probe of Defects in Single Crystal Boron Doped Diamond Electrodes, Electroanalysis. 28 (2016) 2297–2302. doi:10.1002/elan.201600291.

[191] R.A. Lazenby, K. McKelvey, M. Peruffo, M. Baghdadi, P.R. Unwin, Nanoscale intermittent contact-scanning electrochemical microscopy, J. Solid State Electrochem. 17 (2013) 2979–2987. doi:10.1007/s10008-013-2168-2.

[192] R.A. Lazenby, K. MKelvey, P.R. Unwin, Hopping Intermittent Contact-Scanning Electrochemical Microscopy (HIC-SECM): Visualizing Interfacial Reactions and Fluxes from Surfaces to Bulk Solution, Anal. Chem. 85 (2013) 2937–2944. doi:10.1021/ac303642p.

[193] A.R. Perry, R.A. Lazenby, M. Adobes-Vidal, M. Peruffo, K. McKelvey, M.E. Snowden, P.R. Unwin, Hopping intermittent contact-scanning electrochemical microscopy (HIC-SECM) as a new local dissolution kinetic probe: application to salicylic acid dissolution in aqueous solution, CrystEngComm. 17 (2015) 7835–7843. doi:10.1039/c5ce00138b.

[194] S.R. Catarelli, D. Lonsdale, L. Cheng, J. Syzdek, M. Doeff, Intermittent Contact Alternating Current Scanning Electrochemical Microscopy: A Method for Mapping Conductivities in Solid Li Ion Conducting Electrolyte Samples, Front. Energy Res. (n.d.) 8. doi:DOI:103389/fenrg201600014.

[195] M.C. Lafouresse, M.-L. de Bonfils-Lahovary, L. Laffont, C. Blanc, Hydrogen mapping in an aluminum alloy using an alternating current scanning electrochemical microscope (AC-SECM), Electrochem. Commun. 80 (2017) 29–32. doi:https://doi.org/10.1016/j.elecom.2017.05.007.

[196] B.R. Horrocks, D. Schmidtke, A. Heller, A.J. Bard, Scanning electrochemical microscopy. 24. Enzyme ultramicroelectrodes for the measurement of hydrogen peroxide at surfaces, Anal. Chem. 65 (1993) 3605–3614. doi:10.1021/ac00072a013.

[197] K. Eckhard, W. Schuhmann, Alternating current techniques in scanning electrochemical microscopy (AC-SECM), Analyst. 133 (2008) 1486–1497.

[198] C. Gabrielli, F. Huet, M. Keddam, P. Rousseau, V. Vivier, Scanning Electrochemical Microscopy Imaging by Means of High-Frequency Impedance Measurements in Feedback

Mode, J. Phys. Chem. B. 108 (2004) 11620–11626. doi:10.1021/jp0496809.

[199] P.M. Diakowski, Z. Ding, Novel strategy for constant-distance imaging using alternating current scanning electrochemical microscopy, Electrochem. Commun. 9 (2007) 2617–2621. doi:10.1016/j.elecom.2007.08.010.

[200] R.T. Kurulugama, D.O. Wipf, S.A. Takacs, S. Pongmayteegul, P.A. Garris, J.E. Baur, Scanning Electrochemical Microscopy of Model Neurons: Constant Distance Imaging, Anal. Chem. 77 (2005) 1111–1117. doi:10.1021/ac048571n.

[201] D.M. Osbourn, R.H. Sanger, P.J.S. Smith, Determination of Single-Cell Oxygen Consumption with Impedance Feedback for Control of Sample−Probe Separation, Anal. Chem. 77 (2005) 6999–7004. doi:10.1021/ac050326w.

[202] K. Eckhard, T. Erichsen, M. Stratmann, W. Schuhmann, Frequency-Dependent Alternating-Current Scanning Electrochemical Microscopy (4D AC-SECM) for Local Visualisation of Corrosion Sites, Chem. – A Eur. J. 14 (2008) 3968–3976. doi:https://doi.org/10.1002/chem.200701861.

[203] P.M. Diakowski, Z. Ding, Interrogation of living cells using alternating current scanning electrochemical microscopy (AC-SECM), Phys. Chem. Chem. Phys. 9 (2007) 5966–5974.

[204] B. Ballesteros Katemann, Localised electrochemical impedance spectroscopy with high lateral resolution by means of alternating current scanning electrochemical microscopy, Electrochem. Commun. 4 (2002) 134–138. doi:10.1016/s1388-2481(01)00294-6.

[205] D. Trinh, M. Keddam, X.R. Novoa, V. Vivier, Alternating-Current Measurements in Scanning Electrochemical Microscopy, Part 1: Principle and Theory, ChemPhysChem. 12 (2011) 2169–2176. doi:https://doi.org/10.1002/cphc.201001084.

[206] A.S. Bandarenka, K. Eckhard, A. Maljusch, W. Schuhmann, Localized Electrochemical Impedance Spectroscopy: Visualization of Spatial Distributions of the Key Parameters Describing Solid/Liquid Interfaces, Anal. Chem. 85 (2013) 2443–2448. doi:10.1021/ac303490t.

[207] A.S. Bandarenka, A. Maljusch, V. Kuznetsov, K. Eckhard, W. Schuhmann, Localized

impedance measurements for electrochemical surface science, J. Phys. Chem. C. 118 (2014) 8952–8959. doi:10.1021/jp412505p.

[208] D. Trinh, M. Keddam, X.R. Novoa, V. Vivier, Alternating Current Measurements in Scanning Electrochemical Microscopy, Part 2: Detection of Adsorbates, ChemPhysChem. 12 (2011) 2177–2183. doi:https://doi.org/10.1002/cphc.201001085.

[209] V. Kuznetsov, A. Maljusch, R.M. Souto, A.S. Bandarenka, W. Schuhmann, Characterisation of localised corrosion processes using scanning electrochemical impedance microscopy, Electrochem. Commun. 44 (2014) 38–41. doi:https://doi.org/10.1016/j.elecom.2014.04.011.

[210] M. Lucas, J.-F. Boily, Mapping Electrochemical Heterogeneity at Iron Oxide Surfaces: A Local Electrochemical Impedance Study, Langmuir. 31 (2015) 13618–13624. doi:10.1021/acs.langmuir.5b03849.

[211] A. Estrada-Vargas, A. Bandarenka, V. Kuznetsov, W. Schuhmann, In Situ Characterization of Ultrathin Films by Scanning Electrochemical Impedance Microscopy, Anal. Chem. 88 (2016) 3354–3362. doi:10.1021/acs.analchem.6b00011.

[212] I. Morkvenaite-Vilkonciene, P. Genys, A. Ramanaviciene, A. Ramanavicius, Scanning electrochemical impedance microscopy for investigation of glucose oxidase catalyzed reaction, Colloids Surfaces B Biointerfaces. 126 (2015) 598–602. doi:10.1016/j.colsurfb.2015.01.007.

[213] I. Morkvenaite-Vilkonciene, A. Valiūnienė, J. Petroniene, A. Ramanavicius, Hybrid system based on fast Fourier transform electrochemical impedance spectroscopy combined with scanning electrochemical microscopy, Electrochem. Commun. 83 (2017) 110–112. doi:10.1016/j.elecom.2017.08.020.

[214] A. Valiūnienė, J. Petroniene, I. Morkvenaite-Vilkonciene, G. Popkirov, A. Ramanaviciene, A. Ramanavicius, Redox-probe-free scanning electrochemical microscopy combined with fast Fourier transform electrochemical impedance spectroscopy, Phys. Chem. Chem. Phys. 21 (2019) 9831–9836. doi:10.1039/C9CP00187E.

[215] A. Valiūnienė, T. Sabirovas, J. Petronienė, A. Ramanavičius, Towards the application of fast Fourier transform - scanning electrochemical impedance microscopy (FFT-SEIM), J.

Electroanal. Chem. 864 (2020) 114067. doi:https://doi.org/10.1016/j.jelechem.2020.114067.

[216] A. Valiūnienė, J. Petronienė, M. Dulkys, A. Ramanavičius, Investigation of Active and Inactivated Yeast Cells by Scanning Electrochemical Impedance Microscopy, Electroanalysis. 32 (2019) 367–374. doi:10.1002/elan.201900414.

[217] V. Sundaresan, K. Marchuk, Y. Yu, E.J. Titus, A.J. Wilson, C.M. Armstrong, B. Zhang, K.A. Willets, Visualizing and Calculating Tip-Substrate Distance in Nanoscale Scanning Electrochemical Microscopy Using 3-Dimensional Super-Resolution Optical Imaging, Anal. Chem. 89 (2017) 922–928. doi:10.1021/acs.analchem.6b04073.

[218] N. Casillas, P. James, W.H. Smyrl, A Novel Approach to Combine Scanning Electrochemical Microscopy and Scanning Photoelectrochemical Microscopy, J. Electrochem. Soc. 142 (1995) L16–L18. doi:10.1149/1.2043970.

[219] P. James, N. Casillas, W.H. Smyrl, Simultaneous Scanning Electrochemical and Photoelectrochemical Microscopy by Use of a Metallized Optical Fiber, J. Electrochem. Soc. 143 (1996) 3853–3865. doi:10.1149/1.1837308.

[220] G. Shi, L.F. Garfias-Mesias, W.H. Smyrl, Preparation of a Gold-Sputtered Optical Fiber as a Microelectrode for Electrochemical Microscopy, J. Electrochem. Soc. 145 (1998) 2011–2016. doi:10.1149/1.1838591.

[221] E. Sosa, R. Cabrera-Sierra, M.T. Oropeza, F. Hernández, N. Casillas, R. Tremont, C. Cabrera, I. González, Chemical Characterization of Corrosion Films Electrochemically Grown on Carbon Steel in Alkaline Sour Environment, J. Electrochem. Soc. 150 (2003) B530. doi:10.1149/1.1617303.

[222] J. Lee, H. Ye, S. Pan, A.J. Bard, Screening of Photocatalysts by Scanning Electrochemical Microscopy, Anal. Chem. 80 (2008) 7445–7450. doi:10.1021/ac801142g.

[223] J.S. Jang, K.Y. Yoon, X. Xiao, F.-R.F. Fan, A.J. Bard, Development of a Potential Fe2O3-Based Photocatalyst Thin Film for Water Oxidation by Scanning Electrochemical Microscopy: Effects of Ag−Fe2O3 Nanocomposite and Sn Doping, Chem. Mater. 21 (2009) 4803–4810. doi:10.1021/cm901056c.

[224] J.S. Jang, J. Lee, H. Ye, F.-R.F. Fan, A.J. Bard, Rapid Screening of Effective Dopants for Fe2O3 Photocatalysts with Scanning Electrochemical Microscopy and Investigation of Their Photoelectrochemical Properties, J. Phys. Chem. C. 113 (2009) 6719–6724. doi:10.1021/jp8109429.

[225] G. Liu, C. Liu, A.J. Bard, Rapid Synthesis and Screening of ZnxCd1−xSySe1−y Photocatalysts by Scanning Electrochemical Microscopy, J. Phys. Chem. C. 114 (2010) 20997–21002. doi:10.1021/jp1058116.

[226] H. Ye, H.S. Park, A.J. Bard, Screening of Electrocatalysts for Photoelectrochemical Water Oxidation on W-Doped BiVO4 Photocatalysts by Scanning Electrochemical Microscopy, J. Phys. Chem. C. 115 (2011) 12464–12470. doi:10.1021/jp200852c.

[227] D. Yuan, L. Xiao, J. Jia, J. Zhang, L. Han, P. Li, B.-W. Mao, D. Zhan, Combinatorial Screening of Photoelectrocatalytic System with High Signal/Noise Ratio, Anal. Chem. 86 (2014) 11972–11976. doi:10.1021/ac503614h.

[228] Y.-C. Weng, H. Chang, Screening and characterization for the optimization of CdS-based photocatalysts, RSC Adv. 6 (2016) 41376–41384. doi:10.1039/C6RA05245B.

[229] M. Harati, J. Jia, K. Giffard, K. Pellarin, C. Hewson, D.A. Love, W.M. Lau, Z. Ding, One-pot electrodeposition, characterization and photoactivity of stoichiometric copper indium gallium diselenide (CIGS) thin films for solar cells, Phys. Chem. Chem. Phys. 12 (2010) 15282–15290. doi:10.1039/C0CP00586J.

[230] V. Badets, G. Loget, P. Garrigue, N. Sojic, D. Zigah, Combined local anodization of titanium and scanning photoelectrochemical mapping of TiO2 spot arrays, Electrochim. Acta. 222 (2016) 84–91. doi:10.1016/j.electacta.2016.10.151.

[231] R. Gutkowski, C. Khare, F. Conzuelo, Y.U. Kayran, A. Ludwig, W. Schuhmann, Unraveling compositional effects on the light-induced oxygen evolution in Bi(V–Mo–X)O4 material libraries, Energy Environ. Sci. 10 (2017) 1213–1221. doi:10.1039/c7ee00287d.

[232] F. Zhao, N. Plumeré, M.M. Nowaczyk, A. Ruff, W. Schuhmann, F. Conzuelo, Interrogation of a PS1-based photocathode by means of scanning photoelectrochemical microscopy, Small. 13

(2017) 1604093. doi:10.1002/smll.201604093.

[233] F. Zhao, S. Hardt, V. Hartmann, H. Zhang, M.M. Nowaczyk, M. Rögner, N. Plumeré, W. Schuhmann, F. Conzuelo, Light-induced formation of partially reduced oxygen species limits the lifetime of photosystem 1-based biocathodes, Nat. Commun. 9 (2018) 1973. doi:10.1038/s41467-018-04433-z.

[234] F. Zhao, F. Conzuelo, V. Hartmann, H. Li, M.M. Nowaczyk, N. Plumeré, M. Rögner, W. Schuhmann, Light Induced H2 Evolution from a Biophotocathode Based on Photosystem 1 – Pt Nanoparticles Complexes Integrated in Solvated Redox Polymers Films, J. Phys. Chem. B. 119 (2015) 13726–13731. doi:10.1021/acs.jpcb.5b03511.

[235] F. Zhao, F. Conzuelo, V. Hartmann, H. Li, S. Stapf, M.M. Nowaczyk, M. Rögner, N. Plumeré, W. Lubitz, W. Schuhmann, A novel versatile microbiosensor for local hydrogen detection by means of scanning photoelectrochemical microscopy, Biosens. Bioelectron. 94 (2017) 433–437. doi:https://doi.org/10.1016/j.bios.2017.03.037.

[236] F. Zhao, V. Hartmann, A. Ruff, M.M. Nowaczyk, M. Rögner, W. Schuhmann, F. Conzuelo, Unravelling electron transfer processes at photosystem 2 embedded in an Os-complex modified redox polymer, Electrochim. Acta. 290 (2018) 451–456. doi:https://doi.org/10.1016/j.electacta.2018.09.093.

[237] N. Thomas, V. Singh, S. Kuss, Optical fibers in analytical electrochemistry: Recent developments in probe design and applications, TrAC Trends Anal. Chem. 136 (2021) 116196. doi:https://doi.org/10.1016/j.trac.2021.116196.

[238] Y. Lee, A.J. Bard, Fabrication and Characterization of Probes for Combined Scanning Electrochemical/Optical Microscopy Experiments, Anal. Chem. 74 (2002) 3626–3633. doi:10.1021/ac015705d.

[239] K. Maruyama, H. Ohkawa, S. Ogawa, A. Ueda, O. Niwa, K. Suzuki, Fabrication and Characterization of a Nanometer-Sized Optical Fiber Electrode Based on Selective Chemical Etching for Scanning Electrochemical/Optical Microscopy, Anal. Chem. 78 (2006) 1904–1912. doi:10.1021/ac0502549.

[240] F.-R.F. Fan, D. Cliffel, A.J. Bard, Scanning Electrochemical Microscopy. 37. Light Emission by Electrogenerated Chemiluminescence at SECM Tips and Their Application to Scanning Optical Microscopy, Anal. Chem. 70 (1998) 2941–2948. doi:10.1021/ac980107t.

[241] W. Miao, J.-P. Choi, A.J. Bard, Electrogenerated Chemiluminescence 69: The Tris(2,2‘-bipyridine)ruthenium(II), (Ru(bpy)32+)/Tri-n-propylamine (TPrA) System RevisitedA New Route Involving TPrA•+Cation Radicals, J. Am. Chem. Soc. 124 (2002) 14478–14485. doi:10.1021/ja027532v.

[242] R.G. Maus, R.M. Wightman, Microscopic Imaging with Electrogenerated Chemiluminescence, Anal. Chem. 73 (2001) 3993–3998. doi:10.1021/ac010128e.

[243] F. Kanoufi, C. Cannes, Y. Zu, A.J. Bard, Scanning electrochemical microscopy. 43: Investigation of oxalate oxidation and electrogenerated chemiluminescence across the liquid-liquid interface, J. Phys. Chem. B. 105 (2001) 8951–8962. doi:10.1021/jp0108667.

[244] H. Zhou, S. Kasai, T. Matsue, Imaging localized horseradish peroxidase on a glass surface with scanning electrochemical/ chemiluminescence microscopy., Anal. Biochem. 290 (2001) 83–88. doi:10.1006/abio.2000.4941.

[245] R. Lei, L. Stratmann, D. Schäfer, T. Erichsen, S. Neugebauer, N. Li, W. Schuhmann, Imaging Biocatalytic Activity of Enzyme−Polymer Spots by Means of Combined Scanning Electrochemical Microscopy/Electrogenerated Chemiluminescence, Anal. Chem. 81 (2009) 5070–5074. doi:10.1021/ac900192n.

[246] C.J.R. Sheppard, D.M. Shotton, Confocal Laser Scanning Microscopy., Q. Rev. Biol. 74 (1999) 118. doi:10.1086/393067.

[247] N.C. Rudd, S. Cannan, E. Bitziou, I. Ciani, A.L. Whitworth, P.R. Unwin, Fluorescence Confocal Laser Scanning Microscopy as a Probe of pH Gradients in Electrode Reactions and Surface Activity, Anal. Chem. 77 (2005) 6205–6217. doi:10.1021/ac050800y.

[248] S. Cannan, I. Douglas Macklam, P.R. Unwin, Three-dimensional imaging of proton gradients at microelectrode surfaces using confocal laser scanning microscopy, Electrochem. Commun. 4 (2002) 886–892. doi:10.1016/S1388-2481(02)00482-4.

[249] J.M.A. Grime, M.A. Edwards, N.C. Rudd, P.R. Unwin, Quantitative visualization of passive transport across bilayer lipid membranes, Proc. Natl. Acad. Sci. U. S. A. 105 (2008) 14277–14282. doi:10.1073/pnas.0803720105.

[250] F.M. Boldt, J. Heinze, M. Diez, J. Petersen, M. Börsch, Real-time pH microscopy down to the molecular level by combined scanning electrochemical microscopy/single-molecule fluorescence spectroscopy, Anal. Chem. 76 (2004) 3473–3481. doi:10.1021/ac049635x.

[251] R. Mukhopadhyay, Research Profiles: SECM meets fluorescence microscopy, Anal. Chem. 76 (2004) 224 A-224 A. doi:10.1021/ac041588l.

[252] D. Oyamatsu, N. Kanaya, H. Shiku, M. Nishizawa, T. Matsue, Electrochemical/photochemical formation of enzyme patterns on glass substrates using a scanning electrochemical/confocal microscope, Sensors Actuators B Chem. 91 (2003) 199–204. doi:10.1016/s0925-4005(03)00089-3.

[253] S.-Y. Ku, K.-T. Wong, A.J. Bard, Surface Patterning with Fluorescent Molecules Using Click Chemistry Directed by Scanning Electrochemical Microscopy., J. Am. Chem. Soc. 130 (2008) 2392–2393. doi:10.1021/ja078183d.

[254] S.E. Salamifar, R.Y. Lai, Use of Combined Scanning Electrochemical and Fluorescence Microscopy for Detection of Reactive Oxygen Species in Prostate Cancer Cells, Anal. Chem. 85 (2013) 9417–9421. doi:10.1021/ac402367f.

[255] L. Guerret-Legras, J.F. Audibert, G. V Dubacheva, F. Miomandre, Combined scanning electrochemical and fluorescence microscopies using a tetrazine as a single redox and luminescent (electrofluorochromic) probe, Chem. Sci. 9 (2018) 5897–5905. doi:10.1039/c8sc01814f.

[256] L. Guerret-Legras, J.F. Audibert, I.M.G. Ojeda, G. V Dubacheva, F. Miomandre, Combined SECM-fluorescence microscopy using a water-soluble electrofluorochromic dye as the redox mediator, Electrochim. Acta. 305 (2019) 370–377. doi:10.1016/j.electacta.2019.03.069.

[257] L. Guerret-Legras, J.-F. Audibert, I.M. Gonzalez-Ojeda, G. V Dubacheva, G. Clavier, F. Miomandre, Time-Resolved Fluorescence Microscopy Combined with Scanning

Electrochemical Microscopy: A New Way to Visualize Photo-Induced Electron Transfer Quenching with an Electrofluorochromic Probe, J. Phys. Chem. C. 124 (2020) 23938–23948. doi:10.1021/acs.jpcc.0c06896.

[258] S. Szunerits, N. Knorr, R. Calemczuk, T. Livache, New Approach to Writing and Simultaneous Reading of Micropatterns: Combining Surface Plasmon Resonance Imaging with Scanning Electrochemical Microscopy (SECM), Langmuir. 20 (2004) 9236–9241. doi:10.1021/la0492557.

[259] E. Fortin, Y. Defontaine, P. Mailley, T. Livache, S. Szunerits, Micro-imprinting of oligonucleotides and oligonucleotide gradients on gold surfaces: a new approach based on the combination of scanning electrochemical microscopy and surface plasmon resonance imaging (SECM/ SPR-i)., Electroanalysis. 17 (2005) 495–503. doi:10.1002/elan.200403187.

[260] J. Xiang, J. Guo, F. Zhou, Scanning Electrochemical Microscopy Combined with Surface Plasmon Resonance: Studies of Localized Film Thickness Variations and Molecular Conformation Changes, Anal. Chem. 78 (2006) 1418–1424. doi:10.1021/ac051601h.

[261] Y. Xin, Y. Gao, J. Guo, Q. Chen, J. Xiang, F. Zhou, Real-time detection of Cu2+ sequestration and release by immobilized apo-metallothioneins using SECM combined with SPR, Biosens. Bioelectron. 24 (2008) 369–375. doi:10.1016/j.bios.2008.04.012.

[262] Y. Hou, N. Xin, S. Chen, C. Deng, J. Xiang, Controllable Release and High-Efficiency Collection of Hydrogen Peroxide: Application on the Quantitative Investigation of Biomolecule Oxidation Induced by Reactive Oxygen Species, Electroanalysis. 26 (2014) 1497–1503. doi:10.1002/elan.201400012.

[263] Y. Yu, V. Sundaresan, K.A. Willets, Hot Carriers versus Thermal Effects: Resolving the Enhancement Mechanisms for Plasmon-Mediated Photoelectrochemical Reactions, J. Phys. Chem. C. 122 (2018) 5040–5048. doi:10.1021/acs.jpcc.7b12080.

[264] Y. Yu, J.D. Williams, K.A. Willets, Quantifying photothermal heating at plasmonic nanoparticles by scanning electrochemical microscopy, Faraday Discuss. 210 (2018) 29–39. doi:10.1039/c8fd00057c.

[265] Y. Yu, K.D. Wijesekara, X. Xi, K.A. Willets, Quantifying Wavelength-Dependent Plasmonic Hot Carrier Energy Distributions at Metal/Semiconductor Interfaces, ACS Nano. 13 (2019) 3629–3637. doi:10.1021/acsnano.9b00219.

[266] L. Wang, C. Kranz, B. Mizaikoff, Monitoring Scanning Electrochemical Microscopy Approach Curves with Mid-Infrared Spectroscopy: Toward a Novel Current-Independent Positioning Mode, Anal. Chem. 82 (2010) 3132–3138. doi:10.1021/ac902781h.

[267] L. Wang, J. Kowalik, B. Mizaikoff, C. Kranz, Combining Scanning Electrochemical Microscopy with Infrared Attenuated Total Reflection Spectroscopy for in Situ Studies of Electrochemically Induced Processes, Anal. Chem. 82 (2010) 3139–3145. doi:10.1021/ac9027802.

[268] M. Steimecke, G. Seiffarth, M. Bron, In Situ Characterization of Ni and Ni/Fe Thin Film Electrodes for Oxygen Evolution in Alkaline Media by a Raman-Coupled Scanning Electrochemical Microscope Setup, Anal. Chem. 89 (2017) 10679–10686. doi:10.1021/acs.analchem.7b01060.

[269] J. Clausmeyer, M. Nebel, S. Grützke, Y.U. Kayran, W. Schuhmann, Local Surface Modifications Investigated by Combining Scanning Electrochemical Microscopy and Surface-Enhanced Raman Scattering, Chempluschem. 83 (2018) 414–417. doi:https://doi.org/10.1002/cplu.201800031.

[270] Z.T. Gossage, N.B. Schorr, K. Hernández-Burgos, J. Hui, B.H. Simpson, E.C. Montoto, J. Rodríguez-López, Interrogating Charge Storage on Redox Active Colloids via Combined Raman Spectroscopy and Scanning Electrochemical Microscopy, Langmuir. 33 (2017) 9455–9463. doi:10.1021/acs.langmuir.7b01121.

[271] N.B. Schorr, A.G. Jiang, J. Rodríguez-López, Probing Graphene Interfacial Reactivity via Simultaneous and Colocalized Raman–Scanning Electrochemical Microscopy Imaging and Interrogation, Anal. Chem. 90 (2018) 7848–7854. doi:10.1021/acs.analchem.8b00730.

[272] A.C. Hillier, M.D. Ward, Scanning electrochemical mass sensitivity mapping of the quartz crystal microbalance in liquid media, Anal. Chem. 64 (1992) 2539–2554.

doi:10.1021/ac00045a014.

[273] D.E. Cliffel, A.J. Bard, Scanning Electrochemical Microscopy. 36. A Combined Scanning Electrochemical Microscope−Quartz Crystal Microbalance Instrument for Studying Thin Films, Anal. Chem. 70 (1998) 1993–1998. doi:10.1021/ac971217n.

[274] D.E. Cliffel, A.J. Bard, S. Shinkai, Electrochemistry oftert-Butylcalix[8]arene−C60Films Using a Scanning Electrochemical Microscope−Quartz Crystal Microbalance, Anal. Chem. 70 (1998) 4146–4151. doi:10.1021/ac980183w.

[275] B. Gollas, P.N. Bartlett, G. Denuault, An Instrument for Simultaneous EQCM Impedance and SECM Measurements, Anal. Chem. 72 (2000) 349–356. doi:10.1021/ac990796o.

[276] C. Hess, K. Borgwarth, J. Heinze, Integration of an electrochemical quartz crystal microbalance into a scanning electrochemical microscope for mechanistic studies of surface patterning reactions, Electrochim. Acta. 45 (2000) 3725–3736. doi:10.1016/s0013-4686(00)00465-5.

[277] M. Shin, I.C. Jeon, Frequency-Distance Responses in SECM-EQCM – A Novel Method for Calibration of the Tip-Sample Distance, Bull Korean Chem Soc. 19 (1998) 1227–1232.

[278] C. Gabrielli, S. Joiret, M. Keddam, H. Perrot, N. Portail, P. Rousseau, V. Vivier, Development of a Coupled SECM-EQCM Technique for the Study of Pitting Corrosion on Iron, J. Electrochem. Soc. 153 (2006) B68. doi:10.1149/1.2161574.

[279] X. Tu, Q. Xie, C. Xiang, Y. Zhang, S. Yao, Scanning Electrochemical Microscopy in Combination with Piezoelectric Quartz Crystal Impedance Analysis for Studying the Growth and Electrochemistry as Well as Microetching of Poly(o-phenylenediamine) Thin Films, J. Phys. Chem. B. 109 (2005) 4053–4063. doi:10.1021/jp044731n.

[280] C.-Y. Hsu, V.S. Vasantha, K.-C. Ho, A study of ion exchange at the poly(butyl viologen)-electrolyte interface by SECM, Electrochim. Acta. 53 (2008) 6244–6251. doi:10.1016/j.electacta.2008.02.081.

[281] L. Díaz-Ballote, M. Alpuche-Aviles, D.O. Wipf, Fast-scan cyclic voltammetry–scanning electrochemical microscopy, J. Electroanal. Chem. 604 (2007) 17–25.

doi:10.1016/j.jelechem.2007.02.023.

[282] D.S. Schrock, D.O. Wipf, J.E. Baur, Feedback effects in combined fast-scan cyclic voltammetry-scanning electrochemical microscopy, Anal. Chem. 79 (2007) 4931–4941. doi:10.1021/ac0703911.

[283] D.S. Schrock, J.E. Baur, Chemical Imaging with Combined Fast-Scan Cyclic Voltammetry−Scanning Electrochemical Microscopy, Anal. Chem. 79 (2007) 7053–7061. doi:10.1021/ac071155t.

[284] É. Mahé, Electrochemistry in confined microsystems, Electrochim. Acta. 52 (2007) 5018–5029. doi:10.1016/j.electacta.2007.02.018.

[285] J.A. Koch, M.B. Baur, E.L. Woodall, J.E. Baur, Alternating Current Scanning Electrochemical Microscopy with Simultaneous Fast-Scan Cyclic Voltammetry, Anal. Chem. 84 (2012) 9537–9543. doi:10.1021/ac302402p.